Type I Collagen Nanomorphology in Relation to Disease, Tissue Hierarchy, and Fibrillogenesis

by

Ming Fang

A dissertation submitted in partial fulfillment
of the requirements for the degree of
Doctor of Philosophy
(Chemistry)
in The University of Michigan
2013

Doctoral Committee:

       Professor Mark M. Banaszak Holl, Chair
       Clifford M. Les, Henry Ford Hospital
       Professor Michael D. Morris
       Professor Bradford G. Orr

To my parents

Acknowledgements

Table of Contents

List of Figures

List of Tables

Abstract

Although the axial D-periodic spacing is a well-recognized nanomorphological feature of type I collagen fibrils, the existence of a distribution of values has been largely overlooked since its discovery seven decades ago. This dissertation begins with the development of a quantitative method to measure the D-periodic spacing of type I collagen fibrils using Atomic Force Microscopy coupled with a 2D Fast Fourier Transform approach. Recent quantitative characterizations supported that a 10 nm collagen D-spacing distribution is intrinsic to collagen fibrils in various tissues as well as *in vitro* self-assembly of reconstituted collagen. In addition, the distribution was altered in *Osteogenesis Imperfecta* and long term estrogen depletion. The need for fibril-to-fibril analysis was highlighted since it was the D-spacing distribution, not the D-spacing mean, that showed statistically significant differences in diseases.

The observation of D-spacing distribution was further expanded to a higher hierarchical level by examining fibril D-spacing distribution in relation to the microscale tissue organization. In dermis, bone and tendon, one common structure motif of collagen at the micrometer scale is the organization of fibrils into bundles. It was found that in each tissue type, collagen fibril D-spacings within a single bundle were nearly identical, and frequently differing by less than 1 nm. The full 10 nm range in D-spacing values was attributed to different values at the bundle level, independent of species or tissue types.

In order to better understand the origin of D-spacing distribution and its relationship with type I collagen self-assembly, surface-mediated collagen self-assembly as a function of substrate and incubation concentration was investigated. Collagen fibril assembly on phlogopite and muscovite mica, as well as fibrillar gel coextrusion in glass capillary tubes, all exhibited D-spacing distributions similar to those commonly observed in biological tissues. The observation of D-spacing distribution by self-assembly of type I collagen alone is significant as it eliminates the necessity to invoke other pre-assembly or post-assembly hypotheses, such as variation in the content of collagen types, enzymatic

cross-linking, or other post-translational modifications, as mechanistic origins of D-spacing distribution.

Chapter 1   Variation in Type I Collagen Fibril Nanomorphology: The Significance and Origin

1.1   Introduction

Type I collagen, composing 90% of the organic matrix of bone, plays a crucial role in maintaining the structural integrity and functional properties of bone. It modulates signal transduction of bone cells;[1] provides the framework for mineral nucleation and growth;[2] and it contributes to the toughness and resilience of bone.[3] Compositional and conformational changes of bone collagen have profound influence on bone properties, particularly the mechanical performance. Some of the well known examples are amino acid mutations in *Osteogenesis Imperfecta (OI)* resulting in brittle bones;[4] nonenzymatic cross-linking of collagen resulting in accumulation of advanced glycation products and compromised bone strength.[5] Our understanding of bone collagen structure-property-relationship at micron to submicron scale is still sparse. Many questions remain to be answered regarding how microstructural organization, fibril orientation, and fine details of collagen fibril nanomorphology influence bone properties.

Important aspects of collagen nanomorphological features have also been extensively studied in tissues other than bone. For example, tendon collagen fibrils exhibit a distribution of diameters and fibril diameter was shown to influence the mechanical properties.[6,7] Fibril length in general can reach millimeters and tip-to-tip fusion further extends the length.[8] In this review we will focus on one of the most recognized and functionally important aspects of collagen nanomorphology, the axial gap/overlap D-periodic spacing. Bone collagen D-spacing provides open sites for mineral nucleation, proteoglycan binding and cross-links to occur.[3] It also is an effective indicator of fibril strain during bone deformation.[9] Evidence from recent research has demonstrated the close relationship of collagen fibril D-spacing with bone micro-organization,[10] and

significant nanomorphological changes in D-spacing related to bone diseases.[11,12] These findings highlight the significance of bone collagen D-spacing variations, and provide insight into potential mechanisms for the variations in type I collagen fibril D-spacing. Some common features in collagen nano- and microstructures are shared among bone and other biological tissues and connections amongst these tissues will be elucidated.

1.2   The significance of Bone Collagen Nanomorphology

As an characteristic feature of collagen nanomorphology, the D-periodic spacing of collagen fibrils extracted from nerve, skin and cornea was shown in early electron micrographs,[13] and an estimated 64.6 ± 5.3 nm distribution of D-spacing was reported for human skin (Figure 1.1b).[14] The use of X-ray diffraction (XRD) in studying subfibrillar packing of collagen fibrils soon gained popularity and D-spacing values between 64 to 67 nm were reported.[15] In an attempt to explain the periodic D-spacing, Hodge and Petruska proposed a staggered parallel fibril model.[16] A theoretical analysis by Hulmes *et al*. demonstrated that maximal ionic and hydrophobic interactions occur when collagen monomers are offset by 234 ± 1 residues along the fibril axis, which roughly equals to 67 nm.[17] In the following decades, XRD studies provided stunning structural details including 5-strand quasi-hexagonal lateral arrangement of microfibrils and longitudinal supertwist (Figure 1.1a).[18-20] Nevertheless, techniques based on measurements of *individual* fibril's D-spacing continued to report a distribution of D-spacing values (Table 1.1); however, the physical and biological importance of D-spacing variation was not recognized. Textbooks and literature commonly introduce D-spacing as a single value 67 nm.[3] Recently, the importance of the collagen D-spacing distribution was brought to light; significant alterations in bone collagen D-spacing distribution are shown in *Osteogenesis Imperfecta* and long term estrogen depletion.[11,12]

Table 1.1 D-spacing variations reported in literature.

Variations in D-spacing	Tissue and Technique	Implications	Reference
55-80 nm distribution 64.6 ±5.3 nm[a]	Human skin TEM	The 55 to 80 nm range of spacing is not unique to collagen, but also shared by neurotubules	Gross, 1945[14]
64.6 ±0.8 nm in cornea 67.7 ±0.8 nm in tendon	Cornea and tendon XRD	18° axial inclination in cornea explains the D-spacing difference between cornea and tendon ($\cos\alpha = D_c/D_t$)	Marchini, 1986[21]
67.7 ±0.9 nm in central zone 71.3 ±0.4 nm in distal zone	Vitrified predentin TEM	D-spacing differences in the two zones may be due to the presence of proteoglycans and ions that bind to collagen	Beniash, 2000[22]
54-75 nm distribution (predominantly 67-68 nm hydrated; 57, 62, 67 nm dehydrated)	Partially demineralized dentin AFM	Reduced D-spacing may be due to dehydration induced structure disorder and loss of crystallinity	Habelitz, 2002[23]
69.6 ±2.9 nm	Rat Digital Tendon AFM	Fibril D-spacing is preserved independent of fibril diameter	Bozec, 2007[24]
63-73 nm distribution	Mice bone, dentin and tendon AFM	A distribution of D-spacing exist in bone, dentin and tendon, regardless of the presence of mineral, cellular origin, anatomical location or mechanical function of the tissue	Wallace, 2010[25]
68.0 ± 2.6 nm in sham; 65.9 ±3.1 nm in OVX	Sham and OVX ovine radius bone AFM	Estrogen depletion induces changes in type I collagen nanomorphology of bone (p<0.001)	Wallace, 2010[12]
63-74 nm distribution in wild type (WT); 56-75 nm distribution in brtl/+	WT and brtl/+ mice femur bone AFM	D-spacing means between WT and brtl/+ are not different (67.6 nm versus 67.4 nm); D-spacing distributions between the phenotypes are statistically different (p= 0.001)	Wallace, 2011[11]
59-66 nm distribution in sham; 56-67 nm distribution in OVX	Sham and OVX ovine dermis AFM	Estrogen depletion induces changes in type I collagen nanomorphology of dermis (p<0.001)	Fang, 2012[26]
57-69 nm distribution	Ovine bone AFM	Fibrils from one D-bundle share similar D-spacing; a distribution of values arises at the bundle level	Fang, 2012[10]

[a] Estimated from the distribution histogram (Figure 1.1b)
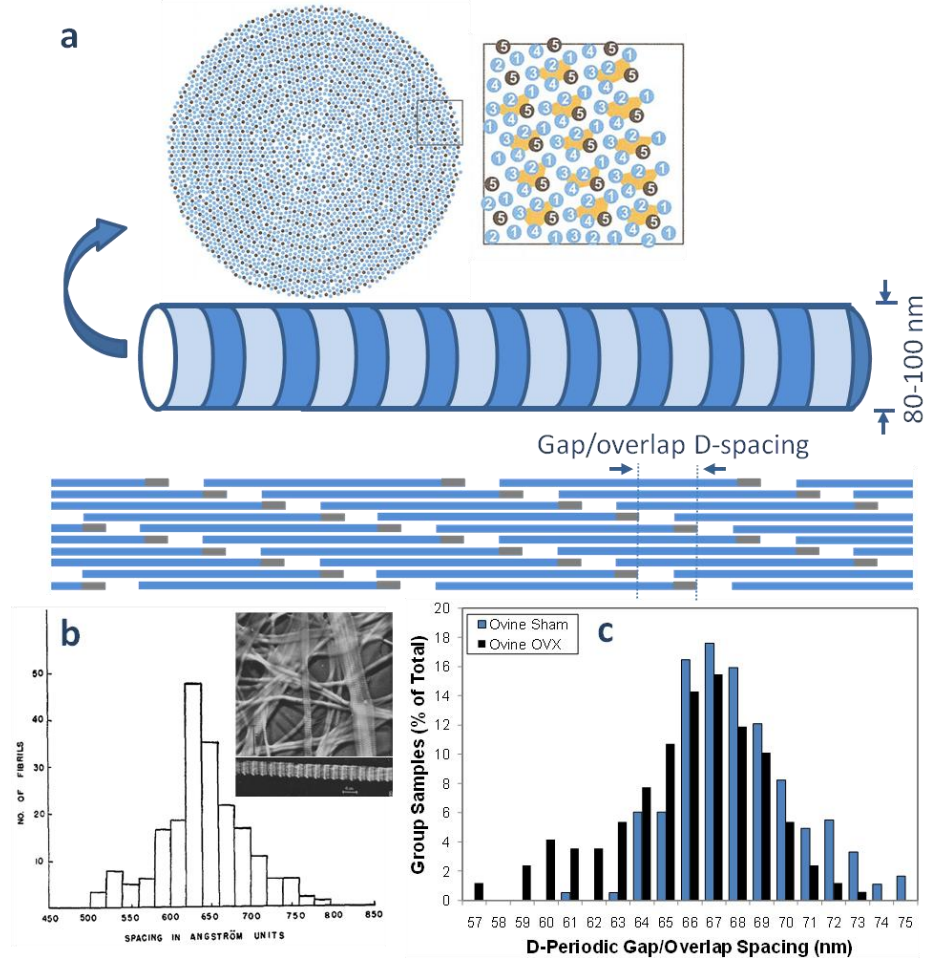
Figure 1.1 Type I collagen fibril structure and nanomorphological heterogeneity. (a) The proposed quasi-hexagonal packing at fibril cross-section, adapted from reference 15 with permission. (b) TEM studies in 1940s showing nanomorphological variations result in a D-spacing distribution, adapted from reference[14] with permission. (c) Significant alteration of D-spacing distribution in OVX ovine bone, adapted from reference[12] with permission.

Point mutations in the collagen amino acid sequence lead to various *Osteogenesis Imperfecta (OI)* phenotypes. On the molecular level, the detrimental effects of *OI* collagen mutations include slower folding of the triple helices, delayed intracellular trafficking and thus over modification,[27] destabilized tropocollagen molecules[28,29], decreased mechanical stiffness of tropocollagen molecules[30] as well as the fibrils.[31] A recent study by Wallace *et al.* showed changes in bone collagen nanomorphology as a result of Glycine 349 to Cysteine substitution in one *col1α1* allele. They used a heterozygous brtl/+ mice model of type IV OI, hence a heterogeneous mixture of mutated

and non-mutated collagen monomers[27]. Interestingly, the resulting collagen fibril D-spacing is also more heterogeneous compared to the wild type (WT) animals. While there was no significant difference between D-spacing means of WT and brtl/+, larger variations along the axial length of brtl/+ bones were noted, and the brtl/+ group contains only 55% of fibrils with D-spacings in 66-70 nm range, versus 75% in wild type (p = 0.001).[11] In a subsequent study, Kemp and Wallace demonstrated correlations between collagen fibril D-spacings and indentation-type nanomechanical properties with tendon fibrils of the brtl/+ OI mouse model. They found that modulus and indentation depth were correlated with brtl/+ fibril D-spacing in dried tendon fibrils, while energy dissipation were correlated with wild type fibril D-spacing in hydrated tendon fibrils.[32] Tensile stretching of an individual collagen fibril indicated correlation between fibril D-spacing and fibril mechanical properties; the nonlinear stress-strain curve suggests increased fibril modulus accompanying D-spacing elongation induced by tensile force.[33,34] In addition, higher elastic modulus in the overlap zone over gap zone has been demonstrated by AFM nanoindentation experiments.[35,36]

Alteration in collagen fibril nanomorphology has also been shown in long term estrogen depletion. Estrogen deficiency in post-menopausal women results in increased bone resorption,[37] reduced bone quantity and mineral density (BMD),[38] changes in the micro-architecture, and other material deterioration of bone.[39] Unlike *OI* which has a genetic origin directly linked to collagen, the knowledge on how estrogen deficiency may impact collagen is limited. Collagen cross-link content has been shown to decrease with osteoporosis.[40,41] The nanomorphology of collagen has been systematically compared between sham and ovariectomized (OVX) ovine bone and dermis.[12,26] In both tissue types, a higher percentage of fibrils with D-spacing values below mean minus 1 standard deviation was associated with estrogen depletion (Figure 1.1c). Specifically, 28% of OVX bone collagen fibrils had D-spacings lower than 64 nm, while only 7% of such fibrils were found in the sham group.[12] Similar results were found in OVX dermis, further supporting the notion that estrogen deprivation affects collagen nanomorphology, regardless of the presence of mineral or not.[26]

The studies of collagen nanomorphology in *OI* and long term estrogen depletion corroborated the important roles of collagen and the need for an effective method to

evaluate the morphology of collagen in bone diseases. Note that in both cases only a sub-portion of fibrils exhibited abnormal nanomorphological values, indicating the importance of methods capable of a fibril-by-fibril analysis. Connecting collagen fibril nanomorphology with biochemical and mechanical properties of collagen fibrils will require combined techniques capable of nm-scale resolution such as AFM/nanoindentation and AFM/Raman. These methods will provide useful information pointing to the biological origin of disease induced collagen nanomorphology variations and functional consequences on bone physiochemical and mechanical properties.

A few practical issues must be taken into consideration when studying bone collagen nanomorphology. Surface demineralization is required to reveal the underlying collagen matrix.[42] Gentle demineralization appears to have a minimal effect on collagen D-spacing since non-mineralized tissues such as tendon and skin showed similar D-spacing distributions with bone (see Table 1.1).[25,26] In addition, samples measured in air, and thus subject to some dehydration, showed minimal changes on D-spacing distribution of healthy and normal collagen fibrils,[43] however dehydration has an impact on *OI* tendon D-spacing distribution,[32] and affects mechanical behavior of bone tissue significantly.[44]

1.3 Collagen Nanomorphology Associated with Tissue Hierarchy

Organization of collagen fibrils into various highly hierarchical structures in bone matrix is a fascinating biological phenomenon. At the ultrastructural level, bone trabeculae and osteons are built by planar or cylindrical lamellar layers of collagen fibrils with different angular orientations between adjacent layers, known as the twisted plywood model.[45] Fibrils within one layer are aligned with each other as a bundle, similar to fibril bundles observed in skin, tendon, cornea and aorta.[46] The birefringence of collagen bundles allows optical techniques such as polarized light microscopy to visualize the different orientation of bone lamellae as alternating dark and bright bands.[47] Collagen fibril orientation is influenced by mechanical strain distribution and in turn enhances the mechanical property of bone.[48,49]

Collagen nanomorphology has a close connection with the coaligned fibril bundle unit-structure. Although a distribution of values ranging from 60-70 nm is frequently

found in tissues, within a single collagen fibril bundle, the variation of D-spacing values can be within ± 1 nm, suggesting uniform axial packing of collagen monomers within a bundle. Collagen bundles with uniform D-spacing has been named D-bundle. Different D-bundles, presumably belonging to different lamellar layers (Figure 1.2), could differ in D-spacing by up to 10 nm which give rise to the full scale distribution. A nested ANOVA analysis partitioned the variance components at the animal, bundle and fibril level, and found that indeed the bundle level variance accounted for 76% of total variance.[10] In other words, fibril D-spacing variance nested within one bundle and variance of different animals are small compared to variance of different D-bundles. It should be noted that this characteristic of the D-bundle was also present in dermis and tendon.
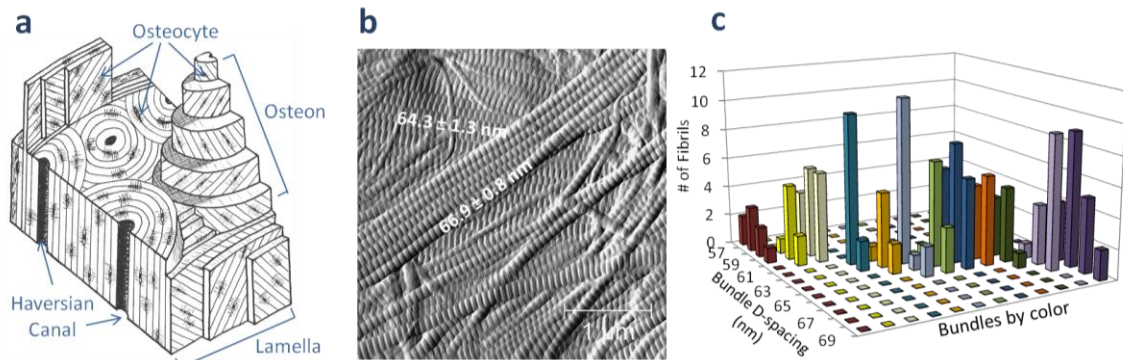
Figure 1.2 Collagen nanomorphology in connection to microscale bone lamellar structure. (a) A schematic of bone microarchitecture, showing lamellae with collagen fibril bundles at different orientations. (b) AFM error images showing two layers of collagen bundles presumably from two lamellae, and different D-spacing values are associated with the two bundles. (c) Three dimentional bar plot showing that bundle D-spacings occupies the full spectrum of distribution ranging from 57 to 59 nm, while fibril D-spacings within one bundle is narrow (± 1 nm). (a-c) are adapted from reference[10].

The observation of narrow D-spacing values within a bundle and large differences across different bundles has important implications in current fibrillogenesis models. Studies carried out in tendon clearly favor the hypothesis that cells play a dominating role in directing the alignment of fibrils.[50-52] Using transverse-sectioned TEM imaging, Canty and coworkers were able to trace collagen fibrils from extracellular bundles to deep within a fibroblast cell. The membrane protrusions of fibroblasts, also called fibripositors, were proposed as nucleation sites of collagen fibrillogenesis, and responsible for projecting collagen fibrils into parallel alignment.[51] By this theory, a collagen bundle is

formed by lateral association of fibrils excreted by one osteoblast and its orientation is determined by the direction in which the cell migrates. In this case, the bundle-to-bundle D-spacing difference could be due to cell-to-cell difference, such as the amount of minor collagens and post-translational modifications. Currently it is unclear to what extent osteoblasts influence bone collagen orientation. Unlike tendon, bone fibrils are orthogonally stacked in the twisted plywood spatial arrangement. *In vitro* osteoblast culture reproduces the orthogonal spatial arrangement of secreted collagen fibrils, however no evidence of osteoblast cells dominating the orthogonal fibril orientation was noted.[53] A different theory emphasizes the importance of the intrinsic liquid crystallinity of collagen.[54-56] Highly concentrated acid soluble collagen has characteristics of a cholesteric liquid crystal, which exhibits a striking resemblance to the twisted plywood structures in bone.[57] It is therefore plausible that high concentrations of procollagen or tropocollagen are pre-aligned prior to fibrillogenesis at the bone resorption pocket, leading to the formation of a fibril bundle with uniform packing of individual collagen monomers, hence the narrow D-spacing within a bundle. To date, no one has observed the motion of osteoblasts in registration with the collagen fibrils they secrete or directly studied the liquid crystallinity of collagen during the in vivo process of fibrillogenesis.

1.4   The Origin of Collagen D-spacing Distribution

For decades collagen D-spacing has been thought as a single value, either 64 nm in skin and cornea, or 67 nm in tendon and bone, based on X-ray diffraction data. Some have proposed a helicoidal fibril model to explain the discrepancy based on the observation of a 18° axial tilting of microfibrils in cornea using freeze etching technique. The 64 nm D-spacing in cornea was explained as 67 cos (18°).[21,58] A distribution of D-spacings has only recently been reported with significant connections to bone diseases and bone tissue micro-architecture.[10-12,25,26,32,43,59] For now, our understanding of the origin and functions of a collagen D-spacing distribution is limited, potential biological and molecular bases for the D-spacing distribution are discussed in this section.

Many collagen constituted tissues are also load bearing tissues. Bone formation and resorption are stimulated by increased mechanical loading and disuse, respectively,

as a part of bone functional adaptation.[60] It is plausible that variation in D-spacing is a reflection of changing local mechanical stresses. Although this hypothesis could explain formation of different bundle D-spacings and narrow D-spacing within a bundle, experimental data by various studies suggest against the possibility of differences in static mechanical loading causing a 10 nm distribution of D-spacings. Gupta *et al*. studied the behavior of fibril strain over tissue strain of bone using small-angle X-ray Scattering (SAXS) and noted that 1% macroscopic tissue strain corresponds with a 0.3 nm increase in D-spacing average as measured by SAXS.[9] Sasaki and Puxkandl have demonstrated similar effect in tendon.[61,62] The noncollagenous components of ECM and interfibril shearing/sliding are thought to account for the majority of bulk scale tissue strain.[63] Therefore, static mechanical stress alone does not cause the 10 nm D-spacing variations. Nevertheless, it doesn't rule out the possibility of fibril bundles with different D-spacings formed by osteoblast cells that are under different mechanical stresses. In addition to responses to mechanical cues, other potential cell-based factors include differential expression level of type V collagen and varing amount of psot-translational modification. Extracellular factors such as cross-links, and proteoglycan binding are also potential factors that could lead to different packing density and thus D-spacing variations.

A recent study has shown that self-assembly of type I collagen in vitro produces similar distributions with that found in biological tissues.[64] Purified type I collagen tropocollagen from rat tail tendon self-assembled into collagen fibrils on mica surfaces as well as fibrillar gels in a confined space of capillary tubes; both resulted in similar D-spacing distributions. It suggests that D-spacing variation is intrinsic to type I collagen and its self-assembly, and it doesn't necessarily require cells, interfibrillar cross-linking, and proteoglycan binding. The variations in fibril D-spacing may be results of variant intrafibrillar interactions including hydrophobic interactions, electrostatic interactions, hydrogen bonding, and cross-links on hydroxylysines and hydroxyprolines. Since an offset of 234 amino acids between collagen monomers maximizes the sum of these interactions, it is possible that D-spacing variations arise from various degrees of tilting or super coiling within a fibril, similar to the idea used to explain the 64 nm vs. 67 nm D-spacing in different tissues. In addition, Bozec *et al.* observed spiral and twisted rope

features in digital tendon fibrils and proposed a classic n-plies rope model which could also explain fibril D-spacing variation.[24] More refined theoretical models incorporating collagen monomer and/or microfibril assembly should also be able to predict a D-spacing distribution.

1.5 Summary and Perspectives

From the 2D Hedge-Petruska model in 1960s[16] to modern computer simulated 3D model,[65] D-spacing has been a key aspect of collagen nanomorphology, yet the intrinsic heterogeneity of collagen D-spacing has rarely been emphasized. An axial D-spacing distribution arises at the bundle level and it is universal among bone and other tissues including skin, tendon, and dentin; it can also be reproduced by self-assembly of type I collagen alone. The alteration of D-spacing distributions in bone diseases underscores the need to better understand the origin of D-spacing distribution and the biochemical/ mechanical consequence of such nanomorphological changes. Different fibril D-spacings may have an impact on mineral nucleation and growth, binding with proteoglycans, and fibril stiffness. Experimental investigations using combined instrumental analyses and theoretical modeling are required to elucidate the details of collagen structure-property-relationship at nano- to micro- scale.

1.6 Reference

(1)   Green, J.; Schotland, S.; Stauber, D. J.; Kleeman, C. R.; Clemens, T. L. *American Journal of Physiology - Cell Physiology* **1995**, *268*, C1090.
(2)   Wang, Y.; Azaïs, T.; Robin, M.; Vallée, A.; Catania, C.; Legriel, P.; Pehau-Arnaudet, G.; Babonneau, F.; Giraud-Guille, M. M.; Nassif, N. *Nature Materials* **2012**, *11*, 724.
(3)   Fratzl, P.; SpringerLink *Collagen Structure and Mechanics*; Springer Science+Business Media, LLC: Boston, MA, 2008.
(4)   Byers, P. H. *Trends Genet.* **1990**, *6*, 293.
(5)   Vashishth, D. *Current Osteoporosis Reports* **2007**, *5*, 62.
(6)   Parry, D. A. D.; Barnes, G. R. G.; Craig, A. S. *Proceedings of the Royal Society of London - Biological Sciences* **1978**, *203*, 305.
(7)   Christiansen, D. L.; Huang, E. K.; Silver, F. H. *Matrix Biol.* **2000**, *19*, 409.
(8)   Graham, H. K.; Holmes, D. F.; Watson, R. B.; Kadler, K. E. *J. Mol. Biol.* **2000**, *295*, 891.

(9)   Gupta, H. S.; Wagermaier, W.; Zickler, G. A.; Raz-Ben Aroush, D.; Funari, S. S.; Roschger, P.; Wagner, H. D.; Fratzl, P. *Nano Lett.* **2005**, *5*, 2108.

(10)   Fang, M.; Goldstein, E. L.; Turner, A. S.; Les, C. M.; Orr, B. G.; Fisher, G. J.; Welch, K. B.; Rothman, E. D.; Banaszak Holl, M. M. *ACS NANO* **2012**, *6*, 9503.

(11)   Wallace, J. M.; Orr, B. G.; Marini, J. C.; Holl, M. M. B. *J. Struct. Biol.* **2011**, *173*, 146.

(12)   Wallace, J. M.; Erickson, B.; Les, C. M.; Orr, B. G.; Banaszak Holl, M. M. *Bone* **2010**, *46*, 1349.

(13)   Schmitt, F. O.; Hall, C. E.; Jakus, M. A. *Journal of Cellular and Comparative Physiology* **1942**, *20*, 11.

(14)   Gross, J.; Schmitt, F. O. *The Journal of Experimental Medicine* **1948**, *88*, 555.

(15)   Bear, R. S. *J. Am. Chem. Soc.* **1944**, *66*, 1297.

(16)   *Recent studies with the electron microscope on ordered aggregates of the tropocollagen molecule*; Hodge, A. J.; Petruska, J. A., Eds.; Academic Press: New York, 1963.

(17)   Hulmes, D. J. S.; Miller, A.; Parry, D. A. D.; Piez, K. A.; Woodhead-Galloway, J. *J. Mol. Biol.* **1973**, *79*, 137.

(18)   Orgel, J. P. R. O.; Miller, A.; Irving, T. C.; Fischetti, R. F.; Hammersley, A. P.; Wess, T. J. *Structure* **2001**, *9*, 1061.

(19)   Orgel, J. P. R. O.; Irving, T. C.; Miller, A.; Wess, T. J. *Proc. Natl. Acad. Sci. U. S. A.* **2006**, *103*, 9001.

(20)   Hulmes, D. J. S.; Wess, T. J.; Prockop, D. J.; Fratzl, P. *Biophys. J.* **1995**, *68*, 1661.

(21)   Marchini, M.; Morocutti, M.; Ruggeri, A.; Koch, M. H.; Bigi, A.; Roveri, N. *Connect. Tissue Res.* **1986**, *15*, 269.

(22)   Beniash, E.; Traub, W.; Veis, A.; Weiner, S. *J. Struct. Biol.* **2000**, *132*, 212.

(23)   Habelitz, S.; Balooch, M.; Marshall, S. J.; Balooch, G.; Marshall Jr, G. W. *J. Struct. Biol.* **2002**, *138*, 227.

(24)   Bozec, L.; Van Der Heijden, G.; Horton, M. *Biophys. J.* **2007**, *92*, 70.

(25)   Wallace, J. M.; Chen, Q.; Fang, M.; Erickson, B.; Orr, B. G.; Banaszak Holl, M. M. *Langmuir* **2010**, *26*, 7349.

(26)   Fang, M.; Liroff, K. G.; Turner, A. S.; Les, C. M.; Orr, B. G.; Holl, M. M. B. *J. Invest. Dermatol.* **2012**, *132*, 1791.

(27)   Forlino, A.; Kuznetsova, N. V.; Marini, J. C.; Leikin, S. *Matrix Biol.* **2007**, *26*, 604.

(28)   Lee, K. H.; Kuczera, K.; Banaszak Holl, M. M. *Biopolymers* **2011**, *95*, 182.

(29)   Lee, K. H.; Kuczera, K.; Holl, M. M. B. *Biophys. Chem.* **2011**, *156*, 146.

(30)   Gautieri, A.; Vesentini, S.; Redaelli, A.; Buehler, M. J. *Protein Sci.* **2009**, *18*, 161.

(31)   Gautieri, A.; Uzel, S.; Vesentini, S.; Redaelli, A.; Buehler, M. J. *Biophys. J.* **2009**, *97*, 857.

(32)   Kemp, A. D.; Harding, C. C.; Cabral, W. A.; Marini, J. C.; Wallace, J. M. *J. Struct. Biol.* **2012**, *180*, 428.

(33)   Gutsmann, T.; Fantner, G. E.; Kindt, J. H.; Venturoni, M.; Danielsen, S.; Hansma, P. K. *Biophys. J.* **2004**, *86*, 3186.

(34)   van der Rijt, J. A. J.; van der Werf, K. O.; Bennink, M. L.; Dijkstra, P. J.; Feijen, J. *Macromol. Biosci.* **2006**, *6*, 697.

(35)   Minary-Jolandan, M.; Yu, M. F. *Biomacromolecules* **2009**, *10*, 2565.

(36)   Grant, C. A.; Phillips, M. A.; Thomson, N. H. *Journal of the Mechanical Behavior of Biomedical Materials* **2012**, *5*, 165.

(37)   Rodan, G. A. *J. Bone Miner. Res.* **1991**, *6*, 527.

(38)   Stone, K. L.; Seeley, D. G.; Lui, L.-Y.; Cauley, J. A.; Ensrud, K.; Browner, W. S.; Nevitt, M. C.; Cummings, S. R. *J. Bone Miner. Res.* **2003**, *18*, 1947.

(39)   Burket, J. C.; Brooks, D. J.; MacLeay, J. M.; Baker, S. P.; Boskey, A. L.; van der Meulen, M. C. H. *Bone* **2013**, *52*, 326.

(40)   Orkoula, M. G.; Vardaki, M. Z.; Kontoyannis, C. G. *Vibrational Spectroscopy* **2012**, *63*, 404.

(41)   Oxlund, H.; Sekilde, L.; Ørtoft, G. *Bone* **1996**, *19*, 479.

(42)   Kindt, J. H.; Thurner, P. J.; Lauer, M. E.; Bosma, B. L.; Schitter, G.; Fantner, G. E.; Izumi, M.; Weaver, J. C.; Morse, D. E.; Hansma, P. K. *Nanotechnology* **2007**, *18*.

(43)   Erickson, B.; Fang, M.; Wallace, J. M.; Orr, B. G.; Les, C. M.; Banaszak Holl, M. M. *Biotechnology Journal* **2013**, *8*, 117.

(44)   Rho, J.-Y.; Pharr, G. M. *J. Mater. Sci. Mater. Med.* **1999**, *10*, 485.

(45)   Giraud-Guille, M. M. *Calcif. Tissue Int.* **1988**, *42*, 167.

(46)   Graham, H. K.; Hodson, N. W.; Hoyland, J. A.; Millward-Sadler, S. J.; Garrod, D.; Scothern, A.; Griffiths, C. E. M.; Watson, R. E. B.; Cox, T. R.; Erler, J. T.; Trafford, A. W.; Sherratt, M. J. *Matrix Biol.* **2010**, *29*, 254.

(47)   Bromage, T. G.; Goldman, H. M.; McFarlin, S. C.; Warshaw, J.; Boyde, A.; Riggs, C. M. *Anatomical Record - Part B New Anatomist* **2003**, *274*, 157.

(48)   Takano, Y.; Turner, C. H.; Owan, I.; Martin, R. B.; Lau, S. T.; Forwood, M. R.; Burr, D. B. *J. Orth. Res.* **1999**, *17*, 59.

(49)   Skedros, J. G.; Dayton, M. R.; Sybrowsky, C. L.; Bloebaum, R. D.; Bachus, K. N. *J. Exp. Biol.* **2006**, *209*, 3025.

(50)   Trelstad, R. L.; Hayashi, K. *Dev. Biol.* **1979**, *71*, 228.

(51)   Canty, E. G.; Lu, Y.; Meadows, R. S.; Shaw, M. K.; Holmes, D. F.; Kadler, K. E. *J. Cell Biol.* **2004**, *165*, 553.

(52)   Canty, E. G.; Kadler, K. E. *J. Cell Sci.* **2005**, *118*, 1341.

(53)   Gerstenfeld, L. C.; Riva, A.; Hodgens, K.; Eyre, D. R.; Landis, W. J. *J. Bone Miner. Res.* **1993**, *8*, 1031.

(54)   Giraud-Guille, M. M. *J. Mol. Biol.* **1992**, *224*, 861.

(55)   Giraud-Guille, M. M.; Mosser, G.; Belamie, E. *Current Opinion in Colloid and Interface Science* **2008**, *13*, 303.

(56)   Gobeaux, F.; Mosser, G.; Anglo, A.; Panine, P.; Davidson, P.; Giraud-Guille, M. M.; Belamie, E. *J. Mol. Biol.* **2008**, *376*, 1509.

(57)   Giraud-Guille, M. M.; Belamie, E.; Mosser, G.; Helary, C.; Gobeaux, F.; Vigier, S. *Comptes Rendus Chimie* **2008**, *11*, 245.

(58)   Wess, T. J. 2005; Vol. 70, p 341.

(59)   Wallace, J. M. *Bone* **2012**, *50*, 420.

(60)   Skerry, T. M. *Arch. Biochem. Biophys.* **2008**, *473*, 117.

(61)   Puxkandl, R.; Zizak, I.; Paris, O.; Keckes, J.; Tesch, W.; Bernstorff, S.; Purslow, P.; Fratzl, P. *Philosophical Transactions of the Royal Society B: Biological Sciences* **2002**, *357*, 191.

(62)   Sasaki, N.; Shukunami, N.; Matsushima, N.; Izumi, Y. *J. Biomech.* **1999**, *32*, 285.

(63)   Gupta, H. S.; Zioupos, P. *Med. Eng. Phys.* **2008**, *30*, 1209.

(64)   Fang, M.; Goldstein, E. L.; Matich, E. K.; Orr, B. G.; Banaszak Holl, M. M. *Langmuir* **2013**, *29*, 2330.

(65)   Gautieri, A.; Vesentini, S.; Redaelli, A.; Buehler, M. J. *Nano Lett.* **2011**, *11*, 757.

Chapter 2   **Nanoscale Structure of Type I Collagen Fibrils:**
                Quantitative Measurement of D-spacing

2.1   **Introduction**

Collagens are the most abundant family of structural proteins in animals.[1,2] These proteins are based on trimeric polypeptide chains, each of which includes a repeating Gly-X-Y triplet region where X and Y are often proline and hydroxyproline. A major class of collagen is the fibrillar-forming type (type I, II, III, V, and XI), which has an approximately 300 nm long, uninterrupted triple helix.[3] Type I collagen accounts for 70% of all collagens and it is found throughout the body in the extracellular matrices (ECMs) of teeth, bones, tendons, skin, arterial walls and cornea.[4]

At the nanoscale, the most prominent feature of Type I collagen fibrils is the ~67 nm axial D-periodic spacing. This feature was observed by X-ray diffraction[5] and imaged by transmission electron microscopy (TEM) as early as 1942 by Schmitt et al.[6] In 1963, the first model of the fibrillar structure was developed by Hodge and Petruska.[7] They proposed that molecules within a fibril are arranged in a staggered parallel alignment, resulting in "gap" and "overlap" regions.[7] Since this original description, X-ray diffraction[8-11] and electron microscopy[12-14] studies have supported a singular spacing of 67 nm. More detailed models of fibrillar structure have been elucidated by the effort of many researchers, including Miller, Brodsky, Hulmes, and Orgel, to name a few.[9,15-22] It has been elucidated that a fibril is composed of five-stranded microfibrils which are supertwisted in the axial direction[22] and quasi-hexagonally packed in the equatorial plane.[16] An atomistic-scale-up simulation based on the state-of-the-art fibril model has elegantly shown the bottom-up design of a collagen fibril resulting in the D-periodicity.[23] Yet all such models are built upon this single valued 67 nm periodicity. Despite this

commonly held view of a singular spacing, the hierarchical complexity of the collagen fibril itself, the variety of tissues into which these fibrils are incorporated, and the potential for morphological variation with damage and disease suggests that a single spacing value for all fibrils is unlikely. Recently, a quantitative approach to measuring this feature allowed the discovery of a distribution of D-periodic spacings ranging from ~60-73 nm in normal bone, dentin, skin, and tendon tissue.[24] This distribution changes as a function of estrogen depletion[25,26] and *Osteogenesis Imperfecta* (OI).[27] This new approach to understanding nanoscale collagen morphology is applicable to understanding the structure of collagen in a wide variety of tissues and ECM-linked diseases.

Quantitative analysis of morphological features in Type I collagen-based tissues is imperative to the understanding of normal tissue architecture.[24] This understanding is requisite for interpretation of any alterations caused by damage and disease. These methods may also serve as techniques for disease diagnosis in collagen-based tissues.[25-27] Here important experimental methodology for the application of atomic force microscopy was provided to the quantitative analysis of Type I collagen D-spacing values. This includes approaches to instrument calibration, data sampling and analysis, and the comparison of the D-spacing values obtained with this method to complementary approaches including electron microscopy[12] and X-ray scattering.[28] The experimental approaches should prove useful for quantifying the changes in collagen structure for a wide range of diseases related to the extracellular matrix.

2.2   Results and Discussion

2.2.1   Aspects of Measuring the D-periodic Spacing in Type I Collagen Fibrils

The axial D-periodic spacing was chosen as the key metric of collagen fibril morphology in this study. This measure captures aspects of collagen's fibrillar structure that may be related to the state of the individual molecular triple helices, post-translational modifications and/or cross-linking within the fibril. Although the functional mechanisms of these activities has not been elucidated, in many cases it has been shown that genetic modification, non-enzymatic cross-linking and other changes at the molecular level lead to significantly compromised bulk tissue properties.[1] As seen in

Figure 2.1A, D-periodic spacing is well resolved by Atomic Force Microscopy (AFM), providing a potential biomarker linked to the state of collagen. Previous studies have relied primarily on line scans and one dimensional Fast Fourier Transformation (1D-FFT) and did not perform quantitative analyses of larger data sets.[30-33] Line scans and 1D-FFTs are subject to user bias in that they both rely on the user drawing a line along the length of a fibril, normal to the D-spacing.[25] From 1D-FFT measurements on fibrils in the current study, as little as a 5° deviation away from normal can alter the value measured for the spacing by as much as 8%. Errors of this magnitude are larger than the population standard deviations noted below, masking important information within the distributions.
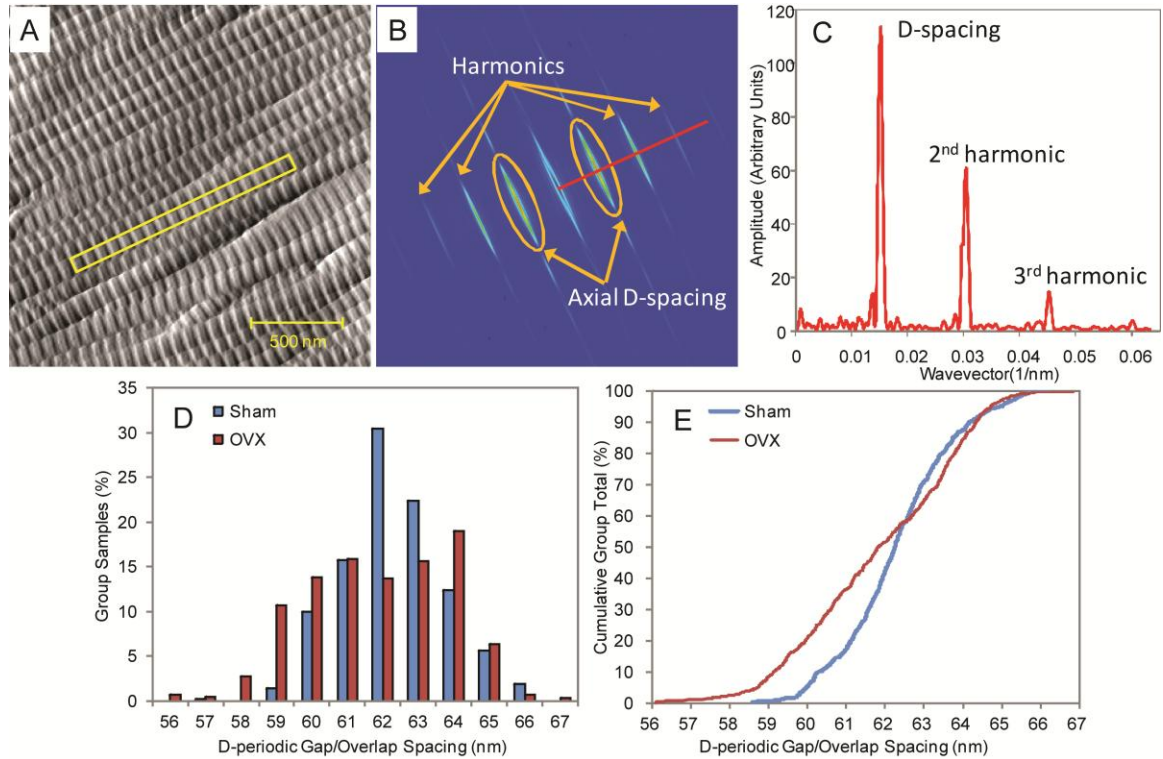
Figure 2.1 Schematic Representation of the 2D-FFT and D-periodic Spacing Measurements from Sham-Operated Versus Ovariectomized Sheep Dermis. Panel A shows an AFM amplitude image of Type I collagen. The D-periodicity is visible as a striped pattern perpendicular to the fibril axis. Panel B shows the 2D-FFT of the selected fibril. The red line runs through the maximum value of the first peak, corresponding to the D-periodic spacing. Panel C shows the 1D-FFT along this line, normal to the D-periodic spacing and through the maxima in the 2D power spectrum. Panel D and E are the histogram and Cumulative Density Functions (CDF) representation of Type I Collagen D-periodic spacing distributions analyzed by 2D-FFT method. The comparison between Sham-operated versus estrogen-depleted (OVX) sheep dermis was derived from

reference[26]. In this case, there was a significant increase of diseased populations towards lower D-periodic spacings.

The type of error noted has provided a significant challenge to the observation of a distribution of D-period spacings in EM and AFM studies over the last seven decades. Employing a 2D-FFT approach decouples the determination of the D-periodic spacing from user bias in line location and angle selection. An example image of a collagen fibril imaged by AFM and measured using a 2D-FFT approach is shown in Figure 2.1. In order to minimize edge effects that can degrade resolution, a rectangular region of interest is drawn and extends from the edge of one gap zone to the edge of another gap zone, remaining within the width of the fibril. Figure 2.1B shows the 2D-FFT power spectrum from the selected region. The red line passes through the maximum value in the fundamental peak, therefore corresponding to the D-periodic spacing along the normal direction of the gap/overlap axis. A 1D-FFT along this line demonstrates that the D-periodic spacing, the second and third harmonics are visible and well resolved (Figure 2.1C).
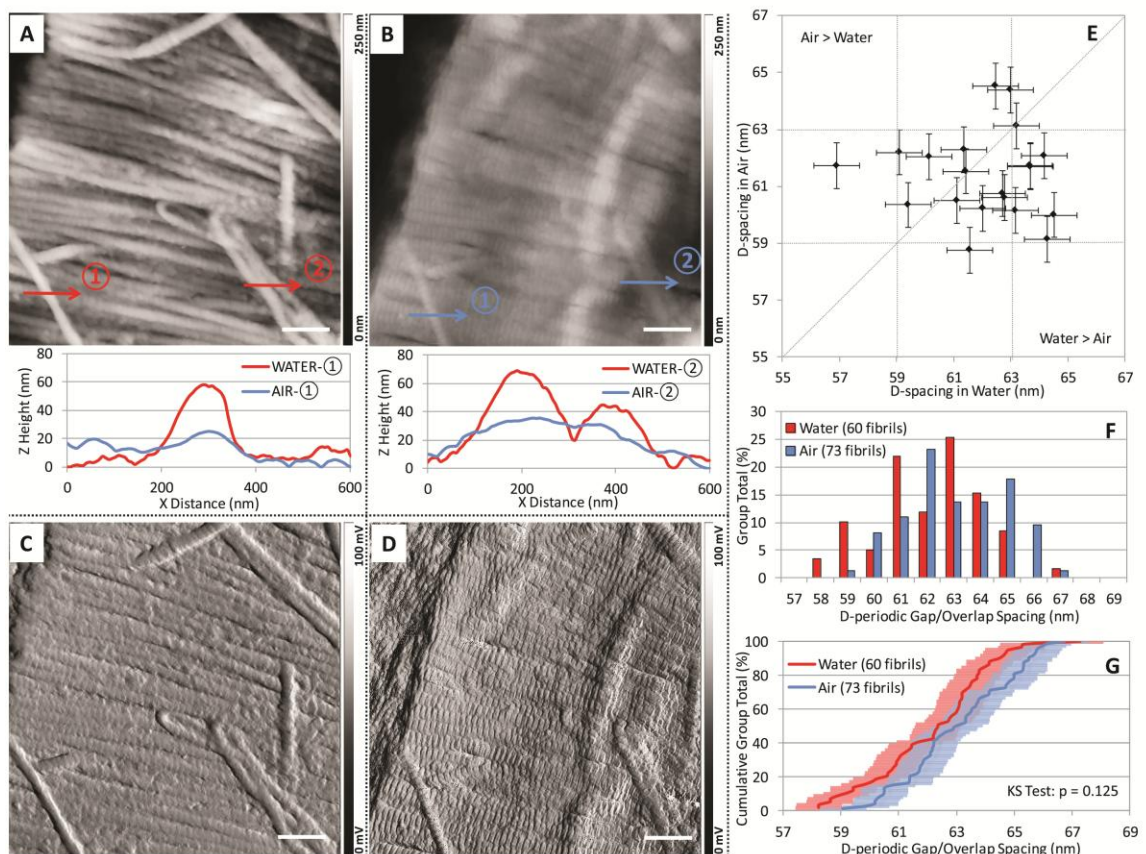
Figure 2.2 Comparison of Sheep Dermal Collagen D-spacings measured in water and air. Panel A and B are height images of sheep dermal collagen fibrils imaged in water and air respectively (both panels A and B are baseline subtracted using 2nd order polynominal fitting). Selected height profiles in the fast scan direction were plotted for the comparison of fibril heights in water and air (the local minimum was set as 0 nm in height). Panel C and D are the error images for regions A and B, respectively. D-spacings from a set of 20 fibrils were measured both in water and air error images. The comparison is provided as a scatter plot (Panel E). Panels F and G are the histogram and CDF representation of the water versus air fibril D-spacings measurement for an uncorrelated set of 133 fibrils. In this case, all the fibrils with discernible D-spacing repeat units from a set of 7 images were included to generate the histogram in panel F and CDF in panel G. The error bars of 1.3 nm shown in Panels E and G were derived from a combination of the absolute measurement error and the uncertainty of the 2D-FFT fibril spacing assessment. The scale bar is 500 nm in panels A-D.

The 2D-FFT analysis can be used to interpret D-spacing data from electron microscopy (EM) and AFM images. AFM was chosen owing to its ability in keeping the tissue specimens relatively close to their native condition during sample preparation and imaging.[35] Absolute dehydration is thought to disrupt collagen molecular structure and increase packing density within a fibril.[36,37] The effect of absolute dehydration has been shown to reduce collagen D-spacing.[38,39] This implies hydration differences in the collagen fibrils could influence the observed distribution of collagen D-spacing. In order to demonstrate the effect of surface air-drying on collagen fibril D-spacing, the metrical parameters of dermal collagen fibrils imaged by AFM in water and air were compared. Dermis tissue was selected for this analysis because of the high water content in its native environment. As shown in height images in Figure 2.2A and Figure *2.2*B, the fibril surface imaged in water has greater height variation than the air-dried surface. The height profiles illustrated by line scans (1) and (2) demonstrate an apparent swelling of the collagen fibrils, and possibly other matrix proteins such as proteoglycans, when imaged in water. Measurement of multiple fibrils indicated as much as a two- to four-fold increase in apparent fibril height in water relative to air. Error images shown in Figure 2.2C and Figure *2.2*D demonstrate that fibril D-spacings can be directly observed in water and air, respectively. Using these images as well as 6 other sets, 20 fibrils with well-resolved D-spacing repeat units were identified in paired water and air images. Using 2D-FFT analysis, the D-spacings from the 20 fibrils were analyzed and are presented in the air versus water scatter plot (Figure 2.2E). As illustrated in Figure 2.2E,

there is no correlation in the small shifts in D-spacings observed as a function of water vs air imaging. Indeed, seven fibrils exhibited larger D-spacings in air and eleven exhibited larger D-spacings in water. Two fibrils were essentially unchanged. In addition to the direct comparison of individual fibril D-spacings, histogram and CDF including every fibril that was observed in either water (60 fibrils) or air imaging (73 fibrils) for the 7 paired air/water images were plotted (Figure 2.2F and Figure *2.2*G). The averages of fibril D-spacing in this analysis are 62.2 ± 2.0 nm and 63.1 ± 1.9 nm in water and air, respectively. The difference in absolute value of the average D-spacing for air vs water imaging obtained from Figure 2.2E and Figure *2.2*F of 0.9 nm is on the same order as our ability to measure the spacings using the 2D-FFT method. The impact of air-drying is small compared to the width of the D-spacing distribution as illustrated in Figure 2.1 (discussed in section 2.2.3). It is interesting to note that although the histogram and CDF (Figure 2.2F and Figure *2.2*G) indicate an average D-spacing increase of 0.9 nm upon air drying, the paired fibril data in Figure 2.2E indicates that this average is obtained by a mix of behaviors ranging from 0 to 4 nm changes in D-spacing and both increases and decreases in D-spacing.   This is also reflected in the substantial red/blue overlap, indicated in purple, in the CDF plot (Figure 2.2G) and the p-value of 0.125 indicating a lack of statistical significance.   In summary, within the reproducibility of the measurement, there is no difference in D-banding spacing between the samples measured in air vs water.

2.2.2   The Nonlinear Relationship between AFM Scanner Error and Scan Size

Making absolute x-y distance measurements with AFM and comparing absolute values measured in different studies has limitations. Absolute measurement relies on accurate calibration of AFM, which depends on the use of appropriate calibration standards, consistent performance of the piezo-material and regular calibration test to maintain the consistency. AFM scanners can be characterized by the sensitivity which is defined as the ratio of piezo movement to piezo voltage (V). The inherent properties of open loop AFM dictate that the sensitivity varies non-linearly with respect to scan size. In order to test to what extent the nonlinear sensitivity affects the AFM scanner error, three calibration standards were used with pitch sizes of 100 nm, 1 μm and 10 μm (Figure 2.3).

The absolute errors of these calibration standards were examined by SEM to be less than 1.5%.
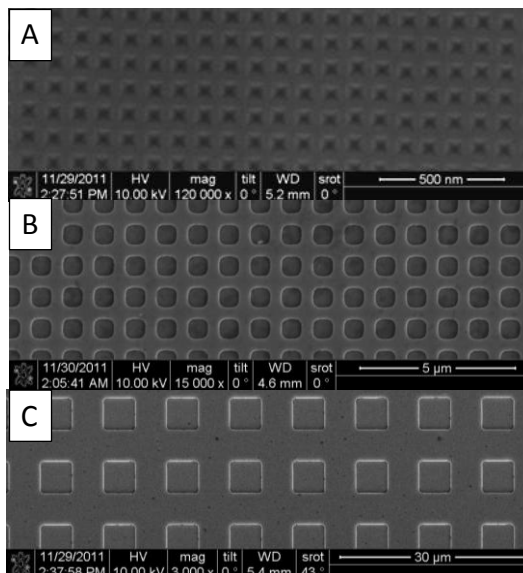
Figure 2.3 SEM characterization of the calibration standards. Panel A–C are SEM images of 100 nm, 1 μm and 10 μm calibration standards. The absolute error of the three calibration standards were less than 1.5 %.

The AFM was calibrated using the manufacturer's recommended method, using a 10 μm pitch calibration standard, scanning over the full 80 μm scale of the AFM scanner. After calibration, the percentage errors on the fast and slow scan direction were 2% and 3% respectively, as shown in Table 2.1. However, as the scan size decreased, the error increased substantially. Using a 100 nm pitch calibration standard to test the scanner calibration on a 3.5 μm scan, the errors on the fast and slow scan direction were 9% and 17% respectively. The Agilent 5500 AFM uses separate piezoelectric elements for X/Y movement and for Z movement. This configuration helps to reduce the cross coupling between different axes, and it also explains the differential responses of piezo-sensitivity on X and Y direction. The effect of nonlinear sensitivity is also shown in Figure 2.4. Since the AFM was calibrated over scans of 80 μm size, sensitivity at high voltage ($Sensitivtity_{high\_v}$) was recorded in the calibration file. Therefore AFM Measured distance always equals voltage times $Sensitivity_{high\_V}$; however the realistic distance on the Standard at small scan sizes equals to voltage times $Sensitivity_{low\_V}$. Comparing the slopes of the linear fittings reveals that $Sensitivity_{low\_V}$ is lower than $Sensitivity_{high\_V}$. This

is confirmed after recalibration using 100 nm pitch sized standard over 3.5 μm scale. The X and Y sensitivities decreased from (209.4, 295.5) nm/V to (187.8, 259.1) nm/V. Depending on the piezoelectric material and its configuration in the AFM, the nonlinear relationship between scanner error and scan size could vary and it should be carefully examined. Calibration at the same scale of the imaging feature size is highly recommended for quantitative analysis.

Table 2.1 The impact of scanner nonlinearity at different scan sizes using the manufacturer's recommended calibration protocol. The table shows the calculation of scanner errors at different scan size. Aglient 5500 AFM was calibrated using 10 μm x 10 μm calibration standard on 80 μm scale. Due to the nonlinear relationship between scanner error and scan size, the percentage error increased with decreasing scan size. As the scan size decrease from 70 μm to 2 μm, the fast scan direction (X)'s percentage error increased from 2% to 9%; the slow scan direction (Y)'s percentage error increased from 3% to 18%.

Calibration Standard	Scan Size (μm)	# of Pitches[a]	Fast Scan Direction (X)				Slow Scan Direction (Y)			
			Pitch Size (μm)[b]	Distance on Standard (μm)[c]	Distance by AFM (μm)	% Error	Pitch Size (μm)[b]	Distance on Standard (μm)[c]	Distance by AFM (μm)	% Error
100 nm	2	10	0.1014	1.014	1.109	9.37	0.1009	1.009	1.188	17.74
100 nm	3.5	20	0.1014	2.028	2.214	9.17	0.1009	2.018	2.366	17.24
100 nm	5	40	0.1014	4.056	4.386	8.14	0.1009	4.036	4.612	14.27
100 nm	7	60	0.1014	6.084	6.587	8.27	0.1009	6.054	6.925	14.39
100 nm	10	80	0.1014	8.112	8.600	6.02	0.1009	8.072	9.039	11.98
1 μm	10	8	1.006	8.048	8.689	7.96	1.01	8.080	9.259	14.59
1 μm	20	16	1.006	16.10	17.14	6.46	1.01	16.16	17.99	11.32
1 μm	35	28	1.006	28.17	29.67	5.32	1.01	28.28	30.53	7.96
10 μm	40	3	10.12	30.36	31.24	2.90	10.15	30.45	31.85	4.60
10 μm	50	4	10.12	40.48	41.70	3.01	10.15	40.60	42.79	5.39
10 μm	70	6	10.12	60.72	61.81	1.80	10.15	60.90	62.56	2.73

[a] Number of pitches included in the measurements;
[b] Pitch size measured by SEM;
[c] Distance on Standard = # of Pitches x Pitch Size;
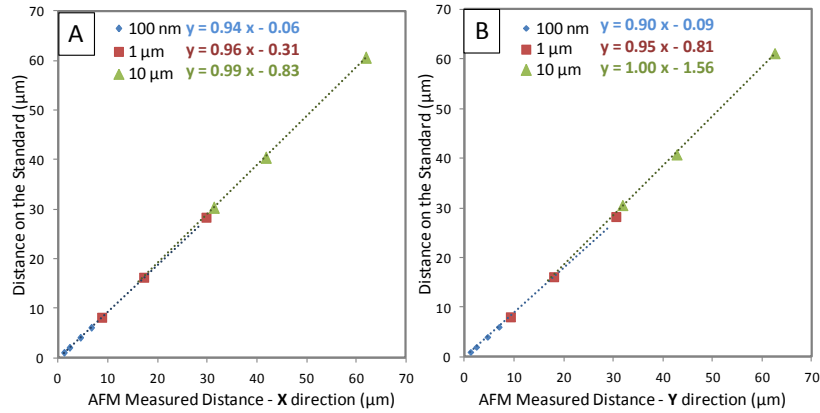
Figure 2.4 The correlation between AFM measured distance and the distance on the calibration standard (based on SEM results). Panel A and B represent the correlation on the fast scan (X) and slow scan (Y) direction respectively. Blue diamonds are measured from 2 – 10 μm scan sizes using 100 nm standard; red squares are measured from 10-35 μm scan sizes using 1 μm standard; green triangles are measured from 40-70 μm scan sizes using 10 μm standard. The equations are linear fitting of these three individual scales; the linear fitting of the blue and green dots is plotted for visual comparison.

Due to the nonlinear relationship between scan size and scanner error, calibration over the range of D-spacing measurement (3.5 µm x 3.5 µm in the current study) using a feature size comparable to the collagen D-spacing (~67 nm) is critical. AFM was calibrated using the 100 nm x 100 nm standard, and limited the scan error to 0.98 % and 0.20 % for X and Y direction at 3.5 x 3.5 µm image size. For a fibril with 67 nm D-spacing, the absolute error in the AFM measurement is less than 1 nm. Note that AFM manufacturer recommended calibration procedure utilizes a 10 µm x 10 µm calibration standard, which is 100 times larger than the collagen feature size. Non-linearity in the piezoelectric scanners introduce substantial error between these size scales. Nevertheless, this calibration process only addresses the absolute calibration (accuracy) of the system. The calibration has no bearing on the differential sensitivity between measurements (precision), and does not limit one's ability to differentiate between population distributions measured using the same AFM with the same calibration parameters.

2.2.3 D-periodic Spacing as a Distribution of Values and Statistical Comparison of the Distributions as a Function of Disease

The 2D-FFT approach was applied to Type I collagen fibrils imaged within sham-operated sheep dermis using AFM (used as a control for a previously published

experiment). The mean D-periodic spacing of the 624 measured fibrils was 62.3 nm, with a population standard deviation of 1.4 nm. Figure 2.1D shows these data plotted as a histogram with a bin size of 1.0 nm. Note that the mean D-spacing value in dermal collagen has been reported to be less than 67 nm.[40] This histogram demonstrates that normal bone contains fibrils with a distribution of D-periodic spacing values. A recent study demonstrated that this type of distribution also exists in other Type I collagen based tissues including dentin and tendon.[24] Based upon these studies, and other tissue samples measured to date,[25,27] the existence of a distribution of D-periodic spacings is a fundamental characteristic of Type I collagen. However, the currently accepted models of Type I collagen fibrillar structure completely overlook the presence of a distribution of spacing values.[15] For example, the possibility of a distribution was not discussed in a recent thorough book review of collagen structure and mechanics.[1]

The existence of a distribution of D-periodic spacings is an important observation, standing in contrast to the fixed 67 nm value put forth 50 years ago. Utilizing an OVX model in sheep which leads to estrogen depletion, an early model of osteoporosis, it was hypothesized that differences between normal skin and skin from animals with a known disease state could be detected through changes in collagen fibril morphology.[26] The mean D-periodic spacing of the Sham population was 62.3 nm, not significantly different than the 61.9 nm value in OVX samples (p = 0.249 using One Way ANOVA). When viewed as histograms (Figure 2.1D), there was an observable increase in the OVX population towards lower D-periodic spacing values. Observing qualitative population differences between the normal and diseased states was an important finding, but proving statistical significance was imperative. Population differences were further highlighted when viewing the data as Cumulative Distribution Functions (CDF, Figure 2.1E). The CDF plot from the Sham population was then compared to that of the OVX population using a Kolmogorov-Smirnov test (K-S test), chosen because it is a non-parametric comparison between distributions. This test is sensitive to changes in means as well as in the width of distributions, and does not require normally distributed data. The two-sample K-S test demonstrated a significant difference in the population distributions between Sham and OVX samples (p < 0.001). These methods were also applied to a mouse model of human type IV OI, where a known genetic mutation on collagen was

created by substituting glycine with cysteine.[27] Similar to the estrogen depletion model, no significant difference was noted in the means of D-spacing between the brittle mouse bones and wild type bones. Significant differences were present in the population distributions of fibril spacings. It was found that 55% of brittle fibrils versus 75% of wild type fibrils were within ± 1 standard deviation (66-70 nm) range, which contributed to the statistically different CDF plots.[27]

The origin of a D-spacing distribution and mechanisms of D-spacing changes that operate in diseases such as osteoporosis and OI are still unclear. Estrogen plays important roles in regulating metabolism, cell activities,[45] and collagen turn-over,[46-48] *etc*. The change in D-spacing induced by estrogen depletion is a complex system to study. In the case of point mutation in OI, inserting a bulkier residue in the molecular structure disrupts or destabilizes the triple helical conformation, through molecular kinking,[49] free energy changes,[50] weakening of intermolecular adhesion and reduction of cross-links.[51] These effects may lead to a change in D-spacing. Although the mechanisms leading to these changes found in estrogen deprived and OI tissues are still unclear, these studies provide evidence to show that collagen nanomorphology is altered, an important information that could potentially explain the compromised tissue properties, and be considered in disease diagnosis.

2.3   Concluding Remarks

This work details a systematic method to measure and analyze nanoscale characteristics of Type I collagen fibrils using the D-periodic spacing as the key metric of nanoscale morphology. The ability to accurately measure the D-periodic spacing using a 2D-FFT approach led to the discovery of a distribution of Type I collagen morphologies in four tissue types, bone, dentin, dermis and tendon. The importance of these observations was highlighted by demonstrating that statistically significant changes in population distributions could be observed in disease models of estrogen depletion and *Osteogenesis Imperfecta*. The facts that distributions were present in both normal and diseased fibril populations, and that there were significant changes in these distributions with multiple diseases, has important implications for the structural model of Type I

collagen fibrils, and possibly to the diagnosis of Type I collagen-based diseases. This type of analysis shows promise for providing important structural information regarding Type I collagen in a wide variety of collagen-related ECM diseases and processes, such as photo aging, Ehlers-Danlos Syndrome, *Osteogenesis Imperfecta*, *Osteoporosis*, wound healing, tissue engineering, and gene knockout model systems. Future work will be focused on the broader application of this method in ECM disease diagnosis and mechanistic studies. This method may find clinical uses in disease diagnosis and is already being employed for assessment of drug therapeutics.

2.4 Experimental

2.4.1 Animals

Five year-old Columbia-Ramboulliet cross sheep were anesthetized and ovariectomized (OVX) or subjected to a sham surgery (Colorado State University, ACUC # 03-010A-02).   After 2 years, the ewes were sacrificed with an intravenous overdose of a barbiturate, and skin samples from the dorsal thoracolumbar region were used as previously described.[29]

2.4.2 AFM Calibration

Calibration of the Agilent 5500 AFM large scanner (80 μm scan range) was carried out with a 100 nm x 100 nm calibration standard (NANOSENSORS, Switzerland), using contact mode and SNL-10 AFM probes (nominal tip radius 2 nm, force constant 0.25 N/m. Bruker AFM probes, CA). The scan size was set at 3.5 μm (35 x 35 pitches) with 512 x 512 pixels and a scan rate of 2 lines/sec. The absolute error of the calibration standard was verified by Scanning Electron Microscopy (SEM) imaging to be less than 1.1 % (FEI NOVA SEM, FEI Company, OR). 1 μm x 1 μm standard (Digital Instrument, CA) and 10 μm x 10 μm standard (Asylum Research, CA) were used to examine the impact of scanner non-linearity on AFM calibration at different scan sizes.

2.4.3 AFM Imaging and Analysis

Tissue samples were processed and imaged in air using a PicoPlus 5500 Atomic Force Microscope (AFM, Agilent) in tapping mode as previously described.[24,25,27] Water and air comparison was carried out using a Dimension Icon AFM (Bruker AXS, Santa Barbara, CA) in scanasyst fluid and air imaging modes. Scansyst fluid+ AFM probes (Bruker probes, nominal tip radius 2 nm, force constant 0.7 N/m) was used in both water and air imaging, in order to reduce differences caused by different tip convolutions. Skin samples were imaged in DI water and then dried by wicking away the water followed by exposure to a gentle stream of air for 30 minutes before re-imaging the same region in air. Following image capture, a rectangular region of interest (ROI) was chosen along straight segments of individual fibrils (Figure 2.1A). The selected regions spanned consistent topographical features (i.e. from gap region to gap region and though the middle of a given fibril). For each evaluated fibril, a two dimensional Fast Fourier Transform (2D-FFT) was performed in SPIP and the 2D power spectrum was analyzed to determine the value of the D-periodic spacing for that fibril.

2.4.4 Statistical Analysis

To investigate differences in fibril morphology due to estrogen deficiency, D-periodic spacing values measured from an individual sample were averaged, yielding a single mean value for that sample, and then statistically compared using One Way ANOVA. Histograms were computed using a 1.0 nm bin size. To examine differences in the distribution of fibril morphologies between sham and OVX sheep, the Cumulative Distribution Function (CDF) of each group was computed. The CDF shows what fraction of a given sample is contained up to a particular value, easily demonstrating differences between distributions in both mean and standard deviation. To test for statistical significance between distributions, two-sample Kolmogorov-Smirnov (K-S) tests were then applied to the data sets.

2.5 References

(1)   *Collagen: Structure and Mechanics*; Fratzl, P., Ed.; Springer: New York, 2008.

(2)   Kadler, K. E.; Holmes, D. F.; Trotter, J. A.; Chapman, J. A. *Biochemical Journal* **1996**, *316*, 1.

(3)   Kadler, K. E.; Baldock, C.; Bella, J.; Boot-Hanford, R. P. *J. Cell Sci.* **2007**, *120*, 1955.

(4)   Canty, E. G.; Kadler, K. E. *J. Cell Sci.* **2005**, *118*, 1341.

(5)   Bear, R. S. *J. Am. Chem. Soc.* **1942**, *64*, 727.

(6)   Schmitt, F. O.; Hall, C. E.; Jakus, M. A. *J. Cell. Comp. Phys.* **1942**, *20*, 11.

(7)   Hodge, A. J.; Petruska, J. A. In *Aspects of Protein Structure*; Ramachandran, G. N., Ed.; Academic Press: New York, 1963, p 289.

(8)   Bigi, A.; Koch, M. H. J.; Panzavolta, S.; Roveri, N.; Rubini, K. *Connect. Tissue Res.* **2000**, *41*, 37.

(9)   Fraser, R. D. B.; MacRae, T. P.; Miller, A.; Suzuki, E. *J. Mol. Biol.* **1983**, *167*, 497.

(10)   Eikenberry, E. F.; Brodsky, B.; Parry, D. A. D. *Int. J.Biol. Macromol.* **1982**, *4*, 322.

(11)   Brodsky, B.; Eikenberry, E. F. In *Methods Enzymol.*; Leon W. Cunningham, D. W. F., Ed.; Academic Press: 1982; Vol. Volume 82, p 127.

(12)   Chapman, J. A.; Tzaphlidou, M.; Meek, K. M.; Kadler, K. E. *Electron Microscopy Reviews* **1990**, *3*, 143.

(13)   Lin, A. C.; Goh, M. C. *Proteins-Structure Function and Genetics* **2002**, *49*, 378.

(14)   Arsenault, A. L. *J. Electron Microsc. Tech.* **1991**, *18*, 262.

(15)   Orgel, J.; Irving, T. C.; Miller, A.; Wess, T. J. *Proc. Natl. Acad. Sci. U. S. A.* **2006**, *103*, 9001.

(16)   Hulmes, D. J. S.; Wess, T. J.; Prockop, D. J.; Fratzl, P. *Biophys. J.* **1995**, *68*, 1661.

(17)   Hulmes, D. J. S.; Miller, A. *Nature* **1979**, *282*, 878.

(18)   Fraser, R. D. B.; MacRae, T. P.; Miller, A. *J. Mol. Biol.* **1987**, *193*, 115.

(19)   Orgel, J. P. R. O.; Miller, A.; Irving, T. C.; Fischetti, R. F.; Hammersley, A. P.; Wess, T. J. *Structure* **2001**, *9*, 1061.

(20)   Trus, B. L.; Piez, K. A. *Nature* **1980**, *286*, 300.

(21)   Piez, K. A.; Trus, B. L. *Biosci. Rep.* **1981**, *1*, 801.

(22)   Orgel, J. P. R. O.; Irving, T. C.; Miller, A.; Wess, T. J. *Proc. Natl. Acad. Sci. U. S. A.* **2006**, *103*, 9001.

(23)   Gautieri, A.; Vesentini, S.; Redaelli, A.; Buehler, M. J. *Nano Lett.* **2011**, *11*, 757.

(24)   Wallace, J. M.; Chen, Q.; Fang, M.; Erickson, B.; Orr, B. G.; Banaszak Holl, M. M. *Langmuir* **2010**, *26*, 7349.

(25)   Wallace, J. M.; Erickson, B.; Les, C. M.; Orr, B. G.; Banaszak Holl, M. M. *Bone* **2010**, *46*, 1349.

(26)   Fang, M.; Liroff, K. G.; Turner, A. S.; Les, C. M.; Orr, B. G.; Holl, M. M. B. *J. Invest. Dermatol.* **2012**, *132*, 1791.

(27)   Wallace, J. M.; Orr, B. G.; Marini, J. C.; Banaszak Holl, M. M. *J. Struct. Biology* **2011**, *173*, 146.

(28)   Fratzl, P.; Fratzlzelman, N.; Klaushofer, K. *Biophys. J.* **1993**, *64*, 260.

(29)   Fang, M.; Liroff, G. K.; Turner, A. S.; Les, C. M.; Orr, B. G.; Banaszak Holl, M. M. *J. Invest. Dermatol.* **2012**.

(30)   Habelitz, S.; Balooch, M.; Marshall, S. J.; Balooch, G.; Marshall, G. W. *Journal of Structural Biology* **2002**, *138*, 227.

(31)   Hassenkam, T.; Fantner, G. E.; Cutroni, J. A.; Weaver, J. C.; Morse, D. E.; Hansma, P. K. *Bone* **2004**, *35*, 4.

(32)   Baranauskas, V.; Garavello-Freitas, I.; Jingguo, Z.; Cruz-Hofling, M. A. *Journal of Vacuum Science & Technology A* **2001**, *19*, 1042.

(33)   Kindt, J. H.; Thurner, P. J.; Lauer, M. E.; Bosma, B. L.; Schitter, G.; Fantner, G. E.; Izumi, M.; Weaver, J. C.; Morse, D. E.; Hansma, P. K. *Nanotechnology* **2007**, *18*.

(34)   Cremer, C.; Kaufman, R.; Gunkel, M.; Pres, S.; Weiland, Y.; Muller, P.; Ruckelshausen, t.; Lemmer, P.; Geiger, F.; Degenhard, S.; Wege, C.; Lemmerman, N. A. W.; Holtappels, R.; Strickfaden, H.; Hausmann, M. *Biotechnology Journal* **2011**, *6*, 1037.

(35)   Wallace, J. M. *Bone* **2012**, *50*, 420.

(36)   Buehler, M. J.; Keten, S.; Ackbarow, T. *Progress in Materials Science* **2008**, *53*, 1101.

(37)   Mogilner, I. G.; Ruderman, G.; Grigera, J. R. *J. Mol. Graphics Model.* **2002**, *21*, 209.

(38)   Price, R. I.; Lees, S.; Kirschner, D. A. *Int. J.Biol. Macromol.* **1997**, *20*, 23.

(39)   Habelitz, S.; Balooch, M.; Marshall, S. J.; Balooch, G.; Marshall Jr, G. W. *J. Struct. Biol.* **2002**, *138*, 227.

(40)   Brodsky, B.; Eikenberry, E. F.; Cassidy, K. *Biochimica et Biophysica Acta (BBA) - Protein Structure* **1980**, *621*, 162.

(41)   Sasaki, N.; Shukunami, N.; Matsushima, N.; Izumi, Y. *J. Biomech.* **1999**, *32*, 285.

(42)   Puxkandl, R.; Zizak, I.; Paris, O.; Keckes, J.; Tesch, W.; Bernstorff, S.; Purslow, P.; Fratzl, P. *Philosophical Transactions of the Royal Society B: Biological Sciences* **2002**, *357*, 191.

(43)   Gupta, H. S.; Zioupos, P. *Med. Eng. Phys.* **2008**, *30*, 1209.

(44)   Drits, V. A.; Eberl, D. D.; Srodon, J. *Clays and Clay Minerals* **1998**, *46*, 38.

(45)   Haczynski, J.; Tarkowski, R.; Jarzabek, K.; Slomczynska, M.; Wolczynski, S.; Magoffin, D. A.; Jakowicki, J. A.; Jakimiuk, A. J. *Int. J. Mol. Med.* **2002**, *10*, 149.

(46)   Dimitrios J, H.; Ioannis I, A. *Ann. N. Y. Acad. Sci.* **2006**, *1092*, 385.

(47)   Brincat, M. P.; Baron, Y. M.; Galea, R. *Climacteric* **2005**, *8*, 110.

(48)   Brincat, M.; Moniz, C. J.; Studd, J. W. W. *Br. J. Obstet. Gynaecol.* **1985**, *92*, 256.

(49)   Chang, S.-W.; Shefelbine, Sandra J.; Buehler, Markus J. *Biophys. J.* **2012**, *102*, 640.

(50)   Lee, K. H.; Kuczera, K.; Banaszak Holl, M. M. *Biopolymers* **2011**, *95*, 182.

(51)   Gautieri, A.; Uzel, S.; Vesentini, S.; Redaelli, A.; Buehler, M. J. *Biophys. J.* **2009**, *97*, 857.

Chapter 3   Estrogen Depletion Results in Nanoscale Morphology Changes in Dermal Collagen

3.1   Introduction

The dermis layer of skin is primarily composed of Type I collagen fibers (85-90%), elastic fibers and glycosaminoproteoglycans (GAGs).[1] Collagen fibrils account for skin's tensile strength and resilience whereas the elastic fibers contribute to the elasticity and extensibility of skin.[2] Unlike collagen in bone, which is frequently remodeled to maintain its mechanical strength, skin collagen has a remarkably long half life under normal conditions,[3] and thus suffers long term degradation due to skin ageing. The severity of skin ageing differs by the anatomical locations: sun protected skin suffers mainly intrinsic ageing effects associated with time such as fine wrinkles and reduced elasticity whereas sun exposed skin suffers both intrinsic and extrinsic ageing (exposure to external influences such as UV radiation), where the severity and rate of the pathological changes including deep wrinkles, pigmentation and melanoma formation are exacerbated.[4-7] The process of skin aging leads to decreased skin collagen content, moisture and elasticity;[8,9] A recent study has shown that collagen fibrils are fragmented in aged human skin. These changes in the extracellular environment affect fibroblast attachment and production of matrix metalloproteinases (MMPs), which in turn accelerates extracellular matrix (ECM) degradation.[10] This work underscores the importance of characterizing collagen in order to better understand mechanisms of effects of aging upon skin.

Estrogen has many beneficial and protective effects on skin physiology and functions including maintenance of hydration and skin thickness, wound healing, and reduction of skin cancer risk.[11] On the molecular level, estrogen exerts its effect by

interacting with surface or intracellular estrogen receptors. Intracellular estrogen receptors ER-α and ER-β have been identified in dermal fibroblasts.[12] The cellular responses triggered by the level of estrogen involve gene transcription/expression, as well as cytoplasmic signaling pathways. On the macroscopic level, aging and especially the onset of menopause causes a series of deteriorations in skin tissue physiology as a consequence of compositional and structural alterations in the ECM proteins. Postmenopausal women suffer from loss of dermal collagen content at an average rate of 2 % per postmenopausal year over a period of 15 years.[8,13-15] Decreased amounts of elastic fibers and GAGs in postmenopausal years lead to compromised skin elasticity and less binding with water respectively.[9,16,17] The thinning of the dermal layer and loss of water gradually results in wrinkle formation. On the microscopic level, little is known about the ultrastructural changes of dermal proteins that accompany aging and menopause. In this study, the effect of estrogen depletion on the nanoscale morphology of ovine dermal collagen fibrils was investigated. The metric of fibril D-spacing was employed because it captures a number of structural features including the molecular structure of the collagen, the three dimensional fibril formation, and the associated post-translational modifications.

Studies indicating the D-spacing in collagen exists as a distribution of values ranging from about 64 to 73 nm were recently reported for murine bone, dentin, and tendon tissue.[18] The importance of using a technique that measures the fibril D-spacing on a fibril by fibril basis, as opposed to X-ray or optical methods which average over micron to millimeter scales when obtaining D-spacing data, was highlighted by studies examining the effect of genetic changes, *Osteogenesis Imperfecta*, or estrogen depletion upon the D-spacing distribution in bone tissue.[19,20] In both cases, the average D-spacing values did not change significantly but the distributions of D-spacings were significantly different.

Long term ovariectomy in ovine leads to compromised compact bone viscoelastic properties, which are similar with the conditions in postmenopausal women.[21] Mineralization, architecture and remodeling parameters of OVX ovine bones have been characterized, and intriguingly only poor correlation between viscoelastic mechanical properties and these parameters were found.[22] Additional quality factors that come from

non-mineral components of bone are speculated to play a crucial role in decreasing bone viscoelastic properties. Similar biochemical and biomechanical effects have been noted between estrogen deprived skin and bone.[23-25] Characterizing the fibrillar collagen D-spacing will help better understanding the mechanisms of mechanical failure in ovariectomized tissue. D-spacing has been demonstrated as an effective evaluation of fibril strain in bone and tendon previously. Mechanical stretching on the tissue level can lead to increased fibril level strain, therefore increased D-spacings.[26,27] Atomic Force Microscopy (AFM) imaging of the ultrastructure of type I collagen provides a means to probe the integrity of the matrix protein and its association with macroscopic pathologies. Previous study reported a dramatic difference in the D-spacing population distribution between sham control and OVX ovine cortical bone, suggesting long term estrogen deprivation leads to a decrease in fibril D-spacing. [19]

In this study, the D-spacing distribution in ovine skin was quantified and the effect of estrogen depletion upon the distribution was examined. It is shown that collagen in skin also exhibits a distribution of D-spacing values, as opposed to the singular value of ~67 nm for tendon and bone or 65 nm for skin, typically discussed in textbooks and reviews, and that this distribution changes upon estrogen depletion. This study demonstrates that the distribution of D-spacings is independent of degree of tissue mineralization. It is particularly interesting to note that estrogen depletion causes similar changes in the nanoscale morphology of fibrils in both skin and bone.

3.2   Results and Discussion

The combination of cryostat sectioning and AFM imaging has been recently highlighted by Graham et al. as an advantageous tool for morphological studies of collagen matrix protein structures in soft tissues.[28]   Although histological data reveal the orientation and organization of collagen fibril bundles in dermis, the resolution is limited in resolving fibril organizations within a bundle. AFM imaging can overcome this issue and representative images of fibril bundles from ovine dermis are illustrated in Figure 3.1. Qualitatively, on the 50 micron scale and above, the fibril bundles were randomly oriented in a wavy pattern; within a fibril bundle, on the order of 10 micron scale,

collagen fibrils were bundled in a parallel longitudinal direction and individual fibrils crossing the bundle domains were frequently observed (see the arrow heads in Figure 3.1b and Figure *3.1*e). The function of these crossing fibrils is unclear.
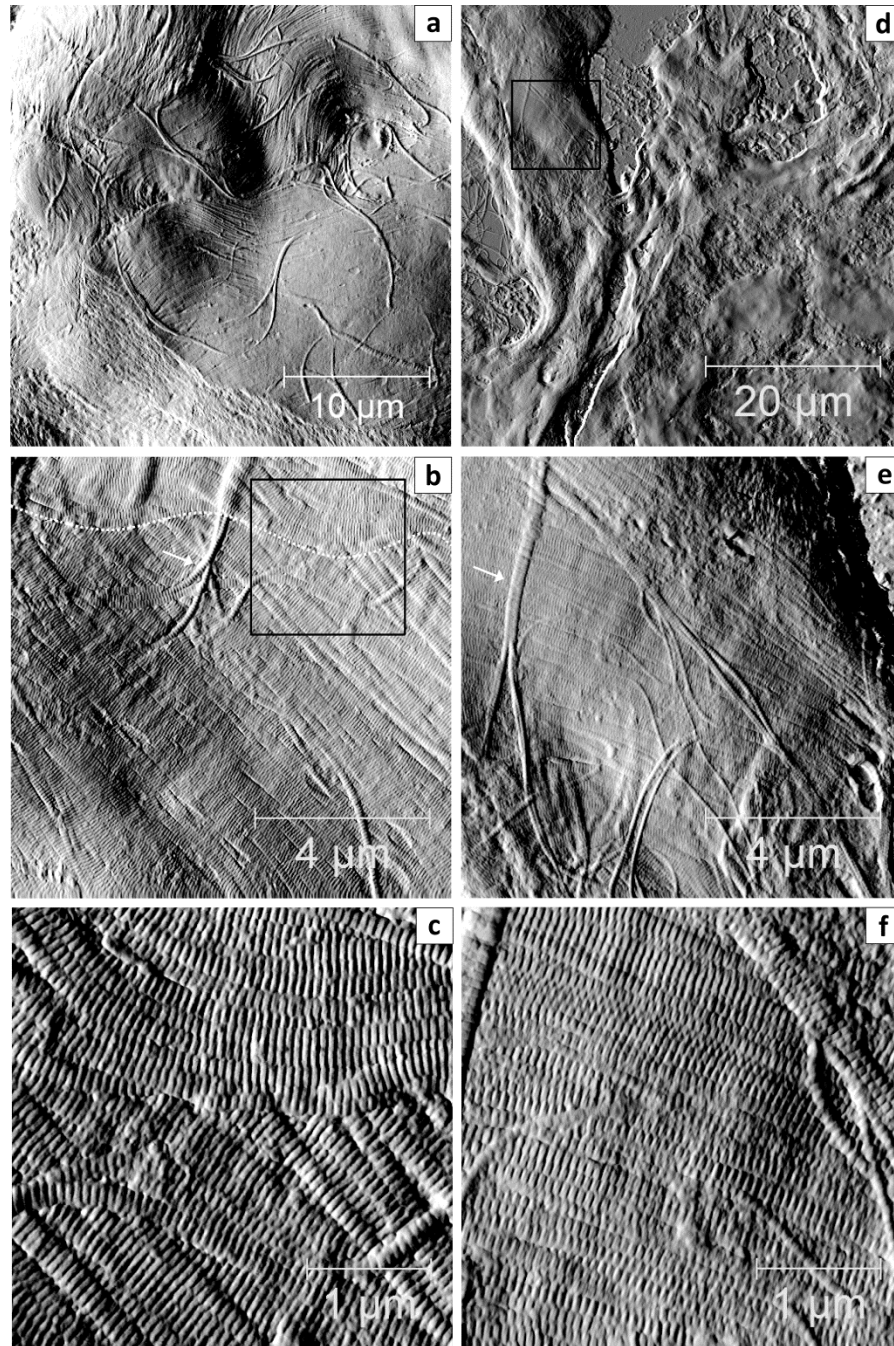
Figure 3.1 AFM deflection images of ovine dermis contain domains of collagen fibril bundles. (a-c) representative images from a sham dermis sample; (d-f) are images from an OVX dermis sample. Panel a captures potentially two fibril bundles (the rough area at the bottom of the scan is coursed by microtome sectioning). Panel b shows one fibril bundle on top of another (The boundary is marked by the white dashed line), note that a

few fibrils (white arrow) that are underneath one bundle are on the surface of another bundle. Panel c is the region marked by the black box in panel b. Panels e and f capture the only region with collagen fibrils found in the 50 micron area of OVX dermis (panel d).

Quantitatively, the characteristic collagen fibril D-spacing was measured and employed as the main morphological metric. For each biopsy, at least 60 fibrils from a minimum of four and an average of five randomly selected 50 μm locations were analyzed. The difference in the number of fibrils obtained for each biopsy is due to variation in collagen abundance at the location of AFM tip engagement. Measurements from each skin biopsy were pooled together to yield the average D-spacing (Figure 3.2). The mean values for five sham ovine were 62.0, 61.6, 62.7, 63.1, and 62.6 nm. The mean values for the OVX ovine were 61.8, 61.3, 60.7 and 62.5 nm. The means from sham and OVX are not significantly different ($p = 0.249$) when compared with the two tailed student T-test.
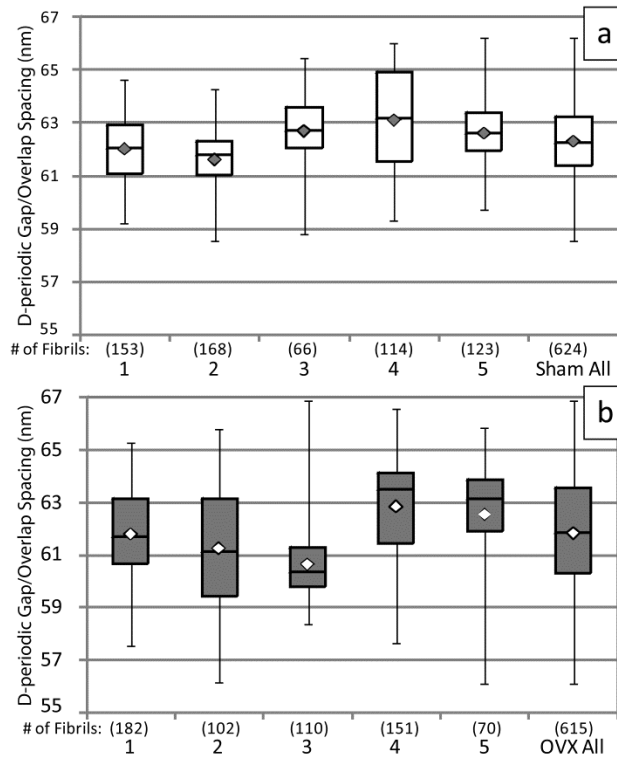
Figure 3.2 Box plot representation of D-Periodic Gap/Overlap spacings from sham and OVX ovine dermis. D-periodic gap/overlap spacing from (a) individual sham (n = 5) and (b) OVX (n = 5) ovine dermis. The box-plot shows the interquartile (middle 50% of data), the horizontal line inside the box is the mean, the diamond is the median, and the whiskers provided the minimum and maximum observation. The numbers in parentheses

are numbers of fibrils measured in each specimen. Two tailed student T-tests between sham and OVX group suggests no differences between the means (p = 0.249).

Examining the population histogram (Figure 3.3a) revealed that the sham D-spacing distribution spans between 59 and 66 nm whereas the OVX population spans between 56 and 67 nm. The major difference between these populations arises from the percentage of fibrils with D-spacings from 56 to 59nm – 14.6% in OVX group and 1.6% in sham group. Note that these changes in distribution do not have a significant impact on the mean D-spacing values which are 61.9 nm for the OVX and 62.3 nm for the sham specimens. The distributions are not strictly Gaussian and the OVX distribution in particular appears bimodal, making the use of the mean value statistically incorrect. It was provided here so that a rough comparison to previous literature can be made; however, to correctly analyze the data a non-parametric method must be employed.
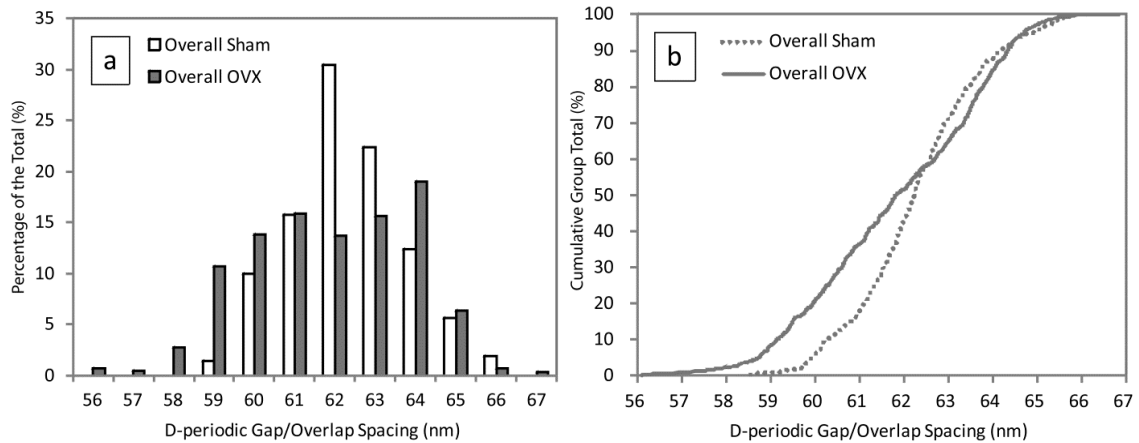
Figure 3.3 Histogram and cumulative distribution function of D-Periodic spacings from sham and OVX ovine skin (each contains five animals). (a) Histogram representation of D-periodic gap/overlap spacings from sham and OVX ovine skin (1 nm bin size). (b) The Cumulative Distribution Function calculated from each group. A Kolmogrov-Smirnov test performed the data distributions indicates significant difference (p < 0.001).

In order to determine the statistical significance of these distributions, a cumulative density function (CDF) was plotted and evaluated using the nonparametric Kolmogrov-Smirnov test (Figure 3.3b). The CDF highlights the cumulative difference in the 56-62 nm region and the distributions were found to be significantly different (p<0.001).

Depending on species and tissue type, mature collagen fibril diameter varies dramatically. In developed ovine dermis, collagen fibril diameter is about 100 nm.[29] To evaluate the effect of estrogen depletion, fibril diameters were measured by averaging from fibril bundle width. The results indicated that OVX ovine dermis have similar fibril diameters with sham ovine. In the case of sham ovine, fibril diameter ranges from 80 nm to 180 nm, with an average of 130 ± 30 nm. OVX ranges from 80 nm to 160 nm and has an average of 120 ± 20 nm. In collective tissues, fibril diameters are typically assessed in the cross-section plane, diameter measurements in the axial plane are limited in accuracy because fibril overlapping is inevitable in tissue sections. Averaging from parallel bundles remedies this problem to a certain degree and ensures ± 10 nm accuracy (for more details see Appendix A.1).
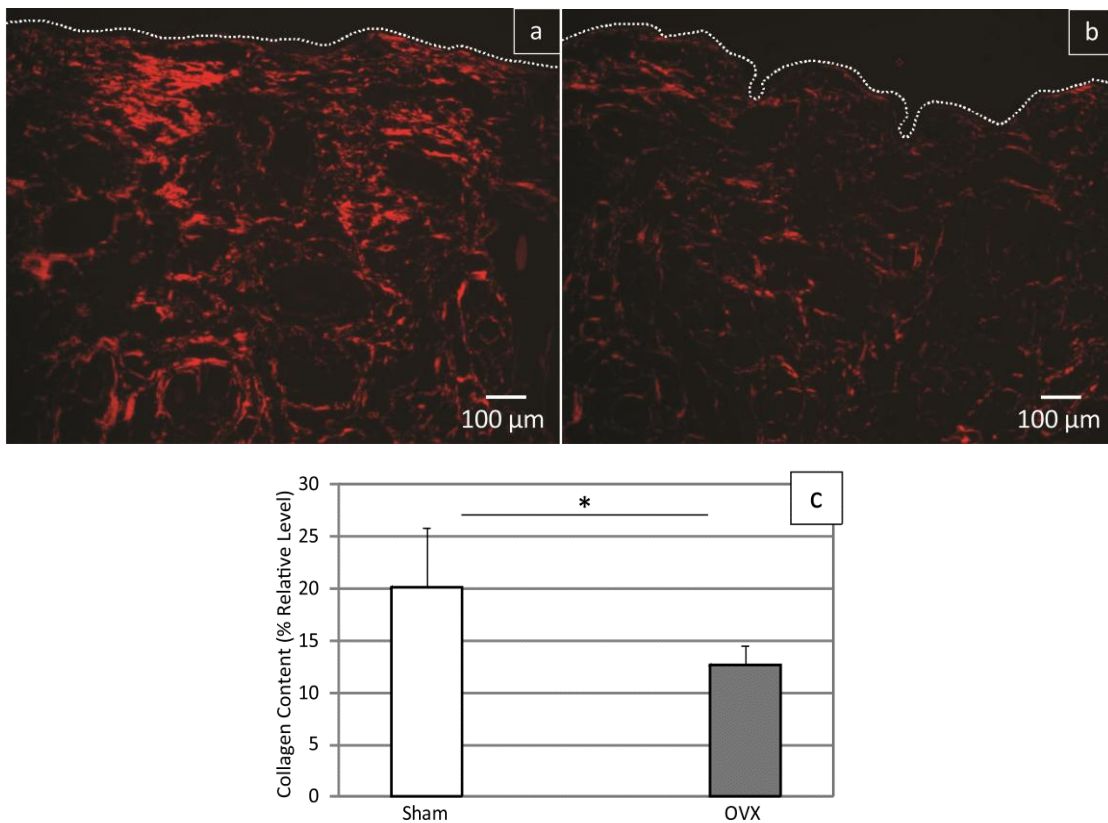
Figure 3.4 Sirius red staining reveals the abundance of fibrillar collagen content in sham and OVX dermis. (a,b) Polarized light microscopic images of sham and OVX dermis, respectively. Original magnification x 10. Dashed lines represent the epidermis. (c) collagen abundance measured from the staining intensity (*p <0.05).

In order to explore the effect of estrogen on collagen content in ovine dermal skin, Sirius red staining followed by polarized light microscopic imaging was performed. Because the birefringence is highly specific to fibrillar collagen due to its uniaxial anisotropy,[30,31] the staining serves as a good indication of collagen fibril abundance. Figure 3.4 indicates higher abundance of fibrillar collagen in sham dermis ($p<0.05$) and a qualitatively thicker fibril bundle width than in OVX dermis.

3.3 Discussion

AFM is a non-destructive alternative for imaging biological tissues under aqueous conditions; however, imaging bulk skin tissue using AFM can be challenging because collagen fibril bundles are surrounded by a sol-gel of hydrophilic GAGs and subcutaneous adipose fat. Recently Graham and coworkers reported a combined tissue cryo-sectioning and AFM imaging method that provides excellent resolution of the ECM components in skin, cartilage, aorta, and lung.[28] The sample preparation greatly facilitates AFM imaging and characterization of biological tissues while in the meantime avoids fixation, chemical staining, and high vacuum.

In order to evaluate the nanomorphology of collagen fibrils present in dermis, the D-spacing was selected as a reliable quantitative marker. It has previously been demonstrated that the application of two dimensional Fast Fourier Transforms (2D-FFT) allows an accurate evaluation of this prominent fibril feature. The D-spacing arises from a parallel staggered packing of collagen monomers which lead to alternating gap and overlap zones along the longitudinal axis of a fibril, as illustrated by the two-dimensional Hodge-Petruska model.[32] Recent X-ray crystallographic work by Orgel *et al.* provides additional three-dimensional insight which supports a supertwist microfibril model.[33] These structural models indicate that quantitative analysis of the D-spacing should be sensitive to changes in the collagen molecule triple helix, the molecular packing, and intermolecular cross-linking effects. For example, the single amino acid substitution of a cysteine residue for glycine-349 results in nanoscale morphology changes observed in the collagen fibril D-spacing distribution. Moreover, the free energy changes induced by amino substitution correlate with clinical severity of *Osteogenis Imperfecta*.[34]

36

Quantitative analysis of ovine dermis collagen D-spacings indicates a distribution of values is present ranging from 56 to 67 nm with a mean value of 62nm. Although AFM has an excellent ability to differentiate differences in the D-spacing within tissue, the absolute value is limited by the calibration process. The average value of the distribution of 62 nm is close with previous literature values obtained by X-ray scattering. Purslow reported 67 nm D-spacing in rat skin;[35] others reported lower values of about 65 nm for skin.[36-38] These techniques have spot sizes of microns and thus average over too large an area of the skin structure for observation of a D-spacing distribution. The observation of this distribution in dermal collagen provides further evidence that a distribution of values is an intrinsic aspect of collagen fibrillar structure. A similar distribution has previously been observed for another non-mineralized Type 1 collagen tissue, murine tail tendon, as well as for the mineralized collagen tissues murine dentin and bone and ovine bone.[18-20] The observation of the distribution is possible because of the fibril by fibril analysis using the AFM data.

The influence of bulk tissue stress on collagen fibril D-spacings has been subject of numerous studies. Gupta *et al.* demonstrated a connection between fibril stain and D-spacing.[27] They noted a 0.3 nm increase in D-spacing in bone as measured by small angle X-ray scattering (SAXS) under mechanical stretching. For bone, fibril strain accounts for only a fraction of the total tissue strain, suggesting that interfibrillar sliding and shear of the proteoglycan-rich matrix takes up the remainder of the tissue strain. With regards to tendon, Puxkandl *et al.* demonstrated up to a 1 nm change when a 3% macroscopic strain was employed and a 0.2 nm change at a 1% strain.[39] D-spacing changes varied between 0.2 and 2 nm at tendon fracture. The most general conclusion from the comparison of this data to the distribution of D-spacings in this study, which has a width of 12 nm, is that materials strain effects on D-spacing are not large enough to explain the D-spacing distribution observed in either mineralized or non-mineralized biological tissues. The strain effects tend to be about an order of magnitude too small.

One limitation of the current study is that dermal samples were from dorsal skin exposed to ultraviolet (UV) radiation as opposed to skin protected from extrinsic UV radiation. Ovine dermis is considerably thicker than human dermis;[40] in addition a layer of wool equivalent of SPF 30 protection also makes it difficult to assess how much

photoageing is induced in these dermal tissue samples as compared with human samples.[41,42] However given that the sham and OVX ovine were provided with the same sheltering condition, the effects observed in this study signify change in the hormonal level rather than differential UV radiation exposure.

Estrogen is known to play important roles in mediating connective tissue physiology and function. Estrogen depletion associated with menopause causes detrimental effects on connective tissues. In skin, estrogen depletion is associated with declining dermal collagen content, skin thickness, water-holding capacity, and skin elasticity. In terms of mechanical properties, a steep increase in skin extensibility was noted in women during perimenopause [24] and ovariectomized rats exhibit an increased Young's Modulus in the skin.[25] Reduced estrogen level also impairs the rate and quality of wound healing: in postmenopausal women and in ovariectomized female rodents, a marked delay in wound healing was reported.[43,44] Hormone replacement therapy was found to partially reverse these effects and topical application of estrogen on wounded skin accelerated wound healing.[45] In addition, Pierard and coworkers noted a positive correlation between bone mineral density and skin viscoelasticity in women.[23]

Collagen ultrastructure in ovine bone demonstrated significant change with estrogen depletion, 28 % of fibrils in OVX ovine have D-spacings lower than 64 nm, while sham-operated ovine contained 7% of such fibrils with low D-spacings.[19] The results presented here show that similar changes occur in dermal collagen nanomorphology upon estrogen depletion. Although the percentage of low D-spacing fibrils (less than 59 nm) is lower in dermis, 14.6% in OVX group and 1.6% in sham group, the result is persistent in all five OVX animals. Bone is a mineralized connective tissue while dermis is only constituted of macromolecular proteins. Thus, the results indicate the changes in collagen nanomorphology results from changes in the protein structure, most likely post-translational modifications, and/or the structural interactions with other tissue proteins such as decorin,[46] and is not a mineralization related structural change.

Fibril diameter has been employed previously as a key measure of ultrastructural change. A number of diseases and tissue malfunctions are associated with changes in collagen fibril diameter. Decorin and lumican knockout rats and type V collagen

38

deficient mice showed one-fold increase in fibril diameters.[47,48] Ovarectomy has been shown to decrease expression level of proteoglycans including decorin[46] and lumican.[49] In this study, average collagen fibril diameter in sham is about 130 ± 30 nm, and 120 ± 20 nm in OVX, the difference is less than 10 % and considered negligible given the limited accuracy in the analysis. Thus, estrogen depletion exerts an anisotropic effect on skin collagen's ultrastructure. It is unclear whether decorin and lumican deficiency are associated to collagen fibril D-spacing changes, this will be the subject of future studies.

3.4 Conclusions

In conclusion, estrogen depletion causes a change in the nanoscale morphology of dermal collagen, quantitatively demonstrated by change in the D-spacing metric. The morphology changes are similar to those previously observed for the changes in bone collagen suggesting that estrogen depletion acts upon a structural aspect of the collagen molecule and/or associated proteins and is intrinsic to the fibril formation process.

3.5 Experimental

3.5.1 Animals

Six-year-old Columbia-Ramboulliet cross ovine were anesthetized and ovariectomized (OVX, n = 5), the control group was subjected to a sham surgery (sham, n = 5) [Colorado State University, ACUC #03-010A-02] as part of a larger study. Two years after the surgery, the animals were sacrificed with an intravenous overdose of a barbiturate, and skin specimens were procured on the dorsal thoracolumbar region centered at the midline, a region that is subject to both intrinsic and extrinsic ageing. Specimens were wrapped in saline-soaked towels, placed in a plastic zip lock bag, and frozen at -20 °C.

3.5.2 Cryostat Sectioning

First, 1 cm x 1 cm skin specimens were cut with subcutaneous fat layer removed using a scalpel blade. Samples were then embedded in Tissue-Tek optimal cutting temperature (OCT) solution (Sakura Finetek Inc., Torrance, CA, USA) and frozen at -20

℃. 10 um thick thin-sections of skin were obtained using Microm HM550 Cryostat (Thermo Scientific Inc., Walldorf, Germany) and transferred onto glass slides. The dermal sections were rinsed with ultrapure water for 5 minutes and kept at -20 ℃ prior to the AFM study on the next day. The combined cryo-section and AFM imaging was described in a recent report by Graham and others.[28]

3.5.3 AFM Imaging and Analysis

The AFM imaging on OVX and sham dermal sections was carried out in air using a PicoPlus 5500 AFM (Agilent), in contact mode with SNL-10 AFM probes (Bruker AFM probes, nominal tip radius 2 nm, force constant 0.25 N/m). The set-point and gains were optimized in each scan to maintain a minimum level of tip-sample contact and no lateral dragging were observed in the images. Line scan rates were set at 2 Hz or lower at 512 lines per frame. Image analysis and measurements were performed using SPIP software (V5.0.8, Image Metrology; Horsholm, Denmark). Collagen fibril D-spacings were measured using 2D fast Fourier Transform (FFT) toolkit of SPIP software, detailed description and validation can be found in previous studies.[19] In short, a straight fibril with at least nine D-bands was selected and marked by a rectangular box as the region of interest (ROI), the 2D FFT transformation is carried out on the ROI, the periodic information (i.e. D-spacing) was obtained from the FFT image. This method provides measurements with an uncertainty of 0.8 nm, based on that the bin size in the population histogram was set to 1 nm.

3.5.4 Statistical Analysis of AFM Data

Statistical analyses utilized PASW (Version 18, SPSS Inc.). A p value of less than 0.05 was considered significant for all analyses. The mean D-spacing values for all sham ovine (n = 5) and OVX ovine (n = 5) were compared using two-tailed student T-test. In order to examine differences in the population distribution of fibril nanomorphology between sham and OVX groups, the Cumulative Distribution Function (CDF) of each group was calculated and Kolmogorov-Smirnov (KS) test was used to test for statistical significance between distributions. This test is sensitive to changes in the mean and standard deviation of a distribution.

3.5.5 Picrosirius Red Staining and Image Capture

7 μm thick tissue sections were thawed for 15 minutes and fixed in 2% paraformaldehyde for 20 minutes. The slides were then incubated in 0.1% Sirius Red in saturated picric acid for 65 minutes at room temperature. After washing in water, they were placed in 1% Acetic Acid for 30 minutes. The sections were then dehydrated through ethanol and xylene and mounted in Permount medium (Fisher Scientific, USA). To visualize the birefringent collagen, a polarized light microscopy (Zeiss Axioskop 2) with a SPOT 2e CCD camera was used to capture the images. Exposure time for red color was 0.1 second. All slides were photographed on the same day. The relative collagen content was calculated based on the staining intensity (normalized by the tissue area), and student t-test was used to compare them statistically.

3.6 References

(1)   Castelo-Branco, C.; Duran, M.; Gonzalez-Merlo, J. *Obstet. Gynecol. Surv.* **1993**, *48*, 277.

(2)   Goldsmith, L. A. *Physiology, biochemistry, and molecular biology of the skin*; Oxford University Press: New York, 1991.

(3)   Verzijl, N.; DeGroot, J.; Thorpe, S. R.; Bank, R. A.; Shaw, J. N.; Lyons, T. J.; Bijlsma, J. W. J.; Lafeber, F. P. J. G.; Baynes, J. W.; TeKoppele, J. M. *J. Biol. Chem.* **2000**, *275*, 39027.

(4)   Naylor, E. C.; Watson, R. E. B.; Sherratt, M. J. *Maturitas* **2011**, *69*, 249.

(5)   Bolognia, J. L. *The American Journal of Medicine* **1995**, *98*, S99.

(6)   El-Domyati, M.; Attia, S.; Saleh, F.; Brown, D.; Birk, D. E.; Gasparro, F.; Ahmad, H.; Uitto, J. *Exp. Dermatol.* **2002**, *11*, 398.

(7)   Gilchrest, B. A. *Br. J. Dermatol.* **1996**, *135*, 867.

(8)   Brincat, M.; Kabalan, S.; Studd, J. W. W.; Moniz, C. F.; De Trafford, J.; Montgomery, J. *Obstet. Gynecol.* **1987**, *70*, 840.

(9)   Uitto, J. *Dermatol. Clin.* **1986**, *4*, 433.

(10)   Fisher, G. J.; Quan, T.; Purohit, T.; Shao, Y.; Moon, K. C.; He, T.; Varani, J.; Kang, S.; Voorhees, J. J. *Am. J. Pathol.* **2009**, *174*, 101.

(11)   Brincat, M. P. *Maturitas* **2000**, *35*, 107.

(12)   Haczynski, J.; Tarkowski, R.; Jarzabek, K.; Slomczynska, M.; Wolczynski, S.; Magoffin, D. A.; Jakowicki, J. A.; Jakimiuk, A. J. *Int. J. Mol. Med.* **2002**, *10*, 149.

(13)   Brincat, M.; Moniz, C. F.; Studd, J. W. W. *Br. Med. J.* **1983**, *287*, 1337.

(14)   Brincat, M.; Moniz, C. J.; Studd, J. W. W. *Br. J. Obstet. Gynaecol.* **1985**, *92*, 256.

(15)   Brincat, M. P.; Baron, Y. M.; Galea, R. *Climacteric* **2005**, *8*, 110.

(16)   Sherratt, M. *AGE* **2009**, *31*, 305.

(17)   Waller, J. M.; Maibach, H. I. *Skin Res. Technol.* **2006**, *12*, 145.

(18)   Wallace, J. M.; Chen, Q.; Fang, M.; Erickson, B.; Orr, B. G.; Banaszak Holl, M. M. *Langmuir* **2010**, *26*, 7349.

(19)   Wallace, J. M.; Erickson, B.; Les, C. M.; Orr, B. G.; Banaszak Holl, M. M. *Bone* **2010**, *46*, 1349.

(20)   Wallace, J. M.; Orr, B. G.; Marini, J. C.; Banaszak Holl, M. M. *J. Struct. Biology* **2011**, *173*, 146.

(21)   Les, C. M.; Vance, J. L.; Christopherson, G. T.; Turner, A. S.; Divine, G. W.; Fyhrie, D. P. *J. Orth. Res.* **2005**, *23*, 869.

(22)   Les, C. M.; Spence, C. A.; Vance, J. L.; Christopherson, G. T.; Patel, B.; Turner, A. S.; Divine, G. W.; Fyhrie, D. P. *Bone* **2004**, *35*, 729.

(23)   Pierard, G. E.; Pierard-Franchimont, C.; Vanderplaetsen, S.; Franchimont, N.; Gaspard, U.; Malaise, M. *Eur. J. Clin. Invest.* **2001**, *31*, 731.

(24)   Pierard, G. E.; Letawe, C.; Dowlati, A.; Pierardfranchimont, C. *J. Am. Geriatr. Soc.* **1995**, *43*, 662.

(25)   Ozyazgan, I.; Liman, N.; Dursun, N.; Gunes, I. *Maturitas* **2002**, *43*, 65.

(26)   Gupta, H. S.; Seto, J.; Krauss, S.; Boesecke, P.; Screen, H. R. C. *J. Struct. Biol.* **2010**, *169*, 183.

(27)   Gupta, H. S.; Zioupos, P. *Med. Eng. Phys.* **2008**, *30*, 1209.

(28)   Graham, H. K.; Hodson, N. W.; Hoyland, J. A.; Millward-Sadler, S. J.; Garrod, D.; Scothern, A.; Griffiths, C. E. M.; Watson, R. E. B.; Cox, T. R.; Erler, J. T.; Trafford, A. W.; Sherratt, M. J. *Matrix Biol.* **2010**, *29*, 254.

(29)   Flint, M. H.; Craig, A. S.; Reilly, H. C.; Gillard, G. C.; Parry, D. A. D. *Connect. Tissue Res.* **1984**, *13*, 69.

(30)   Cuttle, L.; Nataatmadja, M.; Fraser, J. F.; Kempf, M.; Kimble, R. M.; Hayes, M. T. *Wound Repair Regen.* **2005**, *13*, 198.

(31)   Junqueira, L. C. U.; Cossermelli, W.; Brentani, R. *Archivum Histologicum Japonicum* **1978**, *41*, 267.

(32)   Hodge, A. J.; Petruska, J. A., Eds.; Academic Press: New York, **1963**, p 289.

(33)   Orgel, J. P. R. O.; Miller, A.; Irving, T. C.; Fischetti, R. F.; Hammersley, A. P.; Wess, T. J. *Structure* **2001**, *9*, 1061.

(34)   Lee, K. H.; Kuczera, K.; Banaszak Holl, M. M. *Biopolymers* **2011**, *95*, 182.

(35)   Purslow, P. P.; Wess, T. J.; Hukins, D. W. L. *J. Exp. Biol.* **1998**, *201*, 135.

(36)   Gathercole, L. J.; Shah, J. S.; Nave, C. *Int. J.Biol. Macromol.* **1987**, *9*, 181.

(37)   Brodsky, B.; Eikenberry, E. F.; Cassidy, K. *Biochimica et Biophysica Acta (BBA) - Protein Structure* **1980**, *621*, 162.

(38)   Stinson, R. H.; Sweeny, P. R. *Biochimica et Biophysica Acta (BBA) - Protein Structure* **1980**, *621*, 158.

(39)   Puxkandl, R.; Zizak, I.; Paris, O.; Keckes, J.; Tesch, W.; Bernstorff, S.; Purslow, P.; Fratzl, P. *Philosophical Transactions of the Royal Society B: Biological Sciences* **2002**, *357*, 191.

(40)   Dellmann, H.-D.; Eurell, J. A. *Textbook of veterinary histology*; Lippincott Williams&Wilkins: Philadelphia, 1998.

(41)   Fleet, M. R. *Aust. J. Agric. Res.* **2006**, *57*, 751.

(42)   Forrest, J. W.; Fleet, M. R. *Aust. J. Biol. Sci.* **1986**, *39*, 125.

(43)   Calvin, M.; Dyson, M.; Rymer, J.; Young, S. R. *Br. J. Obstet. Gynaecol.* **1998**, *105*, 223.

(44)   Ashcroft, G. S.; Dodsworth, J.; vanBoxtel, E.; Tarnuzzer, R. W.; Horan, M. A.; Schultz, G. S.; Ferguson, M. W. J. *Nat. Med.* **1997**, *3*, 1209.

(45)   Ashcroft, G. S.; Greenwell-Wild, T.; Horan, M. A.; Wahl, S. M.; Ferguson, M. W. J. *The American Journal of Pathology* **1999**, *155*, 1137.

(46)   Danielson, K. G.; Baribault, H.; Holmes, D. F.; Graham, H.; Kadler, K. E.; Iozzo, R. V. *The Journal of Cell Biology* **1997**, *136*, 729.

(47)   Yeh, J. T.; Yeh, L. K.; Jung, S. M.; Chang, T. J.; Wu, H. H.; Shiu, T. F.; Liu, C. Y.; Kao, W. W. Y.; Chu, P. H. *Br. J. Dermatol.* **2010**, *163*, 1174.

(48)   Wenstrup, R. J.; Florer, J. B.; Brunskill, E. W.; Bell, S. M.; Chervoneva, I.; Birk, D. E. *J. Biol. Chem.* **2004**, *279*, 53331.

(49)   Markiewicz, M.; Asano, Y.; Znoyko, S.; Gong, Y.; Watson, D. K.; Trojanowska, M. *J. Dermatol. Sci.* **2007**, *47*, 217.

Chapter 4 Type I Collagen D-spacing in Fibril Bundles of Dermis, Tendon and Bone: Bridging Between Nano- and Micro-Level Tissue Hierarchy

4.1 Introduction

Non-cartilaginous connective tissues, including dermis, tendon and bone, are predominantly composed of type I fibrillar collagen in the organic phase of their extracellular matrix (ECM). As the main ECM building block, collagen fibrils play pivotal roles in maintaining tissue integrity, providing the basis for mechanical properties, and influencing cell activities. Collagen fibrils have an exceptionally long half-life *in vivo*, which is estimated to be 15-95 years. [1,2] They are resistant to common proteases since the tightly packed fibrillar structure prevents access to cleavage sites.[3] Collagen fibrils are mechanically tough; [4] as a structural network, they enhance cell attachment, migration and differentiation.[5,6]

The properties of ECM derive in part from the hierarchical structure of collagen molecules, fibrils, fibril bundles, and higher levels of organization (Figure 4.1). The fibril-forming collagen molecules (type I, III, V, XI, *etc*.) share similar structural motifs. Each of the three α-helices contains Gly-X-Y repeating triplets with proline and hydroxyproline being the most common X and Y residues.[7] The molecular packing of collagen fibril was studied by X-ray in the 1960s to 1980s.[8-15] The fibrils are composed of five-stranded microfibrils that are quasi-hexagonally packed in the equatorial plane[8,9,12-14,16] and supertwisted in the axial direction[3]. Within a fibril, as the Hodge-Petruska model depicts, collagen molecules are aligned in a parallel staggered manner resulting in a repeating Gap/Overlap pattern, resulting in the observed D-spacing.[3,17]
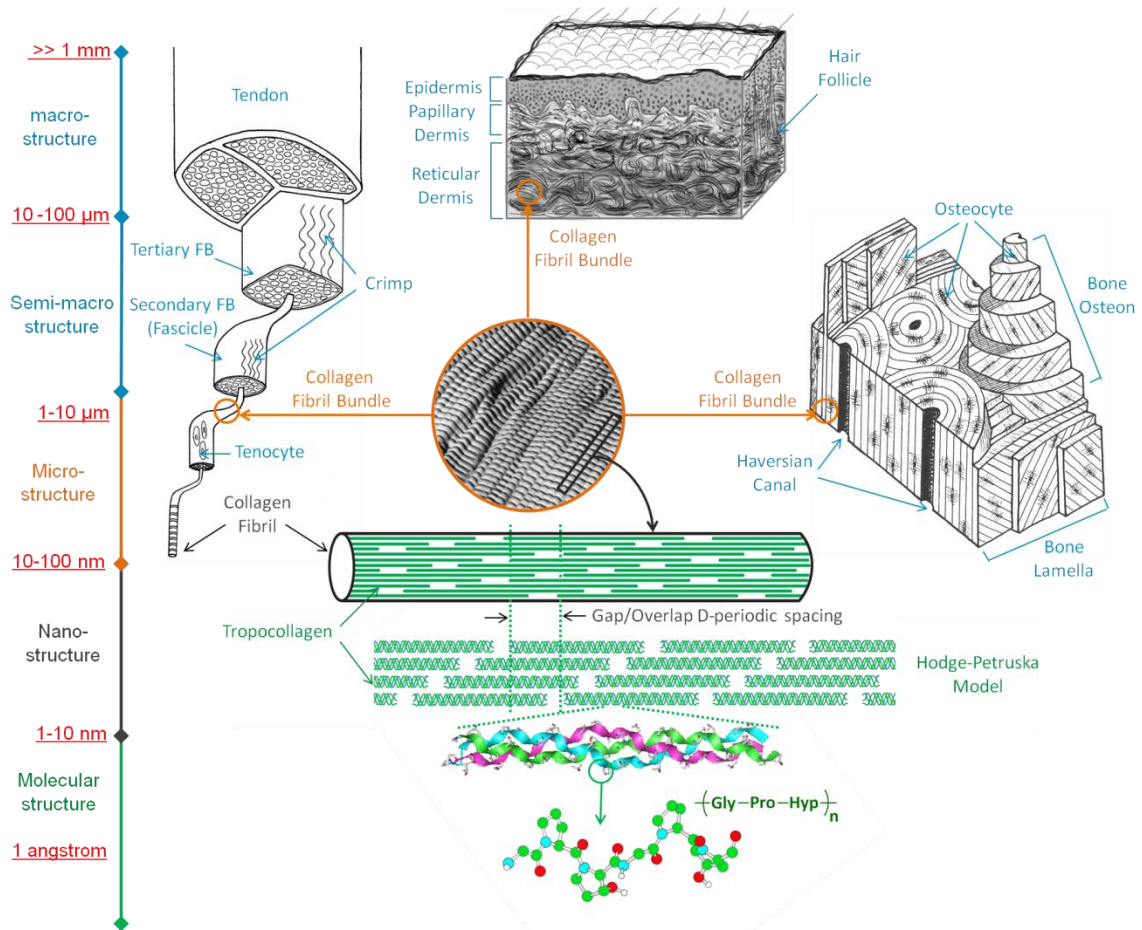
Figure 4.1 Schematic representation of hierarchical tissue structures of tendon, skin and bone. FB is short for fiber bundle.

The next level of collagen hierarchy in ECM is the organization of fibrils into bundles, which occurs at micrometer to millimeter scale (Figure 4.1). Qualitatively, a bundle is a group of parallel fibrils that are generally associated with each other *via* interfibrillar cross-links.[18] In dermis and tendon, a bundle is frequently referred to as a fiber; while in bone it is a lamella sheet of parallel collagen fibrils. The micrometer-scale organization of fibril bundles varies dramatically among tissues. As shown in Figure 4.1, in the dermis, bundles of collagen fibrils with a lateral size ranging from tens of microns to a few hundred microns are randomly oriented in a three dimensional meshwork.[19,20] Tendon has an overall uniaxial structure where collagen fibrils are aligned in parallel arrays [21,22] Bone adapts a twisted plywood structure constructed by lamellae of collagen fibrils with alternating fibril angles among different lamella sheets.[23-25] Despite the

significantly different ECM organizations described above, the grouping of collagen fibrils into micrometer-scale bundles is ubiquitous among collagenous tissues.[26-28]
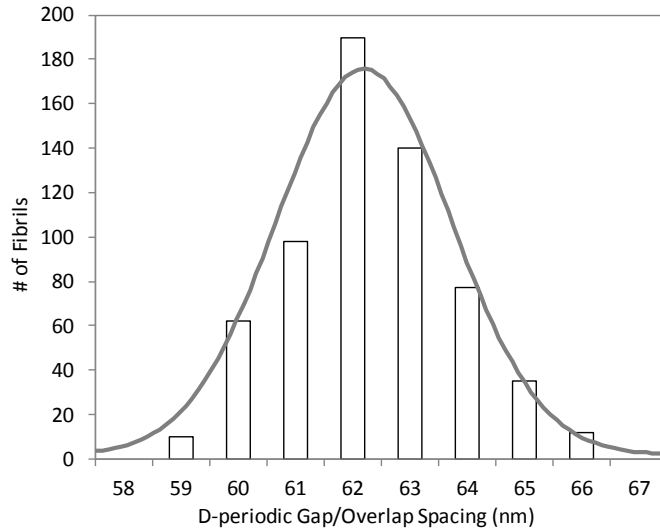
Figure 4.2 A typical D-spacing distribution from ovine dermis. Data were reproduced from AFM imaging and 2D FFT analysis of a sham control study in reference.[33] The distribution is fitted to a Gaussian function shown as the curve.

Characterization of fibril bundles in connective tissues has been limited to qualitative descriptions. For example, scanning electron microscopy (SEM), transmission electron microscopy (TEM) and circularly polarized light microscopy imaging have been used for visualization of dermal fibril bundles and bone lamellae.[19,24,29,30] We have recently developed a quantitative method for D-spacing analysis at the micrometer to sub-micrometer scale, using Atomic Force Microscopy (AFM) imaging and two-dimensional Fast Fourier Transform (2D FFT) analysis.[31,32] Using this method, we have shown that a distribution of nanometer-scale D-spacings is present in a variety of type I collagen based connective tissues, including bone, tooth, tendon and dermis, from a number of species, including murine, ovine, and human.[31,33,34] An example of D-spacing distribution is shown in Figure 4.2. The chemical and physical significance of the *distribution* of D-periodic axial spacing or "D-spacing" values, first characterized by electron microscopy in 1942,[35] has been largely overlooked for seven decades. Only a few publications have quantitatively described collagen D-spacing as a distribution of values to date.[35-38] The majority of publications have adopted the view, largely derived from X-ray scattering data,[39-41] that D-spacing is a single value of about 67 nm and values

deviating from this have generally been attributed to tissue dependent differences,[39,42] and/or artifacts of sample preparation methods such as dehydration.[36,40,43] However, we found that the D-spacing distributions were altered as a function of disease including estrogen deprivation induced osteopenia and *Osteogenesis Imperfecta,* suggesting the biological significance of the D-spacing distribution.[33,34,44]

In this study, the connection between the nanometer-scale collagen fibril D-spacing distribution and the micrometer-scale fibril bundle organization is explored. By comparing fibril D-spacings within a bundle and across different bundles, we wanted to test the two following hypotheses:

H1. The distribution of D-spacing arises from changes at the individual fibril level, *i.e.* the fibril D-spacing is random with respect to the higher level bundle structure.

H2. The distribution of D-spacings arises from changes at the bundle level, *i.e.* differences at the bundle level cause the full range of D-spacing values, whereas D-spacings within a bundle are similar.

We then discuss potential models of collagen fibril structure that describe the origin of the D-spacing morphology as well as the implications for currently proposed mechanisms of fibrillogenesis.

4.2 **Results**

Collagen fibril bundles in healthy adult ovine bone and dermis, human dermis and lamb tendon were imaged and analyzed. Typically a fibril bundle was captured in one 3.5 μm x 3.5 μm AFM scan. In the case of ovine dermis and lamb tendon bundles, we collected images from multiple regions on a bundle. For all the bundle data included in this study, the angular orientations of fibrils within a bundle varied by 10° or less in the XY plane; most fibrils in tendon bundles varied by 3° or less; most fibrils in dermis or bone bundles varied by 5° or less. The small differences of fibril angular orientation represent the laterally ordered organization in a fibril bundle, which serves as a primary criterion for selecting the bundles for quantitative analyses.

4.2.1 **Different D-spacings at Bundle Interfaces**
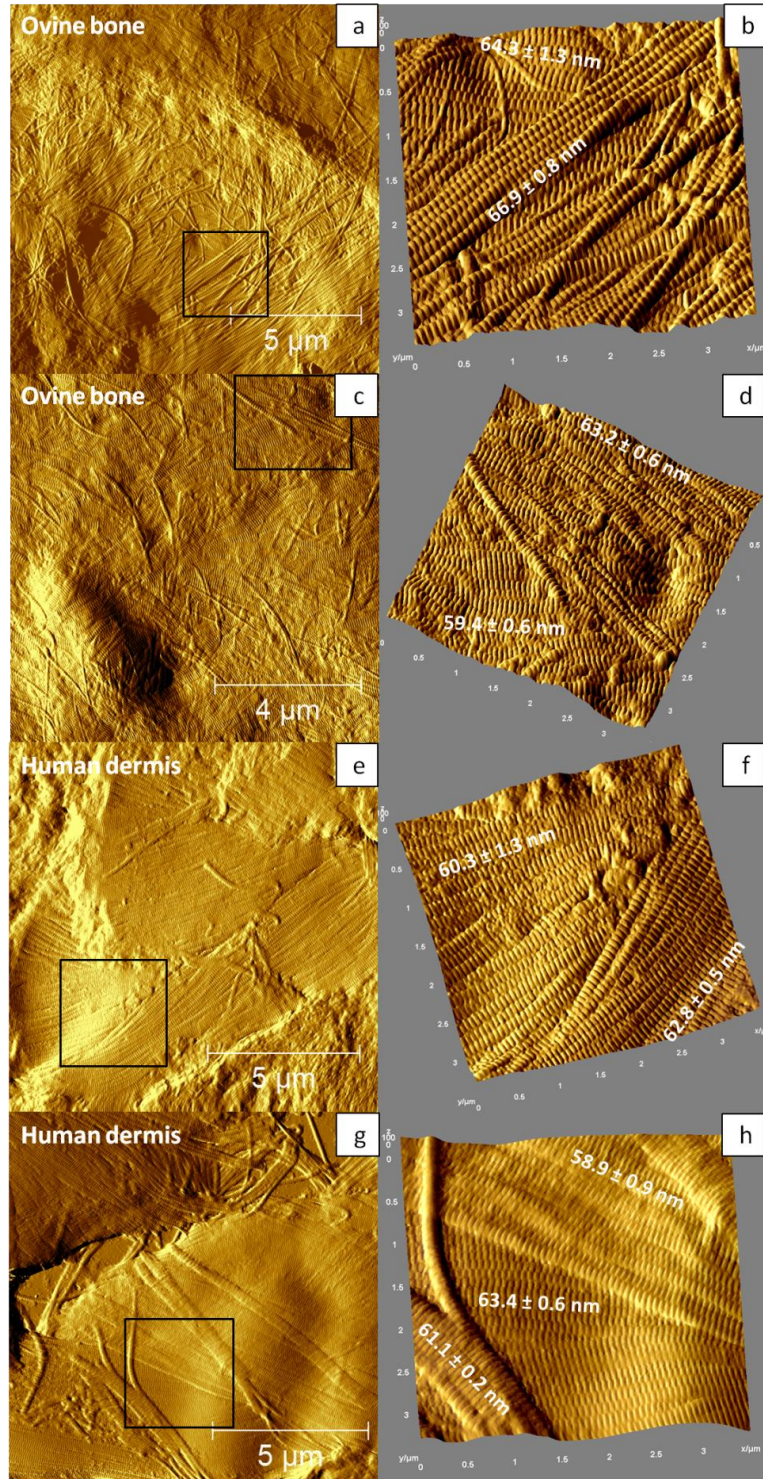
Figure 4.3 AFM images show the domains of fibril bundles and different D-spacings associated with them. (a-d) Exemplary images of ovine bone. (e-h) Exemplary images of human dermis. (b, d, f and h) Three dimensional topography plots of a 3.5 μm area marked by the black box in panel a, c, e and g, respectively. Panel b shows two bundles with 64.3 and 66.9 nm mean D-spacings; panel d shows two bundles with 63.2 and 59.4

nm D-spacing; panel f shows two bundles with 60.3 and 62.8 nm mean D-spacings; panel h shows three bundles with 58.9, 63.4 and 61.1 nm mean D-spacings.

Occasionally two or more bundles were captured in one frame. Examples of these bundle interfaces are shown in Figure 4.3. Interestingly, even though the fibrils are spatially close to each other and captured by the same AFM tip in the same image, fibrils from different bundles exhibit distinctively different D-spacings; fibrils measured from the same bundle share similar D-spacing. Figure 4.3a and Figure *4.3*b illustrate a typical example of two lamella layers in ovine bone: in this instance the underlying bundle has a mean D-spacing of 64.3 ± 1.3 nm, while the top bundle's D-spacing mean is 66.9 ± 0.8 nm. Another example of ovine bone is shown in Figure 4.3c and Figure *4.3*d, where the two bundles have D-spacing means of 63.2 ± 0.6 nm and 59.4 ± 0.6 nm. In addition to aligned fibril bundles, we observed additional interesting structures in bone. Examples of broom-like and interwoven fibril organizations are shown in Appendix A.2. Figure 4.3e shows a set of fibril bundles from human dermis, two of which were captured in Figure 4.3f, with D-spacings of 60.3 ± 1.3 nm and 62.8 ± 0.6 nm. Similarly, Figure 4.3g and Figure *4.3*h are from human dermis, and Figure 4.3h is a zoomed-in region of Figure 4.3g that captured three fibril bundles in one scan. The D-spacings are 58.9 ± 0.9 nm, 63.4 ± 0.6 nm, and 61.1 ± 0.2 nm. Average D-spacing and angular orientations of individual bundles are summarized in Table 4.1. In every case, differences among the bundles were statistically significant ($p < 0.001$).

Table 4.1 D-spacing mean, average angular orientation and number of fibrils of the bundles shown in Figure 4.3b, Figure *4.3*d, Figure *4.3*f and Figure *4.3*h. The standard deviations are included in the parentheses. The angular orientation was measured with respect to the horizontal scan direction. B1-3 stands for bundle 1-3.

	D-spacing (nm)			Angular Orientation (°)			# of Fibrils		
	B1	B2	B3	B1	B2	B3	B1	B2	B3
Figure 4.3b	64.3 (1.3)	66.9 (0.8)	--	-13.4 (4.6)	24.6 (7.7)	--	6	16	--
Figure Figure *4.3*d	63.2 (0.6)	59.4 (0.6)	--	-15.9 (6.2)	22.1 (3.3)	--	8	8	--
Figure Figure *4.3*f	60.3 (1.3)	62.8 (0.5)	--	10.7 (7.1)	38.9 (6.0)	--	9	10	--
Figure Figure *4.3*h	58.9 (0.9)	63.4 (0.6)	61.1 (0.2)	-35.8 (10.0)	-3.0 (4.0)	-52.8 (1.8)	14	15	4

4.2.2 The contribution of Bundle D-spacing Variance to a 10 nm Width Distribution

To illustrate how bundle D-spacings contribute to tissue scale D-spacing distributions, we color coded the distribution histogram to show the contribution from different bundles (Figure 4.4). Taking ovine bone as an example, when plotted in a single histogram (Figure 4.4a and Figure *4.4*b), fibril bundle D-spacings range from 58 nm to 69 nm; however, within each fibril bundle, D-spacing generally spans 1~3 nm. Meanwhile, fibrils from different bundles exhibited independently variant D-spacings that contribute to the full ~10 nm distribution range in these tissues. The narrow intra-bundle D-spacing distribution along with a wide tissue distribution was found for both ovine and human tissues and for both mineralized (bone) and non-mineralized (dermis, tendon) tissue types (Figure 4.4).

When comparing fibril D-spacings from ovine and human dermis, the overall D-spacing averages of 63.0 nm and 62.5 nm, respectively, are not significant different ($p = 0.24$). Upon employing a nested analysis of variance (mixed model ANOVA) to evaluate the contributions of the fibril, bundle and animal variance to the range of D-spacing values, we found that bundle-to-bundle variance was the largest component, accounting for 78% of overall variance. The standard deviation (STD, symbol σ) between bundles is 1.3 nm and the overall STD is 1.5 nm. The bundle STD is significantly different from 0 ($p < 0.0001$). In addition, bundle and fibril level variance are not different between ovine and human by likelihood ratio chi-square test ($p>0.999$ and $p = 0.86$, respectively). The data set exhibited a skewness on the low end of the distribution contributed by bundles with D-spacings as low as 58 nm. As a result, 4.8 % of fibrils were found below $\mu_0 + \tau - 2\sigma$ and none above $\mu_0 + \tau + 2\sigma$.
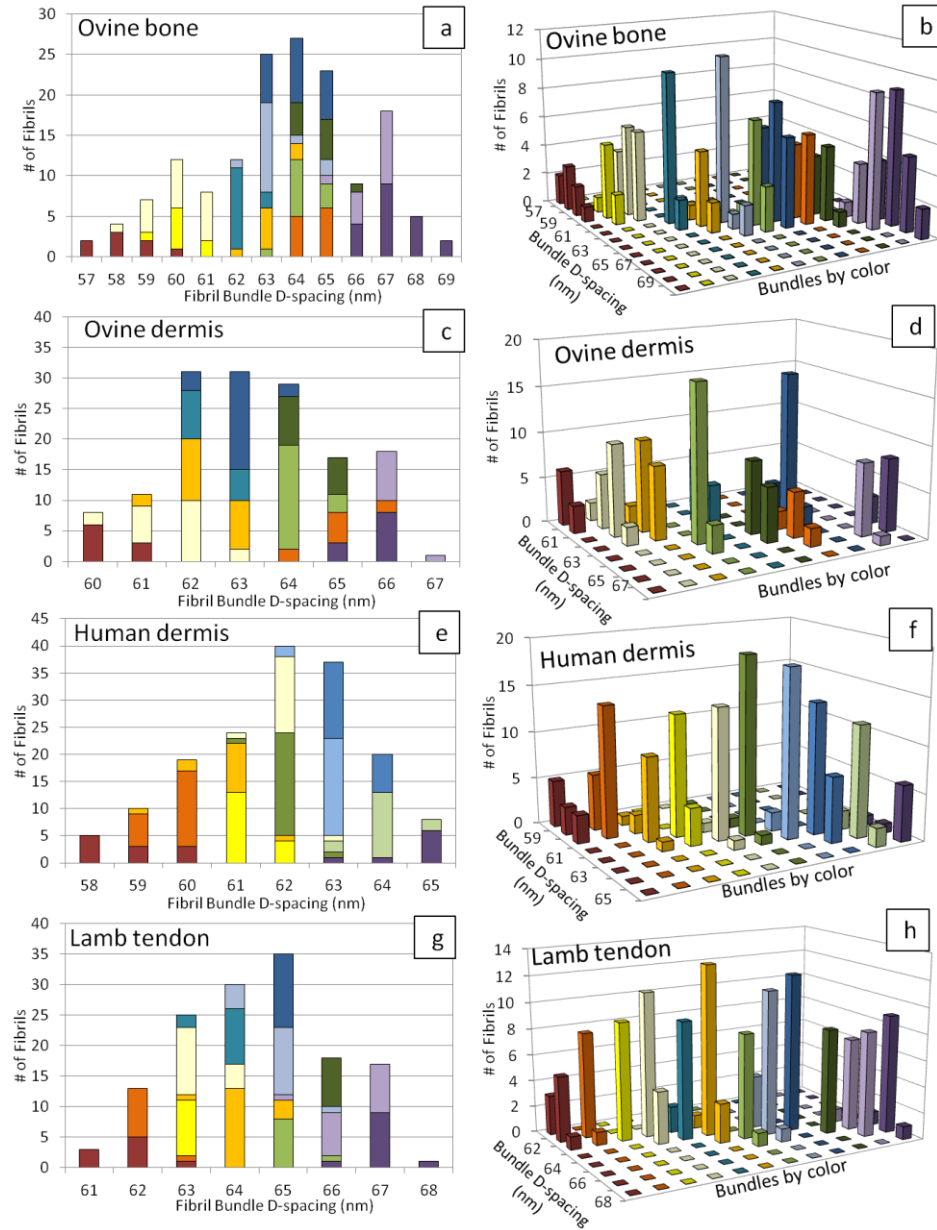
Figure 4.4 Collagen fibril D-spacing distribution arises from narrow bundle D-spacings in ovine bone, ovine dermis, human dermis and lamb tendon. D-spacing distributions plotted in histogram for (a) ovine bone, (c) ovine dermis, (e) human dermis, and (g) lamb tendon. Panel b, d, f and h are 3D histograms of a, c, e and g that show the narrow D-spacing values within a bundle. Each color bar indicates contributions of fibrils from one bundle, while different bundles are denoted by different colors.

The fibril D-spacings averages from ovine dermis, bone and tendon, 62.9 nm, 63.8 nm and 64.0 nm, respectively, are not significantly different from each other ($p = 0.12$). Similar to human/ovine dermis comparison, the nested analysis indicates the

bundle level variance component differed from 0 (p<0.0001), and it accounts for 76% of overall variance. The bundle level and overall STD are 1.6 and 1.8 nm, respectively. Interestingly, bundle variance differs substantially among the three tissues. For dermis, bone and tendon, the estimated $\sigma^2_{bundle(animal)}$ are 1.8, 3.8 and 1.4, respectively (p = 0.074 by likelihood ratio chi-square test). Similarly, the fibril variance is also largest in bone and smallest in tendon. The estimated $\sigma^2_{fibril(bundle(animal))}$ are 0.4, 0.5, 0.2 for dermis, bone and tendon, respectively (p <0.0001). A summary of the statistical analysis is provided in Table 4.2. Additional detail of the nested analysis of variance mixed model ANOVA can be found in Appendix A.3.

Table 4.2 A summary of estimated variance and significance at the level of animal, bundle and fibril.

Test group	Variance component	Estimated variance σ^2 (STD : σ)	P value (compared to 0)
Ovine dermis and human dermis (Analysis 1)	Animal - a_i	0.1 (0.4 nm)	0.2893
	Bundle - b_{ij}	1.8 (1.3 nm)	<0.0001
	Fibril - ε_{ijk}	0.4 (0.6 nm)	<0.0001
	Overall variance	2.3 (1.5 nm)	
Ovine bone, ovine dermis and lamb tendon (Analysis 2)	Animal - a_i	0.4 (0.6 nm)	0.1594
	Bundle - b_{ij}	2.5 (1.6 nm)	<0.0001
	Fibril - ε_{ijk}	0.4 (0.6 nm)	<0.0001
	Overall variance	3.3 (1.8 nm)	
Ovine dermis[a] (Analysis 3)	Animal - a_i	0.5 (0.7 nm)	0.2198
	Bundle - b_{ij}	1.5 (1.2 nm)	0.0021
	Region - r_{ijk}	0.1 (0.4 nm)	0.1358
	Fibril - ε_{ijkl}	0.4 (0.6 nm)	<0.0001
	Overall variance	2.5 (1.6 nm)	
Lamb tendon[a] (Analysis 3)	Animal - a_i	0.3 (0.5 nm)	0.3
	Bundle - b_{ij}	1.3 (1.2 nm)	0.019
	Region[b] - r_{ijk}	0.3-0.4 (0.6 nm)	0.0003
	Fibril - ε_{ijkl}	0.2 (0.5 nm)	<0.0001
	Overall variance	2.2 (1.5 nm)	

[a]See Appendix A.6 for the nested ANOVA model.
[b]Estimated region-to-region variances are 0.4 for axial regions and 0.3 for perpendicular regions; the difference between them are not significant (p = 0.78, likelihood ration chi-square test).

4.2.3 The Persistence Length of D-spacings in Tendon Fascicles and Dermal Samples
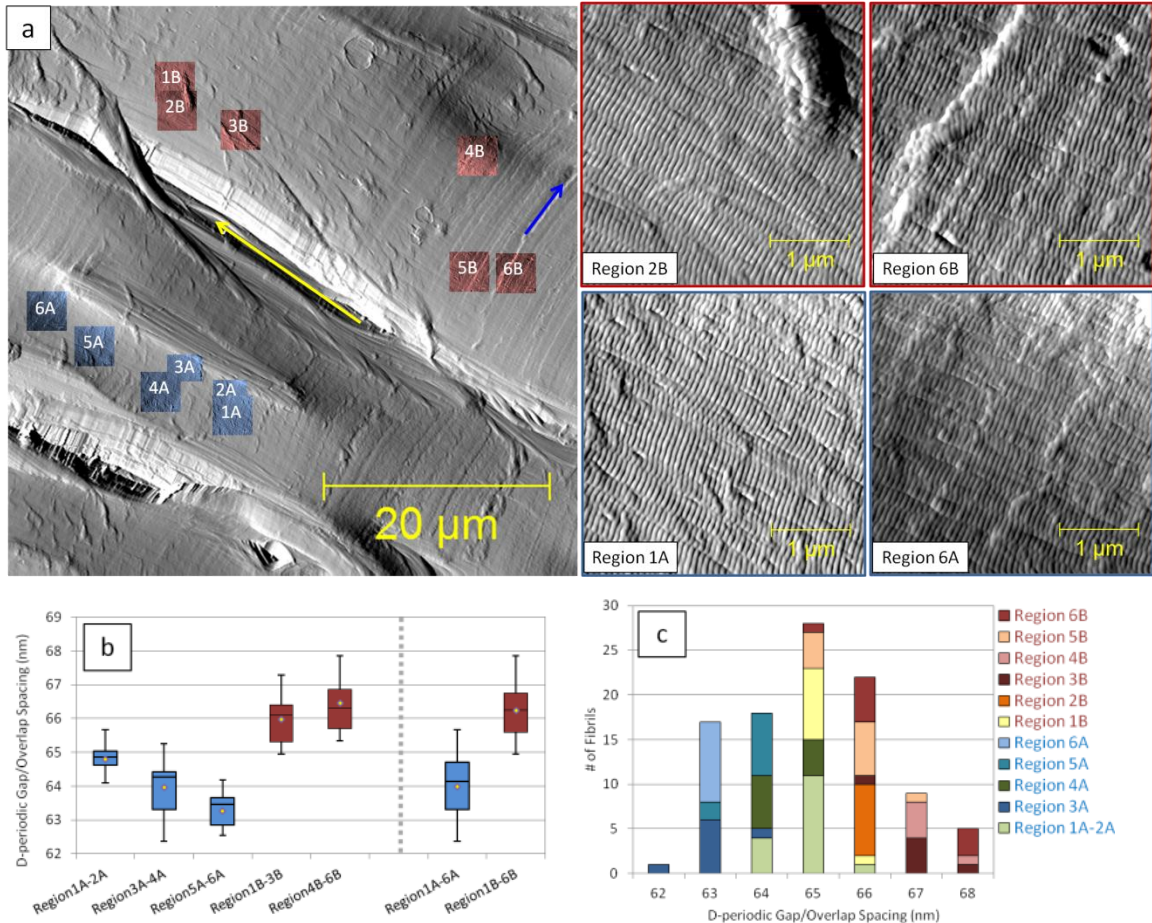
Figure 4.5 Persistence length of D-bundle in lamb tendon fascicle. Panel a is a 50 μm scan of two fascicles in lamb tendon, with the fascicle orientation marked by the yellow arrow. The diagonal lines (indicated by the blue arrow) are artifacts caused by a cryostat blade. Individual regions of 3.5 μm x 3.5 μm size were labeled by sequence and overlaid on the 50 μm scan. Region 1A-6A are noted as fascicle A while region 1B-6B are noted as fascicle B. Panel b is the boxplot that reveals the interquartile, minimum, maximum and mean of the D-periodic gap/overlap spacings measured from individual 3.5 μm scans. Panel c is the color coded histogram of combined region 1A-6A and 1B-6B.

Next, we investigated the persistence length of bundle D-spacings in lamb tendon fascicles and ovine dermis. Figure 4.5a shows two fascicles (A and B) of lamb tendon on the 50 μm-scale. D-spacings were obtained from six 3.5μm x 3.5 μm regions spaced over 20 μm for fascicle A and 40 μm for fascicle B. Fascicles A and B have statistically different D-spacings ($p < 0.001$) of 64.0 ± 0.9 nm, and 66.2 ± 0.9 nm, respectively. D-spacings have a 3.3 nm range in fascicle A and 2.9 nm in fascicle B. Within each fascicle, variations from region to region over a 50 μm-scale are larger than variations within a 3.5μm region. For example, region 1A has a mean D-spacing of 64.9 ± 0.3 nm whereas

region 6A has a mean D-spacing of 62.8 ± 0.3 nm. In another example, regions spaced over 40 μm length of a tendon fascicle give a 4.4 nm range of D-spacing values, with an overall mean of 64.1 ± 0.9 nm (Appendix A.4). Nevertheless, the region-to-region variation is small compared to the full D-spacing width distribution. Nested model ANOVA estimates that region-to-region variance $\sigma^2_{region(bundle(animal))}$ in lamb tendon is 0.4, which is significantly lower than that of bundle-to-bundle variance, $\sigma^2_{bundle(animal)}$ = 1.3 (p = 0.0013 by likelihood ratio chi-square test). We also imaged perpendicular to the axial direction of one or more fascicles (Appendix A.5). In this case, the range of D-spacings is 4 nm, and the region-to-region variance $\sigma^2_{region(bundle(animal))}$ is 0.3. Finally, Figure 4.6 shows a fibril bundle of ovine dermis on the 50 μm scale. Six 3.5 μm x 3.5 μm regions spaced over 30 μm give a set of D-spacings for each region ranging from 61.8 ± 0.6 nm to 62.9 ± 0.4 nm with an overall average of 62.4 ± 0.7 nm. Nested model ANOVA estimates region-to-region variance $\sigma^2_{region(bundle(animal))}$ for ovine dermis is 0.1, significantly lower than bundle-to-bundle variance, $\sigma^2_{bundle(animal)}$ = 1.5 (p = 0.0102 by likelihood ratio chi-square test).
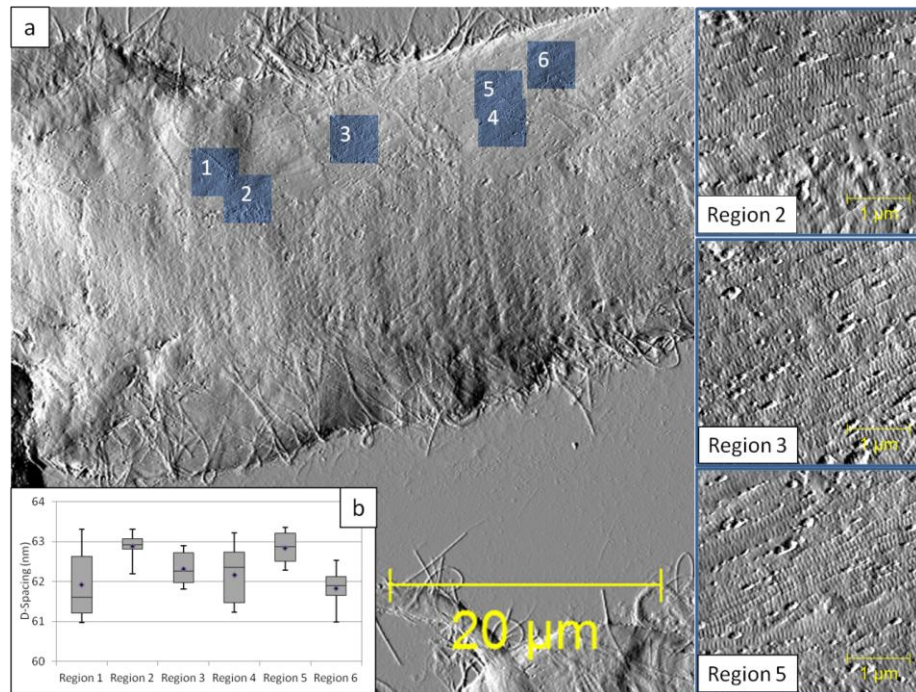
Figure 4.6 Persistence length of D-bundle in ovine dermis. Panel a is a 50 μm scan of a collagen fibril bundle in ovine dermis. Individual scans of 3.5 μm size were labeled by sequence and overlaid on the 50 μm scan (the missing numbers were 10 μm scans). Panel

b is the boxplot that reveals the interquartile, minimum, maximum and mean of the D-periodic gap/overlap spacings measured from individual 3.5 μm scans.

4.3   Discussion

4.3.1   The Origin of D-spacing Distribution: D-bundle

We have observed that collagen fibrils in a single bundle share similar D-spacings (±1 nm), and the full ~10 nm D-spacing distribution found in tissues[31,33,34,44] results from differences in bundle-level D-spacing. This observation is supported by nested mixed model ANOVA analysis. When we evaluate the effect of tissue types, species, animals, bundles nested within animals, and fibrils nested within bundles and animals, the largest component of variance comes from the bundle-to-bundle variance. It accounts for over 76% of total variance, independent of tissue types (bone, dermis and tendon) and species (ovine vs. human). Based on these results, we propose a quantitative definition of a collagen bundle as a bundle of collagen fibrils characterized by identical D-spacing (with ±1 nm STD), and we will refer to fibril bundles with this property as D-bundles. Estimated from 107 D-bundles, STD within a D-bundle is 0.6 nm (see Table 4.2), which is within the error associated with AFM analysis;[31,32] therefore the fibrils in each bundle have similar, if not identical, D-spacings. The bundle-to-bundle variations, as small as 1.3 nm STD in tendon and as large as 1.9 nm STD in bone, are the major component that give rise to the full distribution of 8-10 nm width and 1.5-2 nm STD, typically seen for tissue samples (an example is shown in Figure 4.2). These observations are consistent with hypothesis H2 and inconsistent with H1.

The bundle size, typically on the order of tens of microns, varies among tissues. As observed by AFM, the fibril bundle width in lamb tendon is 20 microns and larger; ovine and human dermis tend to have bundle width of a few microns in papillary dermis, and 50 microns or larger in reticular dermis (similar observations in refs. [38,45]); fibril bundles in ovine cortical bone, in contrast to all the other tissues used in this study, are less frequently observed and are usually of 1-5 μm in lateral size.

The question of persistence length of D-bundles is particularly interesting in tissues such as tendon, where fascicles can extend to millimeters in length. We evaluated

the persistence length of D-bundles by taking D-spacing measurements across 40-50 μm axial and perpendicular directions of tendon fascicles. As shown in Figure 4.5, Appendix A.4, and Appendix A.5, D-spacings from regions of a tendon fascicle vary in a range of 4-5 nm. This range is in between that of a D-bundle (1-3 nm range; 0.6 nm STD) and that of a tissue-scale D-spacing distribution (10 nm range; 1.5-2 nm STD). Based on nested ANOVA analysis, the region-to-region variance in the axial direction in lamb tendon is 0.4 (σ = 0.6 nm) and that of perpendicular direction is 0.3 (σ = 0.6 nm), which is significantly smaller than variance of different tendon bundles, 1.3 (σ = 1.2 nm). It suggests regions within a tendon fascicle vary to a lesser extent than do different D-bundles in tissue consisting of multiple fascicles, and thus are more likely to be related with each over. In ovine dermis, the data in Figure 4.6 indicate that D-bundles can maintain a persistent D-spacing up to 30 μm in the axial direction, which is in agreement with the nested ANOVA analysis since the estimated region-to-region variance is 0.1(σ = 0.4 nm).

4.3.2   The Physical and/or Biochemical Origins of Bundle-Dependent D-spacing

Knowing the physical and/or biochemical origins of tissue scale D-spacing distribution and narrow D-bundle D-spacing range is imperative to our understanding of fibrillogenesis. Although this question remains to be answered, this section is devoted to discussing potential factors that could influence fibril D-spacing. First and foremost, it should be mentioned that biomineralization is not a determinant for the tissue scale distribution of D-spacings, since the 10 nm range of D-spacing and narrow D-spacing range in D-bundles are observed in both mineralized bone and non-mineralized dermis and tendon tissues.[31,34]

Mutations in the collagen composition can change the D-spacing. Based on a previous AFM study using an *Osteogenesis Imperfecta* (OI) mice model and molecular dynamics (MD) simulation, single substitution of glycine to cystein in collagen amino acid composition destabilizes the collagen triple helical structure,[46] and D-spacing distribution in the OI model showed significant shift from the control model.[44]

Some studies have shown D-spacing elongation as a function of strain[47-49]. However, elongation of D-spacing accounts only a small fraction of tissue level strain in the elastic deformation regime. Sasaki[47], Puxkandl[48], and Gupta *et al*[49]. have all shown in

their studies that fibril strain tends to be on the order of 1-2 nm in tendon and bone. In our study, no external stress was applied to the tissues and we observed ~ 10 nm range difference in bundles D-spacings. Therefore it is very unlikely that strain alone is causing the bundle D-spacing differences.

Another hypothesis is that covalent cross-linking is responsible for D-bundle formation. It is possible that hydroxylysine sites are matched between adjacent fibrils during enzymatic cross-linking process, resulting in overlapping gap zones and overlap zones. [50] In addition to enzymatic cross-linking, nonenzymatic glycation (NEG) such as cross-linking between collagen and sugar occurs with ageing and diabetes.[51] However we have found no effect of NEG on collagen fibril D-spacings using ovine bones treated with D-ribose *in vitro* (Appendix A.7). Similar results have been reported by Odetti and others.[37]

Other factors known to interact with collagen during formation and maturation include type V and XI collagen [52,53]; SLRPs such as decorin and lumican[50,54,55]; and fibronectin[56-58]. Knockout studies on collagen V or decorin have shown irregular fibril formation and in some cases early embryonic death[55,59-61], suggesting indispensible roles that the minor collagen types and SLRPs play in regulating collagen fibril formation. However, little is known about whether these small proteins play a role in changing collagen fibril D-spacing.

In summary, the simplest form of the Hodge-Petruska model shown in Figure 4.1 does not address the variations of D-spacings reported here. In particular, this data indicates the need for collagen fibril growth and structural models to account for the collagen fibril D-spacings being organized at the hierarchical level of fibril bundles. As we understand more about the structural complexity of collagen and its dynamic interactions with other ECM components, it becomes increasingly important that we adopt a more sophisticated model of collagen fibril structure that also reflects D-spacing distribution. This model will allow us to better understand normal collagen hierarchy and changes in collagen structure induced by ageing, diseases and mechanical failures.

4.3.3   Collagen Fibril Bundle Formation in Fibrillogenesis Models

The mechanism of D-bundle formation is still an open question, competing theories offer different views on the nucleation and growth of collagen fibrils.
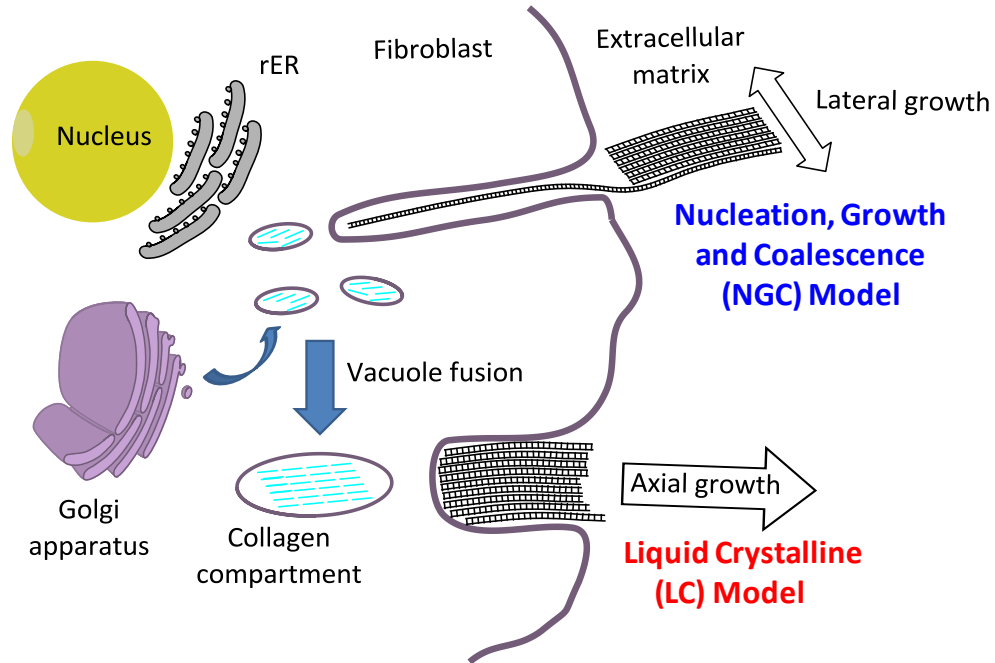
Figure 4.7 Scheme of NGC model and LC model. In the NGC model, the fibroblast forms ruffled protrusions or depressions called fibripositors. Collagen fibril nucleation and growth starts within fibripositors. Individual fibrils then coalesce into bundles when they are excreted into the ECM. In the LC model, collagen precursors pre-align in secretary compartments or the ECM and form a bundle simultaneously.

4.3.3.1 Nucleation, Growth and Coalescence (NGC) Model

EM studies by Birk's and Kadler's groups suggest a nucleation, growth and coalescence model for the formation of collagen fibrils and fibril bundles (NGC model, Figure 4.7). In chick embryonic tendon, single or small groups of fibrils were found in membrane protrusions or depressions near fibroblast cell surfaces, which are called fibripositors.[62-64] Based on this observation, it is hypothesized that single collagen fibrils nucleate in these fibripositors and grow in the axial direction. Side-to-side fusion [26,30,65,62] as well as tip-to-tip fusion[55,66] of fibrils has been observed, which could explain the D-bundle formation. Our quantitative data on fibril D-spacing and their relationship to bundle structure place two interesting constraints on the NGC model. First, if D-spacing is determined by extracellular factors such as binding with proteoglycans and/or mechanical stress, then it is plausible that a bundle could share similar D-spacing if these factors exert uniform effect within a bundle. An alternative hypothesis is that D-spacing is determined at the fibripositor stage, which implies bundle-dependent D-spacing is also cell-dependent. Although there is clear evidence indicating that intracellular information

such as genetic coding can play a vital role in fibril D-spacing formation,[44] further experiments are required to clarify the relationship between collagen fibril D-spacing and the cells that produce collagen.

4.3.3.2 Liquid Crystalline (LC) Model

Driven by the observation of liquid crystalline properties in type I collagen[67-69] *in vitro*, Giraud-Guille and others have proposed that collagen precursors (procollagen or tropocollagen) are pre-aligned in concentrated local environments, which aids in the alignment, undulations and twists in the packing of collagen fibrils (LC model, Figure 4.7).[70] It is also interesting to note that the plywood structure of human compact bone osteons is analogous to the organization of cholesteric liquid crystals, as the direction of fibrils rotates by a constant angle from one lamallar layer to the next.[24,29,68] This model provides a simple physical explanation for the collagen structural organization in collective tissues, and offers the intriguing possibility that D-bundle spacing is synchronized by liquid crystalline alignment. Although aspects of this model are compelling, the liquid crystallinity of collagen has not been demonstrated directly *in vivo*.

4.4 Conclusion

In conclusion, we observed a narrow distribution of D-spacings within D-bundles (±1 nm). In addition, large variations in D-spacings among different bundles contribute to the full distribution (10 nm range) at the tissue scale in bone, dermis, and tendon. The measurements and statistical analysis support the hypothesis that differences at the bundle level cause the full range of D-spacing values, whereas D-spacings within a bundle are similar (H2) and are inconsistent with fibril D-spacing being random with respect to the higher level bundle structure (H1). The formation of D-bundles has important implications in terms of how collagen fibrils are assembled; however, the mechanisms of D-bundle formation and D-spacing variations are poorly understood. Mechanistic pathways for both the NGC and LC models can be proposed that are consistent with the data presented here for the relationship between fibril D-spacing and bundle structure. Future research efforts are needed to answer many questions raised by these studies including: how are cells and/or extracellular proteins involved in forming

collagen fibril bundles? What contributes to a heterogeneous D-spacing distribution? Is the tight distribution of D-spacings within a D-bundle disrupted by disease? Do D-bundles with different D-spacings play varying roles under mechanical stresses? We are pursuing a number of these challenging questions and we hope that these new quantitative observations regarding type I collagen structure can be employed by the broader scientific community to promote a better understanding of collagen fibrillogenesis and ultimately how collagenous tissues are established and maintained.

4.5   Experimental

4.5.1   Animals

Ovine bone and dermis specimens were collected from sham-operated Columbia-Rambouillet ovine, as previously described.[33] Bone specimens were acquired from the mid-diaphysis of the left radius, while dermis specimens were harvested from the dorsal midline, in the thoracolumbar region. Procurement of human skin samples was approved the University of Michigan Institutional Review Board, and conducted according to the Declaration of Helsinki principles. All subjects provided written informed consent. Full-thickness human skin biopsies were taken from sun-protected buttock skin from human donors ranging in age from 20 to 40 years old. Lamb tendons were from 6-month-old rambouillet-dorset ovine, provided by a local butcher. Ovine bone data were collected from 15 animals; ovine dermis data were collected from 4 animals, human dermis data were collected 6 donors; lamb tendon data were collected from 4 animals. We analyzed 32 bundles in ovine bone, 26 in ovine dermis, 32 in human dermis and 17 in lamb tendon for a total of 107 bundles and 1710 fibrils.

4.5.2   Cryostat Sectioning of Dermis and Tendon

Combined tissue sectioning and AFM analysis was highlighted in Graham's recent report.[71] First, skin biopsies were embedded in Tissue-Tek optimal cutting temperature (OCT) solution (Sakura Finetek Inc., Torrance, CA, USA) and frozen at -20 ℃. 10 μm thick thin-sections of dermis were obtained using Microm HM550 Cryostat (Thermo Scientific Inc., Walldorf, Germany) and transferred onto glass slides. Due to the random meshwork nature of dermis collagen bundles, sections parallel to the skin surface

60

and perpendicular to the skin surface (cross-section) are both suited for AFM imaging. The dermal sections were rinsed with ultrapure water for 5 minutes and kept at -20 ℃ prior to the AFM study. Tendon specimens were sectioned in a similar manner and the cutting plane was set to be parallel with the long axis of tendon. No artificial stretching was imposed on tissue samples during sample preparation.

4.5.3 Polishing and Demineralization of Bone

Ovine bones were mounted to a steel disk using cyanoacrylate glue, and a flat surface was polished as described previously.[33] The bones were demineralized using 0.5 M EDTA at a PH of 8.0 for 1 hour with 5 min sonication at every 20 min interval. The bones were then vigorously rinsed with ultrapure water and preserved at 4 ℃ before AFM study.

4.5.4 AFM Imaging and Analysis

All imaging was carried out in air dry condition using a PicoPlus 5500 AFM (Agilent); dermis and tendon specimens were imaged in contact mode using SNL-10 AFM probes (Bruker AFM probes, nominal tip radius 2 nm, force constant 0.25 N/m). Ovine bones were imaged using tapping mode with VistaProbe T300R probes (NanoScience, AZ; nominal radius 10 nm, force constant 40 N/m, resonance frequency 300 kHz). Line scan rates were set at 2 Hz or lower at 512 lines per frame. Random locations on tissue samples were imaged by AFM in search of fibril bundles. Image analysis and measurements were performed using SPIP software (V5.0.8, Image Metrology; Horsholm, Denmark). Collagen fibril D-spacings were measured using 2D fast Fourier Transform (FFT) toolkit of SPIP software, detailed description and validation can be found in previous studies.[31,33]

One concern associated with AFM imaging is the effect of thermal drift and tip convolution which may differ from scan to scan. We have carefully examined the effect of thermal drifting and ruled out the possibility of thermal drifting causing an artificial D-spacing distribution.[32] Furthermore, finding two or more fibril bundles with different D-spacings in single AFM scans (Figure 4.3) rules out the concern that the differences in D-spacings may be caused by using different AFM tips or scanning on different days. All fibril bundle D-spacings were measured within individual 50 μm x 50 μm area. The

limited AFM scan size may underestimate lateral bundle size and persistence length. In addition, due to the cylindrical geometry of bone lamellae, polishing and imaging on a flat surface may cause underestimation in the bundle size and length of fibril bundles in bone tissues.

4.5.5 Statistical Analysis

Mean D-spacings (± standard deviation) from individual bundles were tested using one way ANOVA.

A nested analysis of variance was employed (mixed model ANOVA[72]) to determine the hierarchical level of the sources of variance in the overall D-spacing distribution (Eq. a-e). Arranged by their hierarchical order, fibrils were nested within bundles, and bundles were nested within animals.

$$Y_{ijk} = \mu_0 + \tau + a_i + b_{ij} + \varepsilon_{ijk} \tag{Eq. (a)}$$

$$var\ (a_i) = \sigma^2_{animal} \tag{Eq. (b)}$$

$$var\ (b_{ij}) = \sigma^2_{bundle(animal)} \tag{Eq. (c)}$$

$$var\ (\varepsilon_{ijk}) = \sigma^2_{fibril(bundle(animal))} \tag{Eq. (d)}$$

$$Total\ Variance = \sigma^2_{animal} + \sigma^2_{bundle(animal)} + \sigma^2_{fibril(bundle(animal))} \tag{Eq. (e)}$$

μ_0 – D-spacing mean; τ – fixed effect (described in the analyses below); a_i - random effect of ith animal; b_{ij} – random effect of jth bundle nested within ith animal; ε_{ijk} – random effect of kth fibril nested in jth bundle and in ith animal.

Two sets of mixed model ANOVA analyses were performed based on the model above:

Analysis1) Comparison of two different species: ovine dermis (4 animals, 26 bundles and 340 fibrils) and human dermis (6 humans, 32 bundles and 479 fibrils); in this case the fixed effect τ is the animal type.

Analysis 2) Comparison of three different tissue types in ovine: ovine bone (15 animals, 32 bundles, 340 fibrils), ovine dermis (4 animals, 26 bundles and 340 fibrils), and lamb tendon (4 animals, 17 bundles, 198 fibrils); in this case the fixed effect τ is the tissue type.

Within each nested analysis, differences between D-spacing averages, components of variance, and their significance were examined. In should be noted that only one 3.5 µm x 3.5 µm region per bundle is used in these two analyses.

In 1 of the 26 bundles in ovine dermis (Figure 4.6) and 4 of 17 bundles in lamb tendon (Figure 4.5 and Appendix A.4), we investigated multiple regions along the axial direction of one bundle or fascicle (over ~20-40 µm distance) to assess the axial persistence length of these bundles. We examined regions perpendicular to one fascicle (over ~40 µm distance) in lamb tendon (Appendix A.5). We employed another nested model (see Appendix A.6) to include the variance component of regions:

Analysis 3) Estimate the region-to-region variance, and how it compares to bundle-to-bundle variance: ovine dermis (4 animals, 26 bundles, 31 locations and 376 fibrils); lamb tendon (4 animals, 17 bundles, 49 locations and 515 fibrils).

4.6 **Reference**

(1)   Naylor, E. C.; Watson, R. E. B.; Sherratt, M. J. *Maturitas* **2011**, *69*, 249.
(2)   Verzijl, N.; DeGroot, J.; Thorpe, S. R.; Bank, R. A.; Shaw, J. N.; Lyons, T. J.; Bijlsma, J. W. J.; Lafeber, F. P. J. G.; Baynes, J. W.; TeKoppele, J. M. *J. Biol. Chem.* **2000**, *275*, 39027.
(3)   Orgel, J. P. R. O.; Irving, T. C.; Miller, A.; Wess, T. J. *Proc. Natl. Acad. Sci. U. S. A.* **2006**, *103*, 9001.
(4)   Sasaki, N.; Nakayama, Y.; Yoshikawa, M.; Enyo, A. *J. Biomech.* **1993**, *26*, 1369.
(5)   Sivakumar, P.; Czirok, A.; Rongish, B. J.; Divakara, V. P.; Wang, Y. P.; Dallas, S. L. *J. Cell Sci.* **2006**, *119*, 1350.
(6)   Dallas, S. L.; Chen, Q.; Sivakumar, P. In *Curr. Top. Dev. Biol.*; Gerald, P. S., Ed.; Academic Press: 2006; Vol. Volume 75, p 1.
(7)   Fratzl, P.; SpringerLink *Collagen Structure and Mechanics*; Springer Science+Business Media, LLC: Boston, MA, 2008.
(8)   Miller, A.; Wray, J. S. *Nature* **1971**, *230*, 437.
(9)   Hulmes, D. J. S.; Miller, A. *Nature* **1979**, *282*, 878.
(10)   Fraser, R. D. B.; MacRae, T. P.; Miller, A.; Suzuki, E. *J. Mol. Biol.* **1983**, *167*, 497.
(11)   Fraser, R. D. B.; MacRae, T. P.; Miller, A. *J. Mol. Biol.* **1987**, *193*, 115.
(12)   Trus, B. L.; Piez, K. A. *Nature* **1980**, *286*, 300.
(13)   Traub, W.; Piez, K. A. 1971; Vol. 25, p 243.
(14)   Piez, K. A.; Trus, B. L. *Biosci. Rep.* **1981**, *1*, 801.
(15)   Brodsky, B.; Eikenberry, E. F. 1982; Vol. 82, p 127.

(16)   Hulmes, D. J. S.; Wess, T. J.; Prockop, D. J.; Fratzl, P. *Biophys. J.* **1995**, *68*, 1661.

(17)   Hodge, A. J.; Petruska, J. A., Eds.; Academic Press: New York, **1963**, p 289.

(18)   Knott, L.; Bailey, A. J. *Bone* **1998**, *22*, 181.

(19)   Lavker, R. M.; Zheng, P.; Dong, G. *J. Invest. Dermatol.* **1987**, *88*, 44s.

(20)   Goldsmith, L. A. *Physiology, biochemistry, and molecular biology of the skin*; Oxford University Press: New York, 1991.

(21)   Kannus, P. *Scand. J. Med. Sci. Sports* **2000**, *10*, 312.

(22)   Provenzano, P. P.; Vanderby Jr, R. *Matrix Biol.* **2006**, *25*, 71.

(23)   Weiner, S.; Arad, T.; Sabanay, I.; Traub, W. *Bone* **1997**, *20*, 509.

(24)   Giraud-Guille, M. M. *Calcif. Tissue Int.* **1988**, *42*, 167.

(25)   Weiner, S.; Wagner, H. D. *Annual Review of Materials Science* **1998**, *28*, 271.

(26)   Birk, D. E.; Trelstad, R. L. *J. Cell Biol.* **1986**, *103*, 231.

(27)   Birk, D. E.; Trelstad, R. L. *J. Cell Biol.* **1984**, *99*, 2024.

(28)   Birk, D. E.; Southern, J. F.; Zycband, E. I.; Fallon, J. T.; Trelstad, R. L. *Development* **1989**, *107*, 437.

(29)   Bromage, T. G.; Goldman, H. M.; McFarlin, S. C.; Warshaw, J.; Boyde, A.; Riggs, C. M. *Anatomical Record - Part B New Anatomist* **2003**, *274*, 157.

(30)   Yurchenco, P. D.; Birk, D. E.; Mecham, R. P. *Extracellular matrix assembly and structure*; Academic Press: San Diego, 1994.

(31)   Wallace, J. M.; Chen, Q.; Fang, M.; Erickson, B.; Orr, B. G.; Banaszak Holl, M. M. *Langmuir* **2010**, *26*, 7349.

(32)   Erickson, B.; Fang, M.; Wallace, J. M.; Orr, B. G.; Les, C. M.; Banaszak Holl, M. M. *Submitted* **2012**.

(33)   Wallace, J. M.; Erickson, B.; Les, C. M.; Orr, B. G.; Banaszak Holl, M. M. *Bone* **2010**, *46*, 1349.

(34)   Fang, M.; Liroff, K. G.; Turner, A. S.; Les, C. M.; Orr, B. G.; Holl, M. M. B. *J. Invest. Dermatol.* **2012**.

(35)   Schmitt, F. O.; Hall, C. E.; Jakus, M. A. *J. Cell. Compar. Physl.* **1942**, *20*, 11.

(36)   Habelitz, S.; Balooch, M.; Marshall, S. J.; Balooch, G.; Marshall Jr, G. W. *J. Struct. Biol.* **2002**, *138*, 227.

(37)   Odetti, P.; Aragno, I.; Rolandi, R.; Garibaldi, S.; Valentini, S.; Cosso, L.; Traverso, N.; Cottalasso, D.; Pronzato, M. A.; Marinari, U. M. *Diabetes. Metab. Res. Rev.* **2000**, *16*, 74.

(38)   Gross, J.; Schmitt, F. O. *The Journal of Experimental Medicine* **1948**, *88*, 555.

(39)   Brodsky, B.; Eikenberry, E. F.; Cassidy, K. *Biochimica et Biophysica Acta (BBA) - Protein Structure* **1980**, *621*, 162.

(40)   Bear, R. S. *J. Am. Chem. Soc.* **1944**, *66*, 1297.

(41)   Price, R. I.; Lees, S.; Kirschner, D. A. *Int. J. Biol. Macromol.* **1997**, *20*, 23.

(42)   Stinson, R. H.; Sweeny, P. R. *Biochimica et Biophysica Acta (BBA) - Protein Structure* **1980**, *621*, 158.

(43)	Eikenberry, E. F.; Brodsky, B. B.; Craig, A. S.; Parry, D. A. D. *Int. J.Biol. Macromol.* **1982**, *4*, 393.

(44)	Wallace, J. M.; Orr, B. G.; Marini, J. C.; Holl, M. M. B. *J. Struct. Biol.* **2011**, *173*, 146.

(45)	Verhaegen, P. D. H. M.; van Marle, J.; Kuehne, A.; Schouten, H. J.; Gaffney, E. A.; Maini, P. K.; Middelkoop, E.; van Zuijlen, P. P. M. *J. Microsc.* **2012**, *245*, 82.

(46)	Lee, K. H.; Kuczera, K.; Banaszak Holl, M. M. *Biopolymers* **2011**, *95*, 182.

(47)	Sasaki, N.; Shukunami, N.; Matsushima, N.; Izumi, Y. *J. Biomech.* **1999**, *32*, 285.

(48)	Puxkandl, R.; Zizak, I.; Paris, O.; Keckes, J.; Tesch, W.; Bernstorff, S.; Purslow, P.; Fratzl, P. *Philosophical Transactions of the Royal Society B: Biological Sciences* **2002**, *357*, 191.

(49)	Gupta, H. S.; Zioupos, P. *Med. Eng. Phys.* **2008**, *30*, 1209.

(50)	Orgel, J. P. R. O.; San Antonio, J. D.; Antipova, O. *Connect. Tissue Res.* **2011**, *52*, 2.

(51)	Vashishth, D.; Gibson, G. J.; Khoury, J. I.; Schaffler, M. B.; Kimura, J.; Fyhrie, D. P. *Bone* **2001**, *28*, 195.

(52)	Wenstrup, R. J.; Florer, J. B.; Brunskill, E. W.; Bell, S. M.; Chervoneva, I.; Birk, D. E. *J. Biol. Chem.* **2004**, *279*, 53331.

(53)	Wenstrup, R. J.; Smith, S. M.; Florer, J. B.; Zhang, G.; Beason, D. P.; Seegmiller, R. E.; Soslowsky, L. J.; Birk, D. E. *J. Biol. Chem.* **2011**, *286*, 20455.

(54)	Weber, I. T.; Harrison, R. W.; Iozzo, R. V. *J. Biol. Chem.* **1996**, *271*, 31767.

(55)	Graham, H. K.; Holmes, D. F.; Watson, R. B.; Kadler, K. E. *J. Mol. Biol.* **2000**, *295*, 891.

(56)	Kadler, K. E.; Hill, A.; Canty-Laird, E. G. *Curr. Opin. Cell Biol.* **2008**, *20*, 495.

(57)	Singh, P.; Carraher, C.; Schwarzbauer, J. E. In *Annual Review of Cell and Developmental Biology, Vol 26*; Schekman, R., Goldstein, L., Lehmann, R., Eds. 2010; Vol. 26, p 397.

(58)	Shi, F.; Harman, J.; Fujiwara, K.; Sottile, J. *American Journal of Physiology - Cell Physiology* **2010**, *298*, C1265.

(59)	Reed, C. C.; Iozzo, R. V. *Glycoconj. J.* **2002**, *19*, 249.

(60)	Danielson, K. G.; Baribault, H.; Holmes, D. F.; Graham, H.; Kadler, K. E.; Iozzo, R. V. *The Journal of Cell Biology* **1997**, *136*, 729.

(61)	Zhang, G.; Ezura, Y.; Chervoneva, I.; Robinson, P. S.; Beason, D. P.; Carine, E. T.; Soslowsky, L. J.; Iozzo, R. V.; Birk, D. E. *J. Cell. Biochem.* **2006**, *98*, 1436.

(62)	Canty, E. G.; Kadler, K. E. *J. Cell Sci.* **2005**, *118*, 1341.

(63)	Canty, E. G.; Lu, Y.; Meadows, R. S.; Shaw, M. K.; Holmes, D. F.; Kadler, K. E. *J. Cell Biol.* **2004**, *165*, 553.

(64)	Trelstad, R. L.; Hayashi, K. *Dev. Biol.* **1979**, *71*, 228.

(65)	Hay, E. D. *Cell biology of extracellular matrix*; Plenum Press: New York, 1991.

(66)   Kadler, K. E.; Holmes, D. F.; Trotter, J. A.; Chapman, J. A. *Biochem. J.* **1996**, *316*, 1.

(67)   Giraud-Guille, M. M. *J. Mol. Biol.* **1992**, *224*, 861.

(68)   Giraud-Guille, M. M.; Mosser, G.; Belamie, E. *Current Opinion in Colloid and Interface Science* **2008**, *13*, 303.

(69)   Gobeaux, F.; Mosser, G.; Anglo, A.; Panine, P.; Davidson, P.; Giraud-Guille, M. M.; Belamie, E. *J. Mol. Biol.* **2008**, *376*, 1509.

(70)   Giraud-Guille, M. M.; Belamie, E.; Mosser, G.; Helary, C.; Gobeaux, F.; Vigier, S. *Comptes Rendus Chimie* **2008**, *11*, 245.

(71)   Graham, H. K.; Hodson, N. W.; Hoyland, J. A.; Millward-Sadler, S. J.; Garrod, D.; Scothern, A.; Griffiths, C. E. M.; Watson, R. E. B.; Cox, T. R.; Erler, J. T.; Trafford, A. W.; Sherratt, M. J. *Matrix Biol.* **2010**, *29*, 254.

(72)   West, B. T.; Welch, K. B.; Galecki, A. T.; NetLibrary, I. *Linear mixed models: a practical guide using statistical software*; Chapman & Hall/CRC: Boca Raton, 2007.

Chapter 5 Type I Collagen Self-Assembly: The Roles of Substrate and Concentration

5.1 Introduction

Type I Collagen is the most abundant protein in mammals and provides, particularly in the form of fibrils and fibers, the basic structural component for bone, dermis, dentin, and tendon. As the archetype of fibrillar collagens, the hierarchical structures associated with type I collagen are the most studied and understood. The D-periodic gap/overlap banding pattern (D-spacing) of the fibrils was discovered in early electron microscopy (EM) studies and reported as a distribution of values.[1,2] Hodge and Petruska proposed a model to explain collagen fibril structure as a parallel staggered array of self-assembled collagen monomers;[3] however this model only addressed the presence of a singular value, nominally 64-67 nm depending on the tissue type. A singular value is obtained by small angle X-ray scattering (SAXS) experiments, which typically average over millimeters of tissue, but distributions of D-spacings are imaged using techniques such as EM[1,2] or atomic force microscopy (AFM),[4-8] which can measure individual fibrils in the tissue. The next two decades of X-ray studies indicated a quasi-hexagonal packing of microfibrils within a fibril[9-14] and a supertwist of collagen molecules in the longitudinal direction of a fibril.[15,16] Recently, structural simulations at the atomistic level have provided additional structural insight into how collagen molecules can pack in three-dimensions and form collagen fibrils with the D-spacing pattern.[17] Despite this substantial recent progress, there is still no experimental or theoretical data that predicts or explains the now 70-year-old observation of a distribution of D-spacings in both mineralized and non-minineralized tissues such as bone and dermis.

Understanding the origin(s) of D-spacing distribution is of crucial importance given the connection of this nanostructural parameter to diseases, such as estrogen depletion[6,18] and *Osteogenesis Imperfecta*.[8,19] In work to date, we have shown that the distribution is independent of mineralization. Thus, although the gap zone of collagen fibrils is an important nucleation site for hydroxyapatite minerals,[20-22] mineralization does not appear to drive the presence of the distribution. We therefore decided to focus on the assembly of type I collagen molecules into the fibrillar structures. The origin of the variation in nanoscale collagen fibril structure, exemplified by the change in D-spacing distribution, has a number of possible biochemical origins. The distribution may be intrinsic to the self-assembly process, whether following the nucleation and growth model[23-26] or the liquid crystalline assembly model.[27-29] Change at the level of amino acid composition has an impact on D-spacing distribution, as suggested by previous *Osteogenesis Imperfecta* studies.[19] It should also be noted that collagen fibrils in tissues are heterotypic, composed of type I, III, V and XI collagens, and it is possible that variation in collagen content changes the nanoscale structure. In addition, collagen fibrils are covalently cross-linked intra-fibrillarly and extra-fibrillarly.[30,31] Lastly, small leucine-rich proteoglycans (SLRPs) and fibronectins are known to bind with collagen fibrils and regulate fibril diameter,[32-35] and it is possible they also impact the D-spacing. In short, the known biochemistry of type I collagen fibrils leaves open many possible mechanisms for variation in D-spacing values; amino acid residue and/or heterotypic variation, cross-linking, and/or protein binding all remain as viable hypotheses for the origin of the observed distribution.

Driven by the observation of fibril D-spacing distributions in a variety of type I collagen based tissues, we investigated type I collagen self-assembly *in vitro*. While the process of collagen fibrillogenesis *in vivo* remains to be elucidated, *in vitro* self-assembly of type I collagen molecules provides a controllable alternative approach where we could control both monomer concentration and the nucleation surface. In general, type I collagen self-assembly *in vitro* is an entropy driven process via loss of surface bound solvent molecules.[36] At neutral pH, hydrogen bonding, hydrophobic and electrostatic interactions result in the self-assembly of type I collagen fibrils with D-periodic spacing.[37-39] Using solubilized rat tail tendon (~93% type I collagen), collagen fibrils can

be formed in the absence of most biochemical effects such as heterotypic variation, interfibrillar cross-linking, and binding to proteoglycans and other small proteins. Several different methods have been established to induce collagen fibril formation for applications in tissue engineering and cell culture *in vitro*, including thermal gelation,[40-42] reverse dialysis and evaporation methods,[43,44] coextrusion in fibril forming buffer (FFB),[28,45] and sol-gel transition induced by ammonia vapor.[46] Many studies have explored the influence of pH and ionic strength of electrolytes, in particular K^+, on fibril formation and growth on mica;[47-49] however, the nature and/ or presence of a distribution of D-spacing values has not been quantified.

In this study, we characterized D-spacing of type I collagen fibrils as a function of incubation concentration utilizing two *in vitro* collagen self-assembly methods and three substrates, including surface-mediated collagen self-assembly on phlogopite and muscovite mica, and coextrusion of collagen fibrillar gel in concentrated bulk solution within glass capillary tubes. The main goals were 1) to test whether type I collagen self-assembly alone produces a distribution of D-spacings and 2) if a distribution formed solely under self-assembly conditions is similar in shape and width to that observed in biological tissues. We also explored the influence of collagen incubation concentration on D-spacing distribution and found that D-spacing tilt angle correlates with decreased D-spacing measurement on muscovite mica at high concentrations ($\geq$ 20 μg/ml). Nevertheless, D-spacing tilt is not common in biological tissues and it cannot explain low D-spacing values typically seen in ovariectomized (OVX) dermis and bone.

5.2   Results and Discussion

5.2.1 Selection of Self-Assembly and Imaging Substrates

Phlogopite and muscovite mica and molybdenum disulfide (MoS_2) were chosen as substrates for several reasons. First, it has been shown that collagen self-assembles on muscovite mica to form axially aligned fibrils with D-periodic spacings similar to those observed in tissue[47-49]. Fibrils with D-periodic spacing were also observed on phlogopite mica; however, the axial organization of the fibrils differed.[49] Second, the previous studies demonstrated that collagen interacts strongly with both mica substrates leading to

the observed axially organizations.[49] In order to be certain that the D-periodic spacing variation was not controlled by the surface interactions, we studied both types of mica and added a third surface, MoS_2, with which collagen does not strongly interact. We found that under similar incubation conditions, type I collagen self-assembly on MoS_2 forms a web pattern instead of fibrils (Appendix A.8). Thus, we chose to use MoS_2 as the substrate to deposit collagen fibrillar gel formed in capillary tube, as we could be certain that fibrils observed on MoS_2 arose from gel self-assembly and not self-assembly on the imaging surface. Third, all three surfaces are readily cleaved to form large, atomically flat domains conducive to AFM imaging of the fibrils.

5.2.2 D-spacing Distribution Arises from Type I Collagen Self-Assembly

Solubilized rat tail tendon collagen solution was deposited on freshly cleaved phlogopite mica at three different incubation concentrations: 10, 50, and 100 μg/ml. As illustrated in Figure 5.1, the fibril assembly on phlogopite mica displays a triangular pattern, which reflects the hexagonal symmetry of the phlogopite crystal lattice.[49] Two-dimensional fast Fourier transform (2D-FFT)[5,6] analysis was utilized to quantitatively analyze fibril D-periodic spacing. The D-spacing values obtained for each concentration are plotted as histograms in Figure 5.2 and a distribution of D-spacing values with a width of ~9-10 nm is observed at every concentration, similar to that observed in bone, dermis, dentin and tendon.[5-7] The tenfold change in collagen incubation concentration had no impact on D-spacing distributions. D-spacing means measured for over two hundred fibrils are 65.7 ± 1.1, 65.9 ± 1.0 and 65.7 ± 1.3 nm for 10, 50 and 100 μg/ml, respectively. Cumulative density function (CDF) plots of the three concentrations indicated substantial overlap (Appendix A.9). K-S test indicated no significant difference between 10 and 100 μg/ml ($p = 0.90$), and a possible significant difference ($p = 0.04$) both in 10 vs. 50 μg/ml, and 50 vs. 100 μg/ml comparison; however, it should be noted that p values deemed significant between D-spacing distributions in previous disease based biological studies were below 0.001.[6,18]
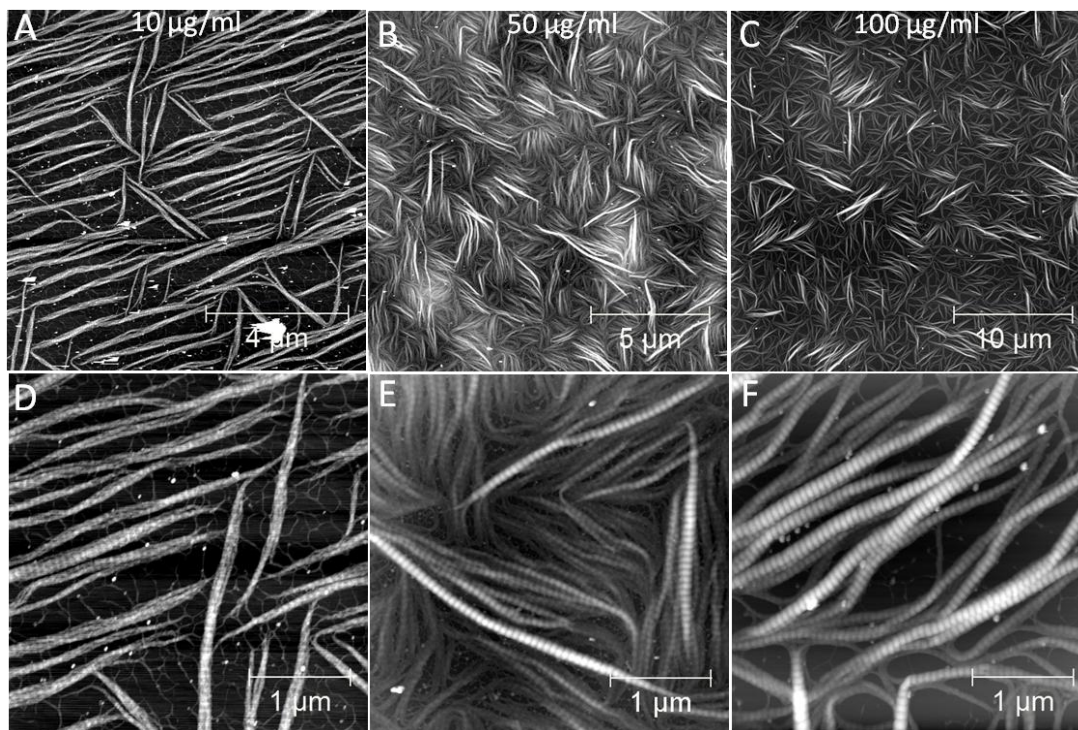
Figure 5.1 Collagen self-assembly on phlogopite mica as a function of concentration. Panels A-C are exemplary topography images of collagen fibrils assembled at 10 μg/ml, 50 μg/ml and 100 μg/ml. Incubation at concentrations lower than 10 μg/ml resulted in no collagen fibril formation. Panels D-F are examples of zoomed-in regions of A-C from which fibril D-spacings were analyzed.

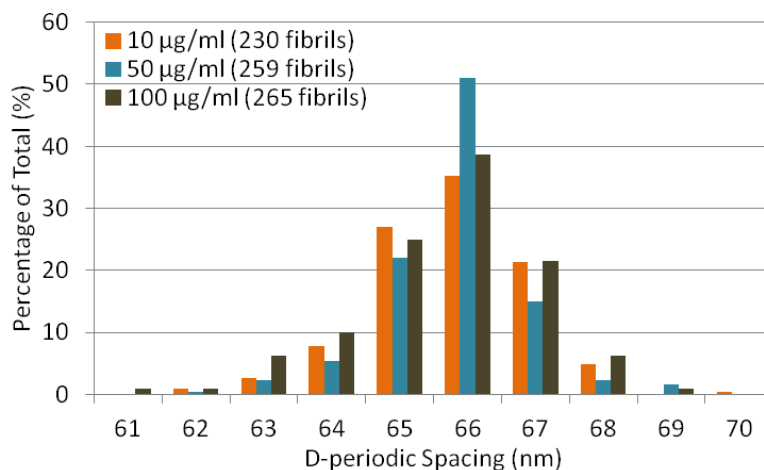**Figure 5.2** D-spacing distributions of self-assembled collagen fibrils on phlogopite mica at three different concentrations: 10, 50 and 100 μg/ml.

Type I collagen is known to interact strongly with the mica surface.[49] In order to rule out the possibility that these interactions incidentally generate a D-spacing distribution, we have also adapted a fibrillar gel coextrusion method as suggested by

Gobeaux and coworkers.[28] Briefly, fibrillar collagen gel formation was induced by submerging glass capillary tubes containing concentrated collagen solution (10 mg/ml) in fibril forming buffer. It was suggested that capillary tubes may assist collagen alignment prior to fibrillogenesis. The fibrillar gel was then deposited on freshly peeled basal planes of MoS_2, as shown in Figure 5.3. Large bundles with branches of collagen fibrils were frequently observed (Figure 5.3A). Similar to the observations on phlogopite mica, the collagen fibrils formed using the gel method also exhibited a distribution of ~10 nm with an overall mean of 65.0 ± 2.1 nm (Figure 5.3C).
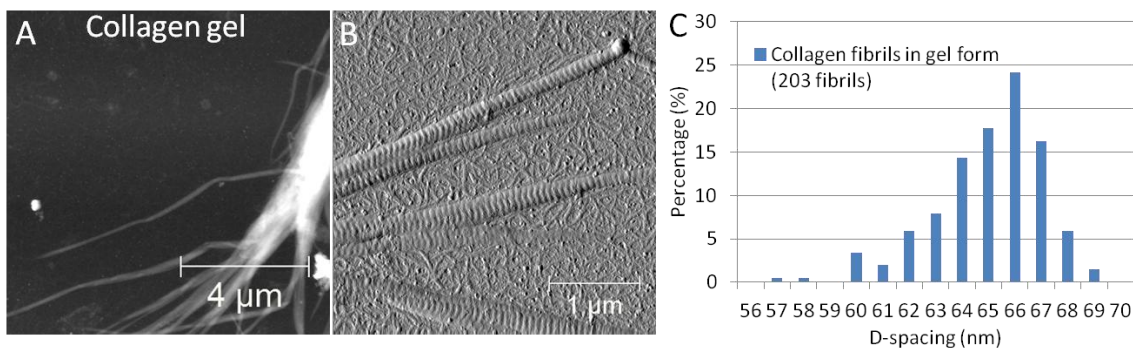

Figure 5.3 Collagen fibrillar gel formed in glass capillary tubes and deposited on MoS2. Panels A and B are representative AFM tapping mode topography and error images of collagen fibrils formed in capillary tubes and then deposited on MoS2. Panel C shows the D-spacing distribution histogram of collagen fibrils formed in capillary tubes.

The D-spacing distribution formed on phlogopite mica and collagen fibrillar gel are similar to that observed in bone, dermis, dentin and tendon in terms of distribution shape and width[5,6], suggesting that it is intrinsic to type I collagen self-assembly. The D-spacing distribution appeared substantially different and highly skewed on the muscovite mica. This striking difference led us to examine the possible impact of the tilted D-spacings in greater detail.

5.2.3 Tilted D-spacing Resulted from Collagen Fibril Self-Assembly on Muscovite Mica

Type I collagen fibrils were self-assembled on muscovite mica from solutions containing 0.5, 5, 20, 50 and 100 μg/ml of solubilized rat tail tendon collagen. Figure 5.4 shows AFM images of self-assembled fibrils at different incubation concentrations. Sporadically spaced microfibrils and fibrils with discernible D-spacings were found in

the 0.5 µg/ml sample. At 5 µg/ml, the surface coverage of collagen fibrils was significantly increased, with lateral and longitudinal fusions frequently present. Fibril fusion is a common observation in type I collagen self-assembly *in vitro* as well as in tendon tissue,[50-52] in contrast to tissues such as cornea where collagen fibril diameter is tightly controlled by minor collagens (type V and XI) and decorin.[32,33,53] At 20 µg/ml and above, collagen fibrils fully cover the mica surface, and fibrils with D-spacing tilt were frequently observed. As shown in Figure 5.4C-E, although all the fibrils are orientated approximately in the same direction, the D-periodic banding patterns are tilted from 45 to 90 degrees with respect to the fibril axis (Appendix A.10).
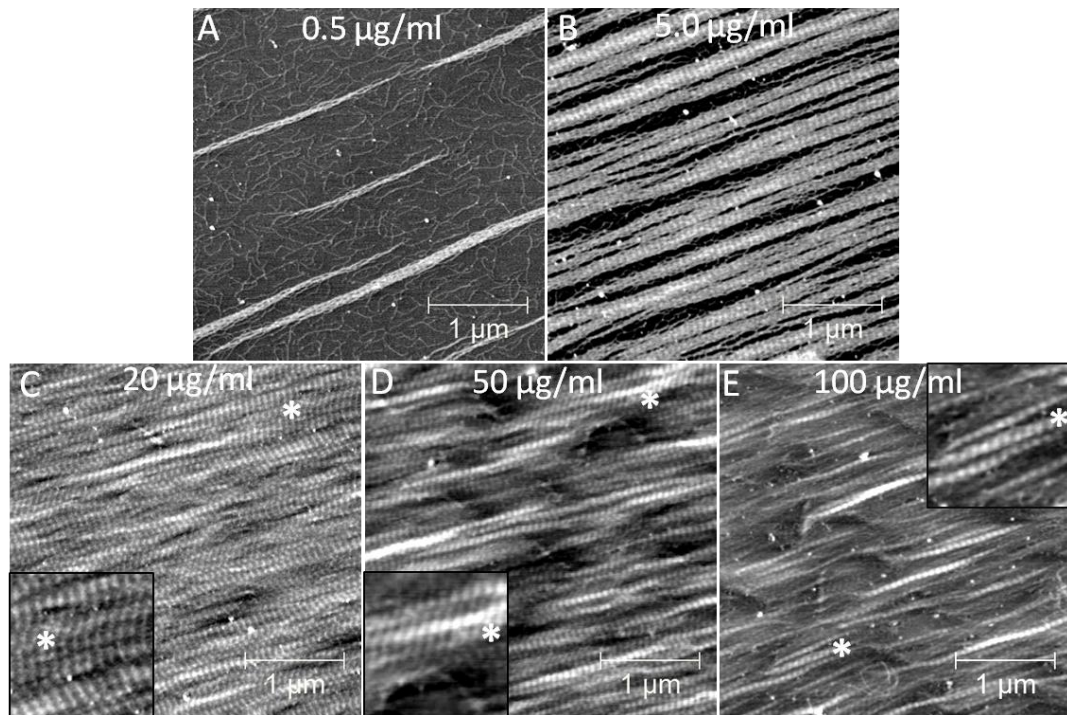
Figure 5.4 Type I collagen self-assembly on muscovite mica as a function of concentration. Panels A-E are representative AFM tapping mode topography images of type I collagen fibrils assembled at 0.5, 5, 20, 50 and 100 µg/ml. At 20 µg/ml and higher concentrations, fibrils with tilted D-spacing were frequently observed. Examples of tilted D-spacing are marked by asterisks and shown as inserts in panels C-E, the inserts are 800 nm in size.
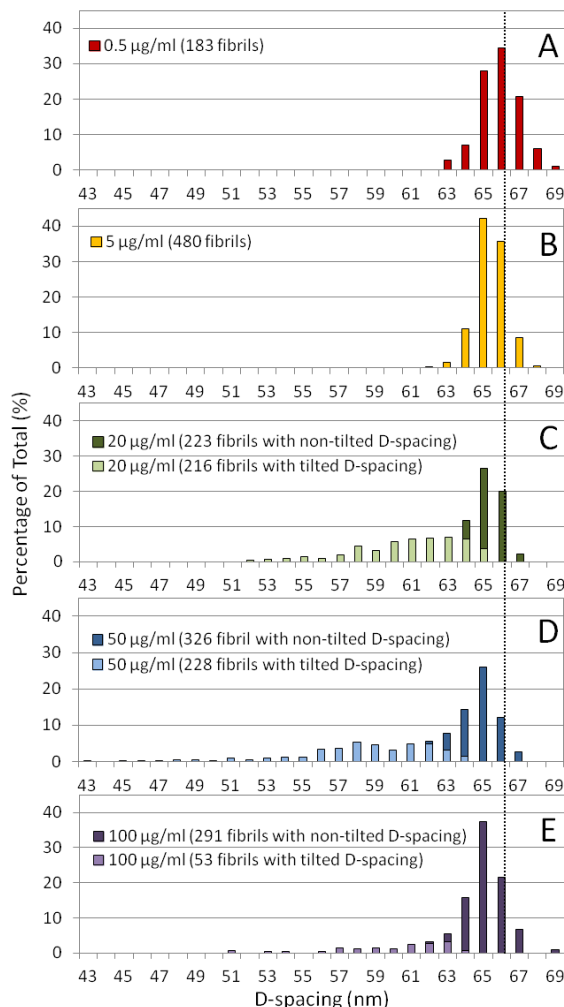
***Figure* 5.5** D-spacing histograms of self-assembled type I collagen fibrils on muscovite mica as a function of concentration. Panels A to E correspond to 0.5, 5, 20, 50 and 100 μg/ml, respectively. Although fibril D-spacings are nominally perpendicular to fibril axis; in 20, 50 and 100 μg/ml, a substantial number of fibrils exhibit tilted D-spacings (tilt angle $< 80^{\circ}$). Contributions from non-tilted D-spacing (in darker colors) and tilted D-spacing (in lighter colors) are shown in the stacked histograms in panels C-E. The dashed line at the 66 nm bin was added for guidance.

Similar with oligothiophene and oligophenyl based organic nanofibers,[54-56] the triangular and parallel self-assembly pattern of collagen fibrils on phlogopite and muscovite mica reflects the mica's surface symmetry. The basal plane of muscovite mica is a dioctahedral sheet with parallel surface corrugations caused by the tilting of SiO_4 tetrahedra. [56,57] This distortion not only reduces the surface symmetry of muscovite mica to plane group pm (with one mirror axis), it also allows OH groups to tilt away from K^{+}.[49] On the other hand, phlogopite mica is a trioctahedral sheet with less distortion on

the surface, resulting in a higher degree of symmetry (plane group p31m with three mirror axes).[54,55] In addition, in phlogopite mica atoms are more vertically aligned, which means the K^+ are closer to OH group leading to reduced binding affinity.[49] It is unclear if muscovite surface distortion plays a role in causing the D-spacing tilt. Since D-spacing tilt was only observed at 20 µg/ml and higher concentrations where adjacent fibrils are in contact with each other, and rarely observed at 0.5 and 5 µg/ml where there are gaps between fibrils, we suspect that tilted D-spacing may be due to the limited packing space and/or influences from adjacent fibrils.

As shown in the distribution histograms in Figure 5.5A-B, D-spacing distributions of 0.5 and 5 µg/ml share similar D-spacing means, 65.9 ± 1.1 and 65.4 ± 0.9 nm; both have a 7 nm width with minute skewness (-0.2 and -0.3, respectively). At 20, 50 and 100 µg/ml (Figure 5.5C-E), D-spacing means are 63.1 ± 3.1, 62.2 ± 4.1, and 64.4 ± 2.4 nm, respectively. The decrease in D-spacing means and increase in standard deviations are due to the severely skewed distributions towards low values, with D-spacing values reaching as low as 43 nm in the 50 µg/ml histogram. The distribution skewness for 20, 50 and 100 µg/ml are -1.3, -1.5 and -2.5, respectively. Interestingly, we noticed that low D-spacing values are from fibrils with tilted D-spacing, including those marked by asterisks in Figure 5.4C-E. Fibrils exhibiting non-tilted D-spacing have values that are within a normal distribution range (62 nm to 69 nm), as shown in Figure 5.5C-E.

In order to probe the relationship between tilted D-spacing and low D-spacing values, we measured D-spacing tilt angle using the same 2D-FFT spectrum from which the D-spacing was derived. As shown in Figure 5.6, we define D-spacing tilt angle θ as the angle of the overlap/gap band with respect to the longitudinal fibril axis, ranging from 0 to 90 degrees. In a normal fibril with non-tilted D-spacing (see model fibril 1 in Figure 5.6A), the overlap/gap band is perpendicular to the fibril axis (tilt angle $\theta = 90^{\circ}$), which is reflected in the orthogonal cross pattern of its 2D-FFT spectrum. A fibril with θ degree of D-spacing tilt, shown as model fibril 2 in Figure 5.6B, results in a 2D-FFT spectrum with θ degree angle present in the cross pattern. In AFM images, fibrils are commonly oriented at an angle (angle φ), such as model fibril 3 in Figure 5.6C. In this case, both D-spacing tilt angle θ and fibril orientation angle φ are reflected in the 2D-FFT spectrum. Figure 5.6D is an example AFM image showing two fibrils with different tilt angles:

fibril 1 has a D-spacing of 65 nm at 84° tilt (Figure 5.6E) and fibril 2 has a D-spacing of 61 nm at 70° tilt (Figure 5.6F). It should be noted that D-spacing values directly measured by 2D-FFT correspond to tilted D-spacing, as shown schematically in Fig 6G. We then define the conventional D-spacing along the fibril axis as fibril axial D-spacing, which equals to tilted D-spacing / $\sin(\theta)$.
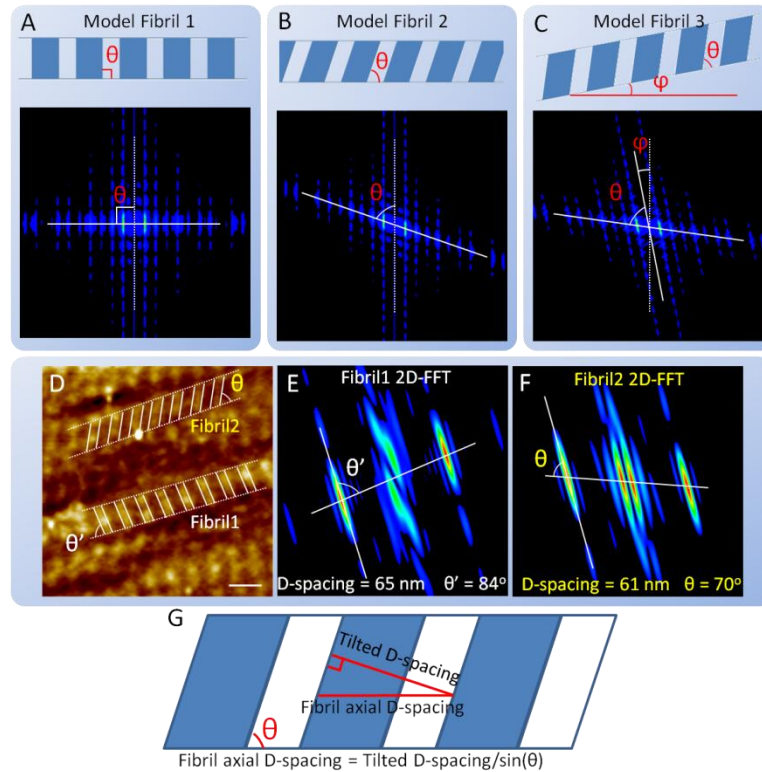

Figure 5.6 Fibril D-spacing tilt angle measured by 2D-FFT. Panels A-C are 2D-FFTs of three model fibrils: 1- a horizontal fibril with a normal D-spacing; 2 - a horizontal fibril with a D-spacing tilted θ degree; 3 - a φ degree rotated fibril with a D-spacing tilted θ degree (models are shown beneath the 2D-FFTs). Panel D is a zoomed-in topography image including a fibril with normal D-spacing (fibril 1) and a fibril with a D-spacing tilt (fibril 2), scale bar is 100 nm. Angle θ and θ' are the D-spacing tilt angles ($90^o \geq \theta$ and θ' $\geq 0^o$). Panels E and F are the 2D-FFT's of fibrils 1 and 2, respectively. Panel G is a schematic showing the conversion between tilted D-spacing and fibril axial D-spacing. Tilted D-spacing is directly measured by 2D-FFT, fibril axial D-spacing is the Gap/Overlap distance along the axial direction of a fibril, which equals to tilted D-spacing/$\sin(\theta)$.
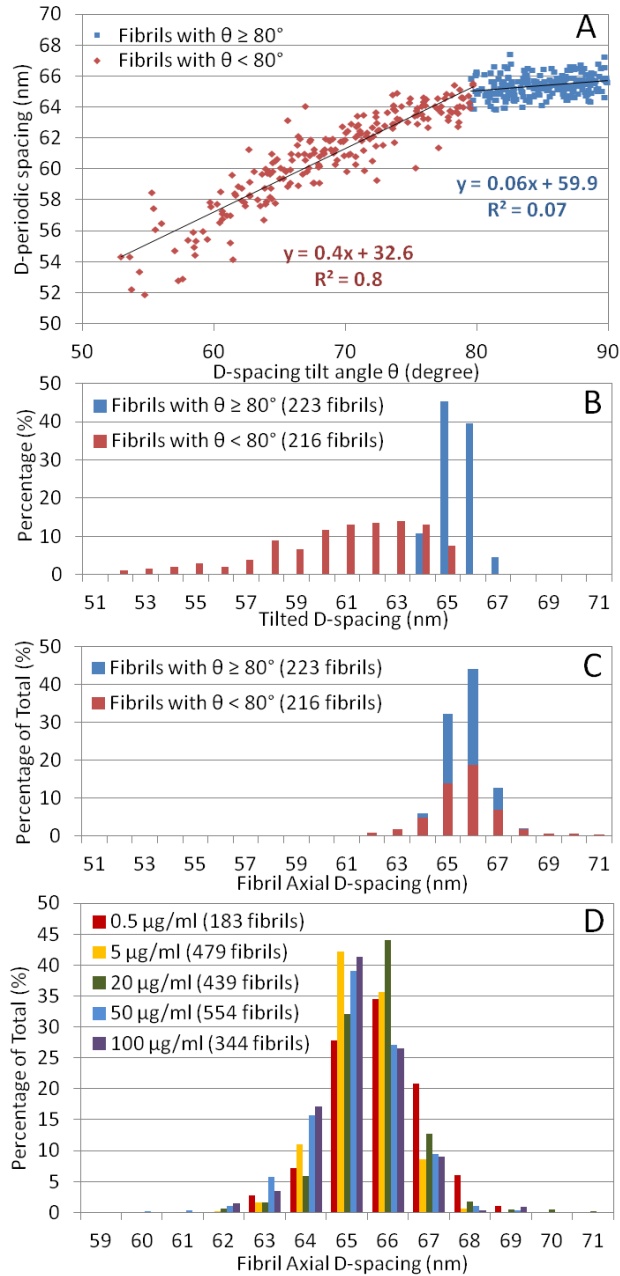
Figure 5.7 The influence of tilt angle on fibril D-spacing at 20 μg/ml. Panel A is the scatter plot showing the linear correlation between fibril D-spacing and tilt angle: red diamonds are fibrils with a large D-spacing tilt (θ < 80o); blue squares are normal fibrils with a small D-spacing tilt ($90^{o} \geq \theta \geq 80^{o}$). Panel B shows the histograms of tilt D-spacing distributions in fibrils with normal and tilted D-spacings, as measured by 2D-FFT; Panel C shows the stacked histogram of fibril axial D-spacing distributions after angle correction: fibril axial D-spacing = tilt D-spacing/sin (θ). Panel D shows histograms of all five concentrations after tilt angle correction.

We analyzed D-spacing values and their corresponding tilt angles for 20, 50 and 100 μg/ml collagen self-assembly on muscovite mica using 2D-FFT. Figure 5.7A is the scatter plot showing the linear correlation between D-spacing tilt angles and tilted D-spacing values in 20 μg/ml concentration. When the D-spacing tilt angle θ is greater than 80°, the fibril D-spacing is within the range of 64 nm to 67 nm, and it shows no correlation with tilt angle ($R^2 = 0.07$). When the D-spacing tilt angle θ is less than 80°, the tilted D-spacing is linearly correlated with D-spacing tilt angle ($R^2 = 0.83$). Thus, more tilt results in a lower D-spacing value. As seen in Figure 5.7B, tilted D-spacings with $θ<80^o$ (in red bins) account for the entire tailing population from 52 nm to 63 nm. When we converted the tilted D-spacings to fibril axial D-spacings using the tilt angle correction shown in Figure 5.6G, all of the low D-spacing values disappeared. Furthermore, the overall D-spacing distribution of the corrected values (as shown in Figure 5.7C) has a skewness of 0.26, compared to -1.3 before the conversion. Similar effects before and after fibril axial D-spacing conversion were observed in 50 and 100 μg/ml (Appendix A.11). Figure 5.7D shows the fibril axial D-spacing histograms at different concentrations: the difference in skewness before the tilt angle correction (Figure 5.5) has disappeared; all five concentrations from 0.5 μg/ml to 100 μg/ml have similar D-spacing means (65.9 ± 1.1, 65.4 ± 0.9, 65.7 ± 1.0, 65.2 ± 1.4, and 65.2 ± 1.1 nm); the distributions are in the range of 60 to 71 nm, similar to that seen in phlogopite mica and collagen fibrillar gel. The cumulative density function plots of different concentrations on muscovite mica before and after tilt angle correction are shown in Appendix A.12. K-S test indicated no significant difference between 50 μg/ml and 100 μg/ml (p = 0.831), and significant differences (p < 0.001) among other concentrations. The shift in CDF plots is within the error of 2D FFT analysis[4] and inconsistent with the trend of concentration change, suggesting that D-spacing distribution on muscovite mica is not concentration dependent.

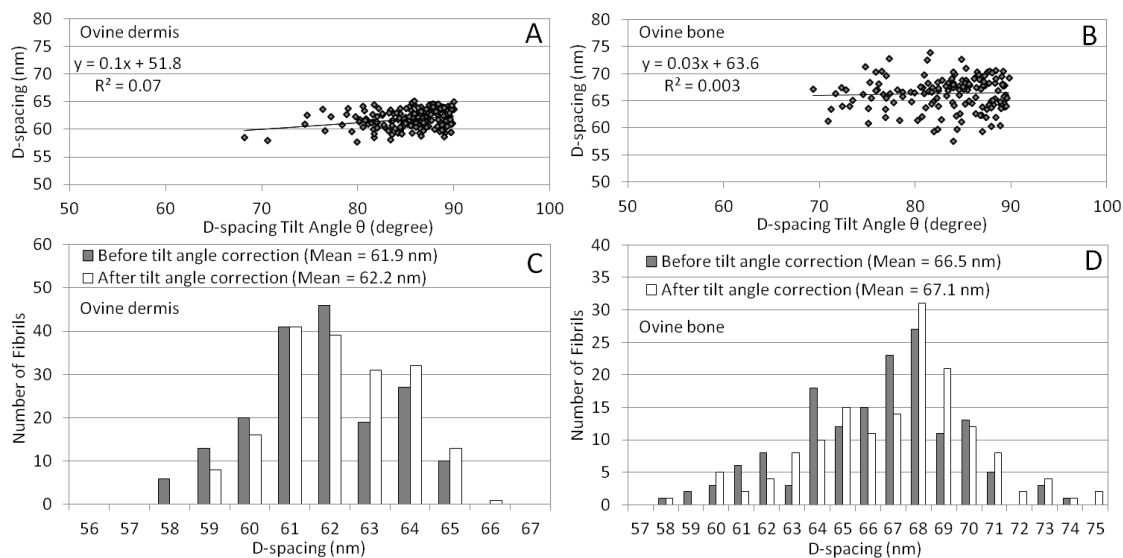**5.2.4 Low D-spacing Values in Ovariectomized (OVX) Tissues**

Figure 5.8 Analysis of fibril D-spacing tilt angles in OVX ovine dermis and OVX bone samples. Scatter plot showing no linear correlation between 2D-FFT measured D-spacing and D-spacing tilt angle in (A) OVX ovine dermis and (B) ovine bone. Histogram comparison of fibril D-spacings before and after D-spacing tilt angle correction in (C) OVX ovine dermis and (D) ovine bone.

The observation of low D-spacing values caused by D-spacing tilt on muscovite mica raises two important questions. The first question is whether tilted D-spacing is common in collagen fibrils formed in biological tissues; the second is whether low D-spacing values previously reported in OVX ovine dermis and bone can be explained by tilted D-spacing. Since we now know 2D-FFT measures the tilted D-spacing and not the fibril axial D-spacing, a fibril with severely tilted D-spacing would have a low D-spacing value. To answer these questions, we analyzed D-spacings and tilt angles in OVX ovine dermis and bone, and converted 2D-FFT measured D-spacing to fibril axial D-spacing using tilt angle correction. Tilted D-spacings in dermis and bone are not very common: 11 out of 181 ovine dermis fibrils (6%) have a tilt angle below 80° (min = 68°), and 36 out of 151 ovine bone fibrils (24%) have a tilt angle below 80° (min = 69°). Figure 5.8A-B are scatter plots showing no correlation between D-spacing tilt angle and 2D-FFT measured D-spacing: the R^2 values for ovine dermis and bone are 0.07 and 0.003, respectively. Overlaying the scatter plots of ovine dermis, ovine bone and 20 µg/ml collagen self-assembled on muscovite mica (Appendix A.13) shows that D-spacings in dermis and bone spread the entire range regardless of the tilt angle, dramatically different

from the correlation between D-spacing and tilt angle found on muscovite mica. Since the percentage of fibrils with tilted D-spacing and the extent of tilt are limited, the impact of D-spacing tilt angle on D-spacing population distribution is negligible. Before tilt angle correction, 22 % of OVX dermal fibrils showed D-spacing values less than 61 nm, compared to 13% after tilt angle correction. In OVX ovine bone, 15% versus 13% of fibrils have D-spacings below 64 nm, before and after tilt angle correction. The comparison between D-spacing distributions as measured by 2D-FFT and fibril axial D-spacing distribution (Figure 5.8C-D) indicates that correction of tilt angle has a small impact on the absolute values of D-spacing, but does not affect the difference in D-spacing distribution as a function of disease.

Tilted D-spacing arises during collagen self-assembly on muscovite mica; however, we did not observe it for self-assembly on phlogopite mica or from gel, and the majority of collagen fibrils in dermis and bone don't have tilted D-spacings. It is important to note that the presence of low D-spacing tilt angle correlates with reduced 2D-FFT D-spacing values due to the sinθ relationship. This study makes it clear that when low D-spacing values are reported, it is important to consider the role of D-spacing tilt angles and the measured values. As we have demonstrated, the fibril axial spacing in collagen fibrils maintains a constant value even as the tilted D-spacing value changes.

5.2.5 The Role of Self-Assembly in the Type I Collagen D-spacing Variations

The data presented in this study demonstrates that self-assembly of type I collagen molecules is sufficient to generate fibrils with the variable D-periodic axial spacing observed in tissue. This indicates that neither the D-spacing itself, nor the variation in the spacing, requires the presence of other matrix proteins, heterotypic collagens, enzymatic cross-linking processes, or an external biological templating device such as a fibripositor.[25] These observations are consistent with previous reports regarding the formation of D-spacings for collagen self-assembly on mica[47-49] as well as studies of the nucleation and growth of fibrils from collagen fibril seeds.[58] These data suggest that theoretical modeling of the self-assembly process,[17] along the lines of studies previously carried out for type I collagen and related model systems,[58,59] should be able to fully model the observed D-spacing variation observed for both the self-assembled systems reported herein as well as in tissue.

5.3 Conclusions

In conclusion, the D-spacing distribution for self-assembly of type I collagen was observed to be substrate independent for two different fibril formation mechanisms. In addition, the D-spacing distribution was similar to that observed for four different tissues (bone, dermis, dentin, tendon) in terms of distribution shape and width. Although D-spacing tilt angle was observed to lower D-spacing on muscovite mica, the effect is reversed with a tilt angle correction and is not the reason for low D-spacings observed in OVX dermis and bone. Type I collagen self-assembly *in vitro* produces the same distribution of D-spacing values observed in biological tissues. The observation of the same distribution of D-spacing by type I collagen self-assembly *in vitro* is significant as it indicates that the mechanism for the origin of distribution does not require heterotypic collagens, enzymatic or non-enzymatic cross-links, or interactions with other small proteins.

5.4 Experimental

5.4.1 Materials and Reagents

Solubilized type I collagen derived from rat tail tendon was purchased from BD Biosciences (4.01 mg/ml, > 90% purity by SDS-PAGE, Franklin Lakes, NJ).The collagen stock solution was prepared by dilution with 0.1 % acetic acid to 1.65 mg/mL (pH = 2.5) and stored at 4 ^{o}C. The stock was used for experiments for up to 2 months. 10 mg/ml solubilized type I collagen was also purchased from BD Biosciences and used for collagen gel formation. Muscovite mica (grade V), phlogpite mica sheets (grade I), and Molybdenum disulfide crystal (grade II) were purchased from SPI supplies (West Chester, PA). AFM pucks of 15 mm diameter were purchased from SPI supplies (West Chester, PA).

5.4.2 Sample Preparation

Mica and MoS_2 substrates were glued onto AFM pucks. Prior to an AFM experiment, a fresh-cleaved substrate surface was produced by peeling off with scotch tape. A fresh aliquot of collagen solution was prepared from collagen stock solution

diluted with a buffer containing 30 mM Na_2HPO_4, 10 mM KH_2PO_4 and 200 mM KCl. A 30-60 μL aliquot of collagen solution was deposited on a mica surface and incubated in a moisture chamber for 2 hours at room temperature. To induce collagen gel formation in capillary tubes, the 10 mg/ml concentrated collagen solution was transferred into capillary tubes, and was then incubated in a fibril forming buffer (FFB) containing 135 mM NaCl, 30 mM Tris base and 5 mM Na_2HPO_4 at room temperature for 2 days. The gel formation was indicated by increased opacity occurring first near the ends of the capillary tube where the collagen solution was in contact with FFB buffer, and slowly penetrating the entire capillary tube. The collagen gel was then transferred onto the MoS_2 surface and incubated for 10 minutes. The mica or MoS_2 surface was then rinsed vigorously with deionized water and wicked with a tissue. After at least 10 minutes of air drying, the substrate surface was imaged with AFM.

5.4.3 AFM imaging and Analysis

All imaging was carried out in air dried conditions with VistaProbes T300R probes in tapping mode (NanoScience, AZ; nominal radius 10 nm, force constant 40 N/m, resonance frequency 300 kHz). All imaging on Muscovite mica was carried out using a PicoPlus 5500 AFM and large scanner (Agilent); all imaging on Phlogopite mica was carried out using a Nanoscope III AFM and JZ scanner (Veeco). Both AFMs were calibrated using a 100 nm x 100 nm calibration standard (2D-100, NANOSENSORS, Switzerland). After calibration, the percentage errors of the Agilent and Nanoscope AFMs are -1.4% and -0.6% respectively (Appendix A.14). Random locations on the samples were imaged by AFM. For the concentration dependent study, each concentration was repeated three times. Image analysis and measurements were performed using SPIP software (Image Metrology; Horsholm, Denmark). Collagen fibril D-spacings were measured using the 2D Fast Fourier Transform (FFT) toolkit of SPIP software. A detailed description and validation can be found in a previous study.[4]

5.5 Reference

(1)   Schmitt, F. O.; Hall, C. E.; Jakus, M. A. *J. Cell. Compar. Physl.* **1942**, *20*, 11.

(2)   Gross, J.; Schmitt, F. O. *The Journal of Experimental Medicine* **1948**, *88*, 555.

(3)   Hodge, A. J.; Petruska, J. A., Eds.; Academic Press: New York, **1963**, p 289.

(4)   Erickson, B.; Fang, M.; Wallace, J. M.; Orr, B. G.; Les, C. M.; Banaszak Holl, M. M. *Biotechnology Journal* **2013**, *8*, 117.

(5)   Wallace, J. M.; Chen, Q.; Fang, M.; Erickson, B.; Orr, B. G.; Banaszak Holl, M. M. *Langmuir* **2010**, *26*, 7349.

(6)   Fang, M.; Liroff, K. G.; Turner, A. S.; Les, C. M.; Orr, B. G.; Holl, M. M. B. *J. Invest. Dermatol.* **2012**, *132*, 1791.

(7)   Odetti, P.; Aragno, I.; Rolandi, R.; Garibaldi, S.; Valentini, S.; Cosso, L.; Traverso, N.; Cottalasso, D.; Pronzato, M. A.; Marinari, U. M. *Diabetes. Metab. Res. Rev.* **2000**, *16*, 74.

(8)   Kemp, A. D.; Harding, C. C.; Cabral, W. A.; Marini, J. C.; Wallace, J. M. *J. Struct. Biol.* **2012**, *180*, 428.

(9)   Miller, A.; Wray, J. S. *Nature* **1971**, *230*, 437.

(10)   Hulmes, D. J. S.; Miller, A. *Nature* **1979**, *282*, 878.

(11)   Trus, B. L.; Piez, K. A. *Nature* **1980**, *286*, 300.

(12)   Traub, W.; Piez, K. A. 1971; Vol. 25, p 243.

(13)   Piez, K. A.; Trus, B. L. *Biosci. Rep.* **1981**, *1*, 801.

(14)   Hulmes, D. J. S.; Wess, T. J.; Prockop, D. J.; Fratzl, P. *Biophys. J.* **1995**, *68*, 1661.

(15)   Orgel, J. P. R. O.; Miller, A.; Irving, T. C.; Fischetti, R. F.; Hammersley, A. P.; Wess, T. J. *Structure* **2001**, *9*, 1061.

(16)   Orgel, J. P. R. O.; Irving, T. C.; Miller, A.; Wess, T. J. *Proc. Natl. Acad. Sci. U. S. A.* **2006**, *103*, 9001.

(17)   Gautieri, A.; Vesentini, S.; Redaelli, A.; Buehler, M. J. *Nano Lett.* **2011**, *11*, 757.

(18)   Wallace, J. M.; Erickson, B.; Les, C. M.; Orr, B. G.; Banaszak Holl, M. M. *Bone* **2010**, *46*, 1349.

(19)   Wallace, J. M.; Orr, B. G.; Marini, J. C.; Holl, M. M. B. *J. Struct. Biol.* **2011**, *173*, 146.

(20)   Landis, W. J.; Hodgens, K. J.; Arena, J.; Song, M. J.; McEwen, B. F. *Microsc. Res. Tech.* **1995**, *33*, 192.

(21)   Fratzl, P.; Fratzl-Zelman, N.; Klaushofer, K.; Vogl, G.; Koller, K. *Calcif. Tissue Int.* **1991**, *48*, 407.

(22)   Fratzl, P.; Groschner, M.; Vogl, G.; Plenk Jr, H.; Eschberger, J.; Fratzl-Zelman, N.; Koller, K.; Klaushofer, K. *J. Bone Miner. Res.* **1992**, *7*, 329.

(23)   Birk, D. E.; Trelstad, R. L. *J. Cell Biol.* **1984**, *99*, 2024.

(24)   Birk, D. E.; Trelstad, R. L. *J. Cell Biol.* **1986**, *103*, 231.

(25)   Canty, E. G.; Lu, Y.; Meadows, R. S.; Shaw, M. K.; Holmes, D. F.; Kadler, K. E. *J. Cell Biol.* **2004**, *165*, 553.

(26)   Canty, E. G.; Kadler, K. E. *J. Cell Sci.* **2005**, *118*, 1341.

(27)   Giraud-Guille, M. M. *J. Mol. Biol.* **1992**, *224*, 861.

(28)   Gobeaux, F.; Mosser, G.; Anglo, A.; Panine, P.; Davidson, P.; Giraud-Guille, M. M.; Belamie, E. *J. Mol. Biol.* **2008**, *376*, 1509.

(29)   Giraud-Guille, M. M.; Mosser, G.; Belamie, E. *Current Opinion in Colloid and Interface Science* **2008**, *13*, 303.

(30)   Ricard-Blum, S.; Ville, G. *Int. J. Biochem.* **1989**, *21*, 1185.

(31)   Knott, L.; Bailey, A. J. *Bone* **1998**, *22*, 181.

(32)   Reed, C. C.; Iozzo, R. V. *Glycoconj. J.* **2002**, *19*, 249.

(33)   Zhang, G.; Ezura, Y.; Chervoneva, I.; Robinson, P. S.; Beason, D. P.; Carine, E. T.; Soslowsky, L. J.; Iozzo, R. V.; Birk, D. E. *J. Cell. Biochem.* **2006**, *98*, 1436.

(34)   Kadler, K. E.; Hill, A.; Canty-Laird, E. G. *Curr. Opin. Cell Biol.* **2008**, *20*, 495.

(35)   Shi, F.; Harman, J.; Fujiwara, K.; Sottile, J. *American Journal of Physiology - Cell Physiology* **2010**, *298*, C1265.

(36)   Kadler, K. E.; Hojima, Y.; Prockop, D. J. *J. Biol. Chem.* **1987**, *262*, 15696.

(37)   Usha, R.; Ramasami, T. *Thermochimica Acta* **1999**, *338*, 17.

(38)   Schnell, J. *Arch. Biochem. Biophys.* **1968**, *127*, 496.

(39)   Na, G. C.; Phillips, L. J.; Freire, E. I. *Biochemistry (Mosc).* **1989**, *28*, 7153.

(40)   Gross, J.; Kirk, D. *The Journal of biological chemistry* **1958**, *233*, 355.

(41)   Leikin, S.; Rau, D. C.; Parsegian, V. A. *Proc. Natl. Acad. Sci. U. S. A.* **1994**, *91*, 276.

(42)   Comper, W. D.; Veis, A. *Biopolymers* **1977**, *16*, 2113.

(43)   Wang, Y.; Silvent, J.; Robin, M.; Babonneau, F.; Meddahi-Pellé, A.; Nassif, N.; Giraud Guille, M. M. *Soft Matter* **2011**, *7*, 9659.

(44)   Knight, D. P.; Nash, L.; Hu, X. W.; Haffegee, J.; Ho, M. W. *J. Biomed. Mater. Res.* **1998**, *41*, 185.

(45)   Pins, G. D.; Christiansen, D. L.; Patel, R.; Silver, F. H. *Biophys. J.* **1997**, *73*, 2164.

(46)   Mosser, G.; Anglo, A.; Helary, C.; Bouligand, Y.; Giraud-Guille, M. M. *Matrix Biol.* **2006**, *25*, 3.

(47)   Jiang, F.; Hörber, H.; Howard, J.; Müller, D. J. *J. Struct. Biol.* **2004**, *148*, 268.

(48)   Loo, R. W.; Goh, M. C. *Langmuir* **2008**, *24*, 13276.

(49)   Leow, W. W.; Hwang, W. *Langmuir* **2011**, *27*, 10907.

(50)   Cisneros, D. A.; Hung, C.; Franz, C. M.; Muller, D. J. *J. Struct. Biol.* **2006**, *154*, 232.

(51)   Graham, H. K.; Holmes, D. F.; Watson, R. B.; Kadler, K. E. *J. Mol. Biol.* **2000**, *295*, 891.

(52)   Kadler, K. E.; Holmes, D. F.; Trotter, J. A.; Chapman, J. A. *Biochem. J.* **1996**, *316*, 1.

(53)   Birk, D. E. *Micron* **2001**, *32*, 223.

(54)   Simbrunner, C.; Nabok, D.; Hernandez-Sosa, G.; Oehzelt, M.; Djuric, T.; Resel, R.; Romaner, L.; Puschnig, P.; Ambrosch-Draxl, C.; Salzmann, I.; Schwabegger, G.; Watzinger, I.; Sitter, H. *J. Am. Chem. Soc.* **2011**, *133*, 3056.

(55)   Simbrunner, C.; Hernandez-Sosa, G.; Oehzelt, M.; Djuric, T.; Salzmann, I.; Brinkmann, M.; Schwabegger, G.; Watzinger, I.; Sitter, H.; Resel, R. *Physical Review B* **2011**, *83*, 115443.

(56)   Balzer, F.; Kankate, L.; Niehus, H.; Rubahn, H. G. 2005; Vol. 5925, p 1.

(57)   Kuwahara, Y. *Phys Chem Min* **2001**, *28*, 1.

(58)   Holmes, D. F.; Tait, A.; Hodson, N. W.; Sherratt, M. J.; Kadler, K. E. *J. Mol. Biol.* **2010**, *399*, 9.

(59)   O'Leary, L. E. R.; Fallas, J. A.; Bakota, E. L.; Kang, M. K.; Hartgerink, J. D. *Nat Chem* **2011**, *3*, 821.

Chapter 6   **Conclusions and Future Directions**

6.1   **Summary**

First reported in 1940s, the biological significance of collagen fibril D-spacing distribution has been largely neglected. D-spacing measurements frequently report mean ± standard deviation, which reflects the conventional view that D-spacing is a singular value and deviations from the mean value are due to instrumental noise or tissue handling artifacts. In this dissertation, a quantitative method for collagen D-spacing characterization has been developed and validated; the biological importance of D-spacing distribution is highlighted in the study of long term estrogen depletion as well as the study of collagen D-spacing in connection to microscale tissue hierarchy. The origin of D-spacing distribution has been explored using in vitro fibrillogenesis.

Chapter 2 described the quantitative method to measure the D-periodic spacing of type I collagen fibrils using Atomic Force Microscopy (AFM) coupled with analysis using the two dimensional Fast Fourier Transform (2D-FFT) approach. AFM was chosen due to its ability to analyze collagen nanomorphology at the individual fibril level. In addition, it excels at keeping the tissue specimens relatively close to their native conditions. The effect of surface dehydration on collagen fibril D-spacing was explored by paired comparison of hydrated and surface dehydrated dermal collagen fibril D-spacing. No correlation was found in the small shifts in D-spacing as a function of surface dehydration. Due to the nonlinear sensitivity of piezoelectric scanners, calibration of AFM at the length scale of collagen D-spacing is required. Variations in the distribution induced by diseases such as *OI* and long term estrogen depletion were identified using the combined AFM and 2D-FFT method. A non-parametric statistical analysis, K-S test, was used to compare different distribution populations, as it is sensitive not only to the mean values, but also the width of distribution. The effectiveness of this quantitative analysis was demonstrated throughout the rest of this dissertation.

Chapter 3 examined the effect of estrogen depletion on dermal collagen using fibril D-spacing as the key metric. Macroscopically, estrogen depletion is known to reduce collagen content and compromise the resilience of skin. This chapter explored the ultrastructural change of dermal collagen in ovariectomized dermis. Similar to what was previously reported in OVX bone, OVX dermis was associated with increased percentage of fibrils with D-spacing values below mean − 1 standard deviation. In contrast to significant difference between Sham and OVX D-spacing distributions, no difference was found when comparing D-spacing means, indicating the importance of using a fibril-by-fibril analysis. The studies in OVX bone and dermis together suggest that estrogen depletion have similar effect on collagen nanomorphology regardless of the mineralization state.

The organization of collagen fibrils into higher level fibril bundles is a common observation in bone, dermis and tendon. Chapter 4 investigated collagen fibril D-spacing as a function of fibril bundles. Fibril D-spacings within a bundle were found to be similar if not identical, given the uncertainty associated with the analysis. A fibril bundle characterized by singular D-spacing was named a D-bundle. A full distribution of D-spacing arises from the differences at the bundle level. A nested mixed model ANOVA analysis further supported the latter observation as over 75% of total variance was attributed to bundle variance, regardless of the animal type and tissue type. These findings have important implications in the existing fibrillogenesis models, particularly the Nucleation, Growth and Coalescence (NGC) model and Liquid Crystallinity (LC) model.

The studies in chapter 3 and 4 led to the question regarding the origin of the D-spacing distribution. The complex biochemical modification and interactions associated with collagen in biological tissues poses challenges in studying the origin of D-spacing distribution. Therefore, chapter 5 investigated type I collagen D-spacing formed using two in vitro methods: surface-mediated collagen self-assembly on phlogopite and muscovite mica, and coextrusion of collagen fibrillar gel in glass capillary tubes. The main finding was that the self-assembly of type I collagen alone could reproduce a distribution of D-spacing values, similar to that observed in tissues. The concentration of collagen in the incubation solution was found to have no impact on D-spacing

distribution. D-spacing tilt with respect to fibril axis was found on muscovite mica, with larger tilt angle correlating to lower D-spacing. However, this effect was reversed with a tilt angle correction and it couldn't explain low D-spacings observed in OVX dermis and bone.

6.2   Future Directions

Systematic analysis of nanoscale characteristics of type I collagen provide important structural information regarding type I collagen and the assembly of fibril networks in model and tissue specimens. It could be used to evaluate the degradation of collagen in diseases and effectiveness of drug therapeutics, which is important both in terms of clinical applications as well as fundamental research of disease mechanisms. Estrogen depletion induced D-spacing variations is one promising example. Clinical diagnosis of Osteoporosis uses bone mineral density (BMD) as the key predictor and overlooks the material property changes associated with collagen. D-spacing analysis could serve as a complementary technique in the early diagnosis of osteoporosis. Other applications include assessing the effect of photo aging on dermal collagen degradation; the impact of X-ray irradiation on tissue collagen in cancer treatment; and characterization of bioengineered tissue scaffolding.

It is unclear how estrogen depletion affects collagen D-spacing. Estrogen plays important roles in regulating cell activities and collagen turn-over; long term estrogen depletion increases bone fracture risk by exacerbated bone resorption. Analysis of D-spacing distribution in estrogen depletion noted a sub-portion of abnormally low D-spacings. A combined fluorescent and AFM imaging experiment could answer whether fibrils with low D-spacings are formed before or after ovarectomy. Bone remodeling could be tracked with a fluorescent marker, such as tetracycline, allowing selective AFM imaging and analysis of fibril D-spacing from newly remodeled versus older bone. Such experiment could provide critical information and explain why only a small percentage of fibrils are severely affected.

The close association of D-spacing with bundle organization has been demonstrated in chapter 4. Yet it is still unclear what controls the narrow D-spacings

within a single D-bundle and what differentiates different D-bundles. Questions include to what extent cells and liquid crystallinity of collagen are involved in forming collagen fibril bundles; whether other extracellular proteins influence D-spacing; whether different D-bundles with variant D-spacings behave differently under mechanical stresses. Knockout animal models are available for D-spacing investigations. For example, type V and decorin deficient mice models exhibit abnormally large collagen fibril diameters, suggesting their roles in regulating collagen fibril fusion. Incorporation of type V collagen occurs in intracellular and paracellular regions, whereas decorin binding occurs extracellularly. The relationship between D-spacing and collagen fibril bundles in type V and decorin deficient animals will have profound implications in NGC fibrillogenesis model which suggests the important role of cells in collagen fibril bundle formation.

The in vitro collagen self-assembly system described in chapter 5 provides an alternative approach to study collagen nanomorphology under controlled conditions. For example, studying the nanomorphology of mixed types (I, III and V) collagen self-assembly using this model system could help decipher the importance of heterotypical collagen fibrils. Chemically induced cross-linking is also readily achievable via UV irradiation or cross-linking reagents. Combined AFM and Raman investigation will allow correlation of collagen D-spacing with cross-link intensity. Furthermore, drug molecules may be introduced to this model system if one is interested in knowing how a drug may affect collagen self-assembly.

With more studies incorporating collagen D-spacing measurement in their tissue or material characterizations, a better understanding of the relationship between D-spacing and other properties will be possible, and D-spacing analysis may find new applications in early disease diagnosis.
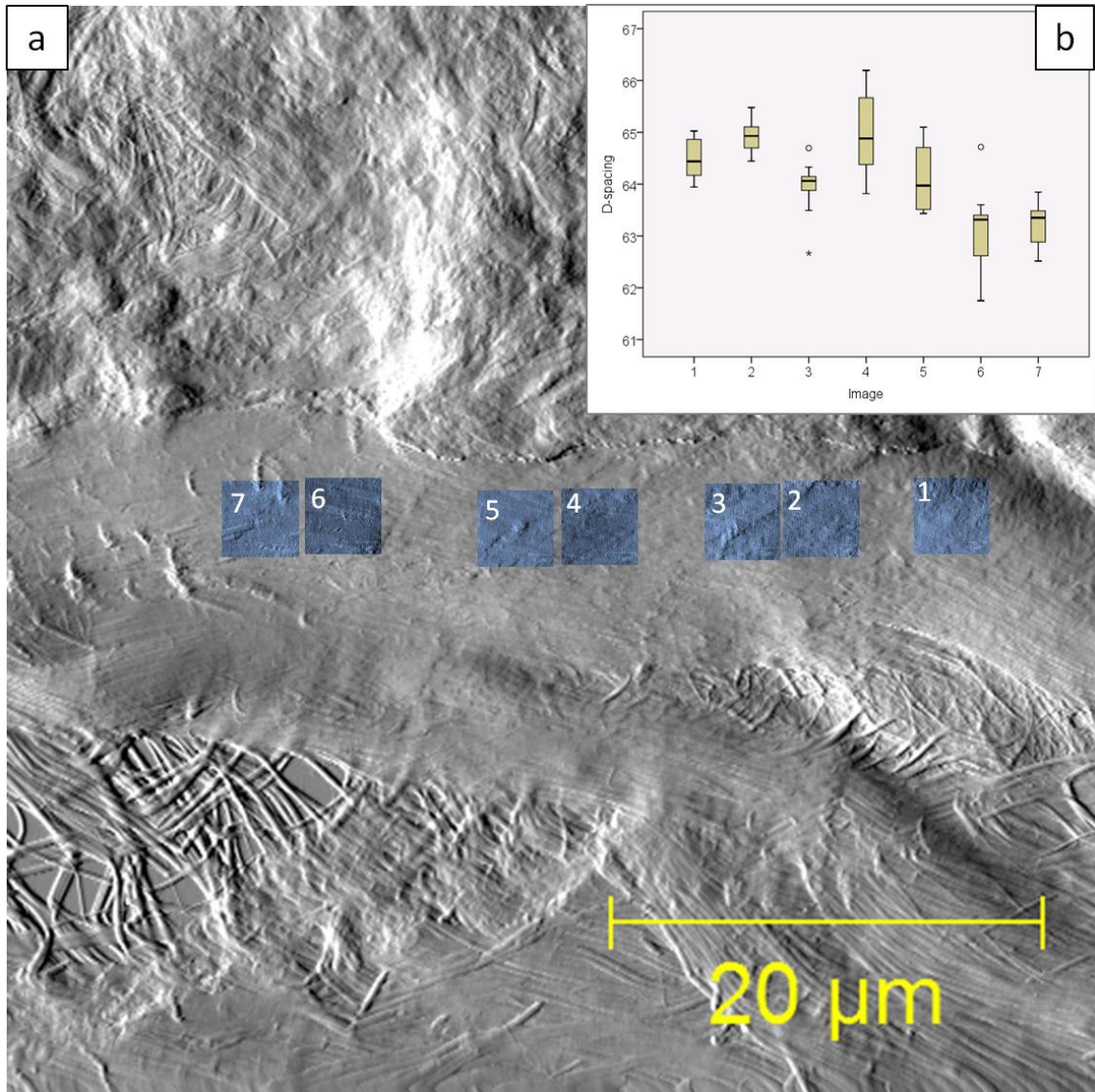
Appendix A
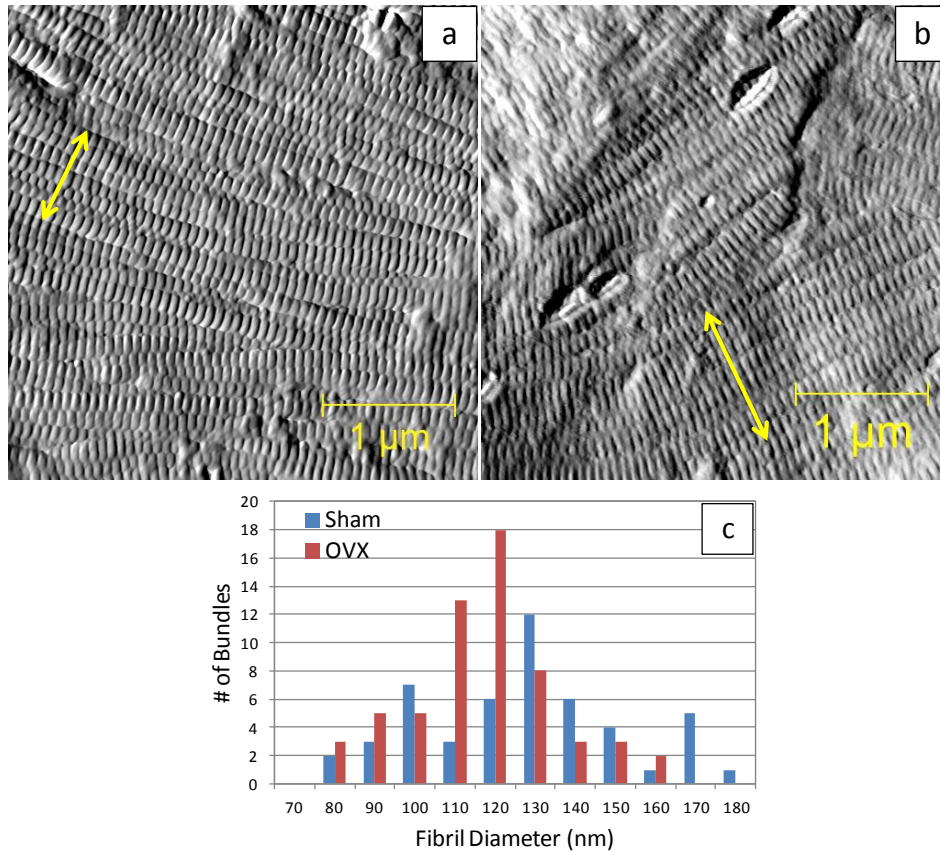
Appendix A.1 The comparison of collagen fibril diameter between sham and OVX ovine dermis. Panel a and b are exemplary AFM images showing bundles of collagen fibrils. An average fibril diameter was estimated for each bundle as indicated by the arrows. Panel c reveals the diameter distribution in sham and OVX dermis.
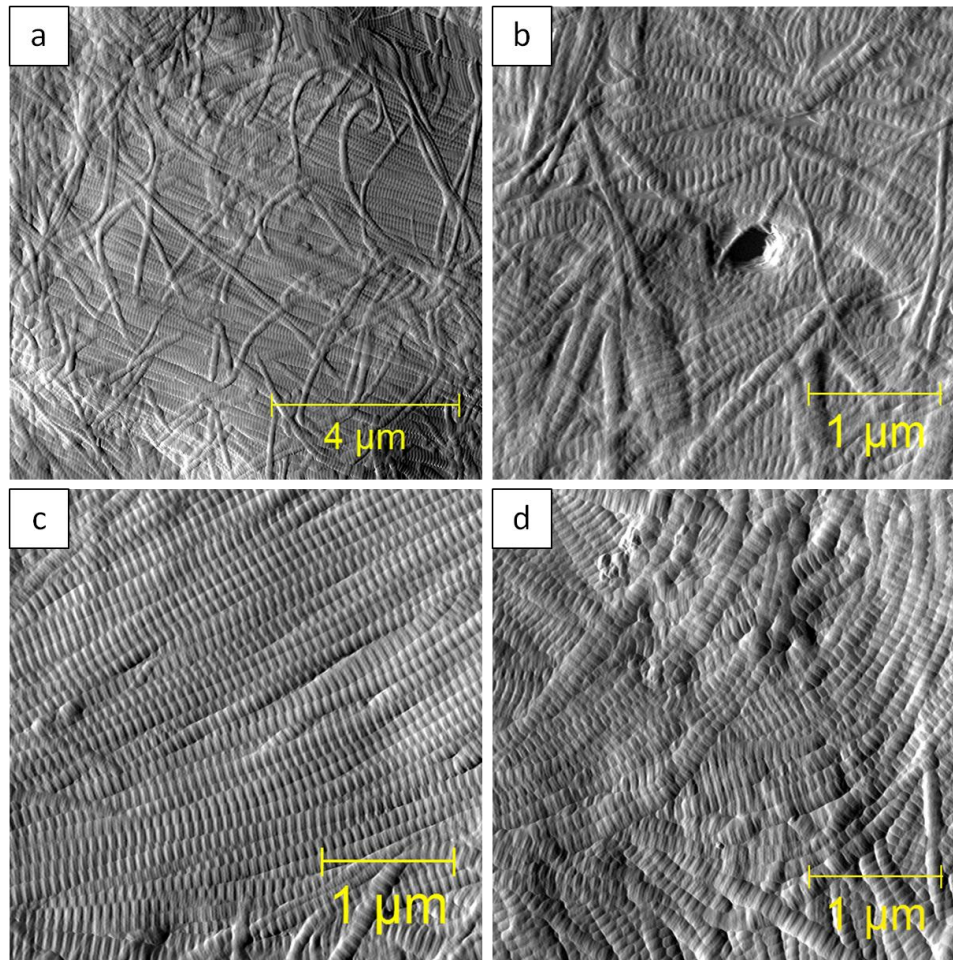
Appendix A.2 Examples of diverse fibril organization in bone. (a) Broom-like organization of collagen fibrils; (b) Interwoven fibril organization near a canaliculi; (c) A rare case of uniformly packed fibril bundle; (d) Curved fibril bundles overlapping with each other(about 1 μm lateral diameter).

Appendix A.3 A summary of nested mixed model ANOVA analysis.

Ovine dermis and human skin	Ovine		Human		p (compare ovine vs human)
D-spacing mean	63.02		62.52		0.2369

Variance components	Pooled	p (compared to 0)	Ovine	Human	p (compare ovine vs human, likelihood ratio χ2 test)
σ^2_{animal}	0.14	0.2893	-	-	-
$\sigma^2_{\text{bundle(animal)}}$	1.75	<0.0001	1.76	1.74	>0.999
$\sigma^2_{\text{fibril(bundle(animal))}}$	0.37	<0.0001	0.38	0.36	0.86

Ovine dermis, bone and tendon	Dermis	Bone	Tendon	p (compare dermis, bone and tendon)
D-spacing mean	62.91	63.84	64.02	0.1169

Variance components	Pooled	p (compared to 0)	Dermis	Bone	Tendon	p (compare dermis, bone and tendon, likelihood ratio χ2 test)
σ^2_{animal}	0.40	0.16	-	-	-	-
$\sigma^2_{\text{bundle(animal)}}$	2.48	<0.0001	1.77	3.82	1.43	0.074
$\sigma^2_{\text{fibril(bundle(animal))}}$	0.40	<0.0001	0.38	0.54	0.22	<0.0001

Appendix A.4 50 μm-scale longitudinal persistence of D-spacing in a lamb tendon fascicle. Panel a is a 50 μm AFM image of a tendon fascicle; 7 different locations (3.5 μm in size) along the longitudinal axis of this fascicle were imaged and overlaid here as the blue images. Panel b is the boxplot representation of the minimum, maximum and interquartile range of D-spacings from these 7 images.
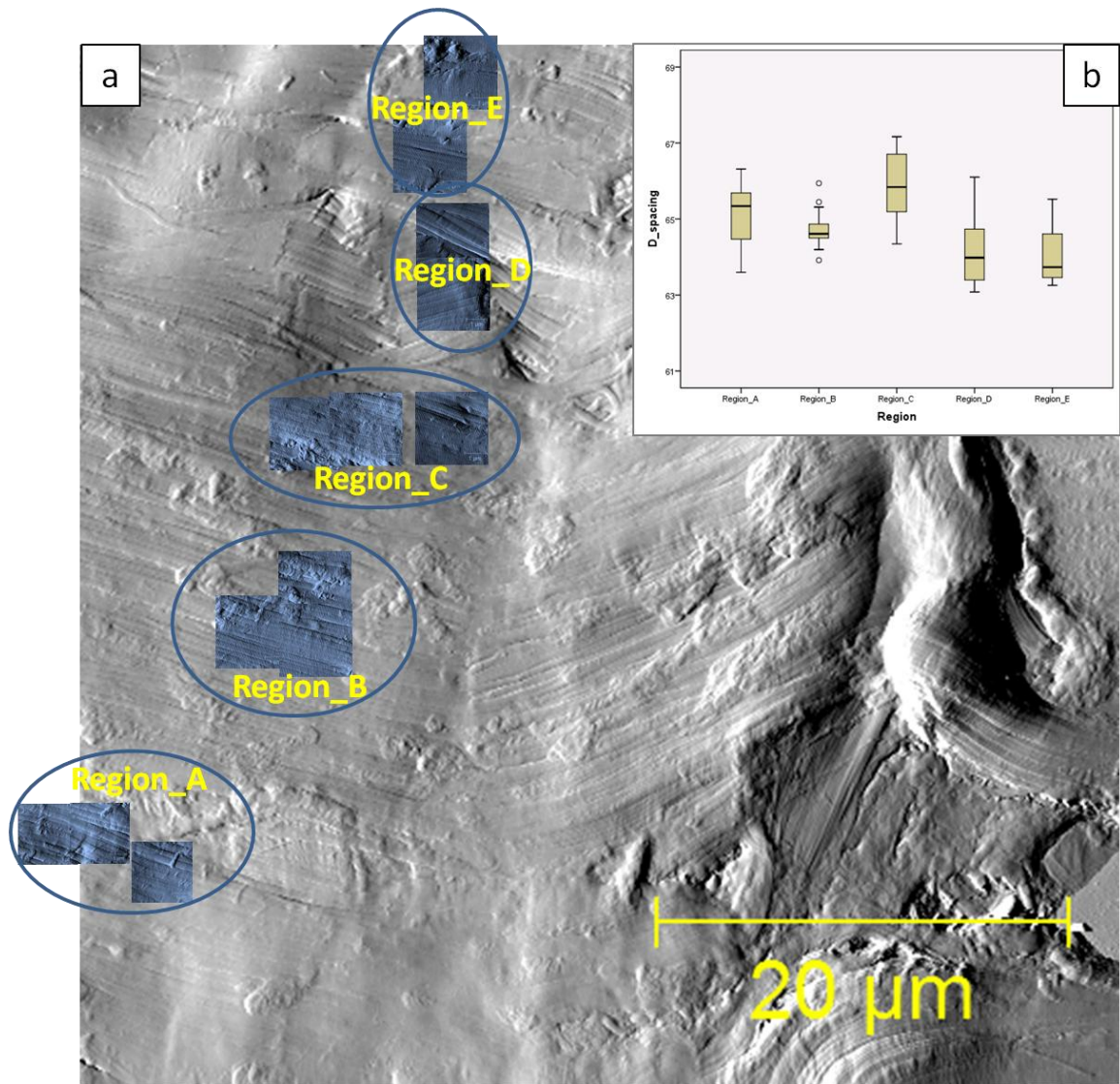
Appendix A.5 The persistence of D-spacing in 40 μm-scale perpendicular regions of a lamb tendon fascicle. Panel a is a 50 μm AFM image of a tendon fascicle; 5 different regions perpendicular to the axial direction of this fascicle were imaged and overlaid here as the blue images, each region contains 2-3 images of 3.5 μm size. Panel b is the boxplot representation of the minimum, maximum and interquartile range of D-spacings from these 5 regions.

Appendix A.6 The nested ANOVA model for bundle persistence length assessment:

$$Y_{ijk} = \mu_0 + a_i + b_{ij} + r_{ijk} + \varepsilon_{ijkl} \qquad\qquad \text{A.6. Eq. (a)}$$

$$var\,(a_i) = \sigma^2_{animal} \qquad\qquad \text{A.6. Eq. (b)}$$

$$var\,(b_{ij}) = \sigma^2_{bundle(animal)} \qquad\qquad \text{A.6. Eq. (c)}$$

$$var\,(r_{ijk}) = \sigma^2_{location(bundle(animal))} \qquad\qquad \text{A.6. Eq. (d)}$$

$$var\,(\varepsilon_{ijkl}) = \sigma^2_{fibril(location(bundle(animal)))} \qquad\qquad \text{A.6. Eq. (e)}$$

$$Total\ Variance = \sigma^2_{animal} + \sigma^2_{bundle(animal)} + \sigma^2_{region(bundle(animal))} +$$

$$\sigma^2_{fibril(region(bundle(animal)))} \qquad\qquad \text{A.6. Eq. (f)}$$

μ_0 – D-spacing mean;
a_i – random effect of ith animal;
b_{ij} – random effect of jth bundle nested within ith animal;
r_{ijk} – random effect of kth region nested in jth bundle and ith animal;
ε_{ijkl} – random effect of lth fibril nested in kth region, jth bundle and ith animal.

| Treatment	# of Fibrils	Mean	SD
NEG Initial	213	69.00	1.89
NEG – 7 days	224	68.49	1.92
NEG – 14 days	221	68.48	1.84
NEG – 21days	217	68.68	2.04
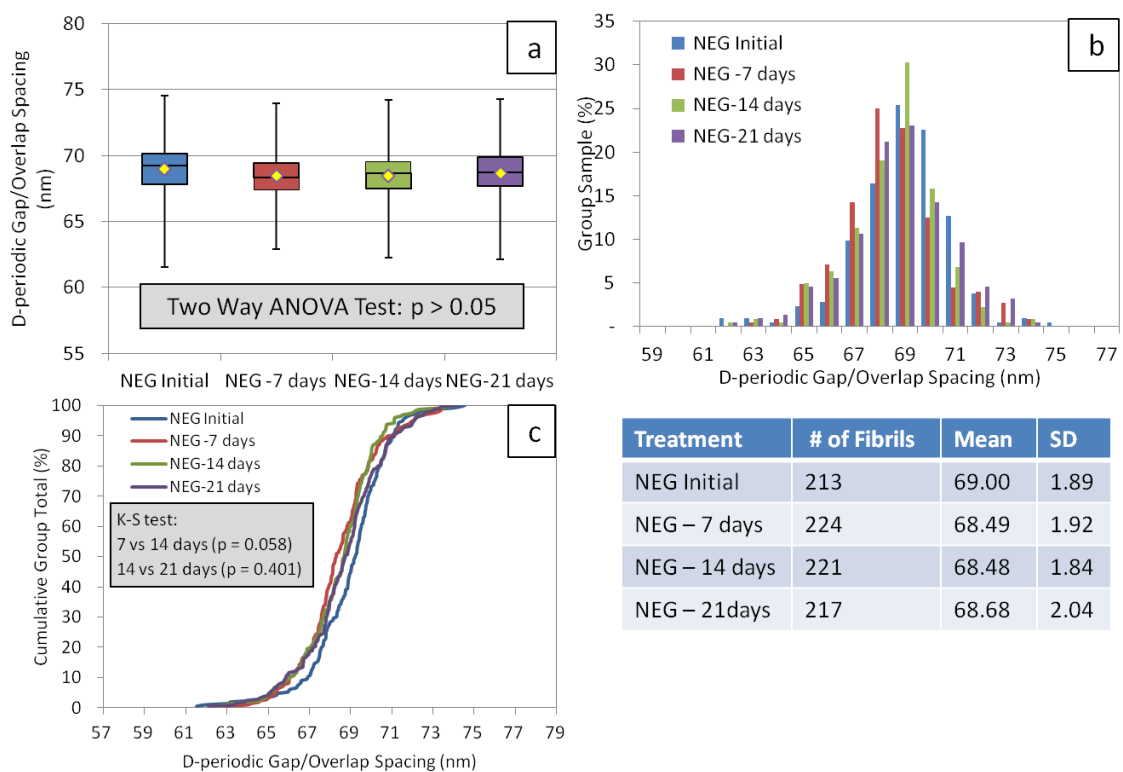
Appendix A.7 Ovine bone collagen D-spacing distribution is unaffected by Non-Enzymatic Glycation (NEG) treatment. (a) Boxplot representation of mean, minimum, maximum and interquartile range of D-spacing distribution at day 0, 7, 14 and 21 of *in vitro* NEG treatment with D-ribose. (b) and (c) are the histogram and cumulative density function (CDF) plot showing no effect of NEG cross-linking on the bone collagen D-spacing distribution. A two way ANOVA test on the D-spacing means and K-S tests on the CDF plots all suggest no statistical significance. The table listed the number of fibrils analyzed in each group and the means and standard deviations.
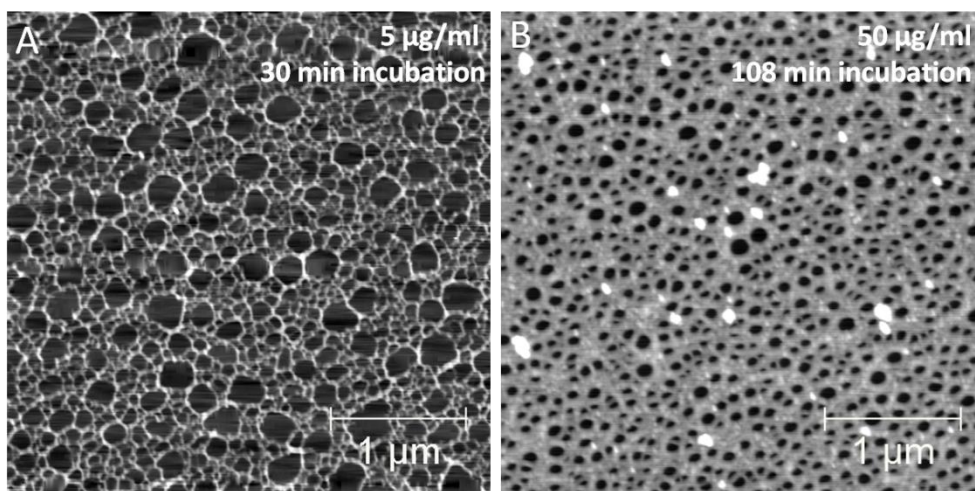
Appendix A.8 Type I collagen self-assembles into web-like pattern on MoS$_2$. Panels A and B are AFM topography images after 30 min and 108 min incubation of collagen solutions containing 5 μg/ml and 50 μg/ml type I collagen, respectively.
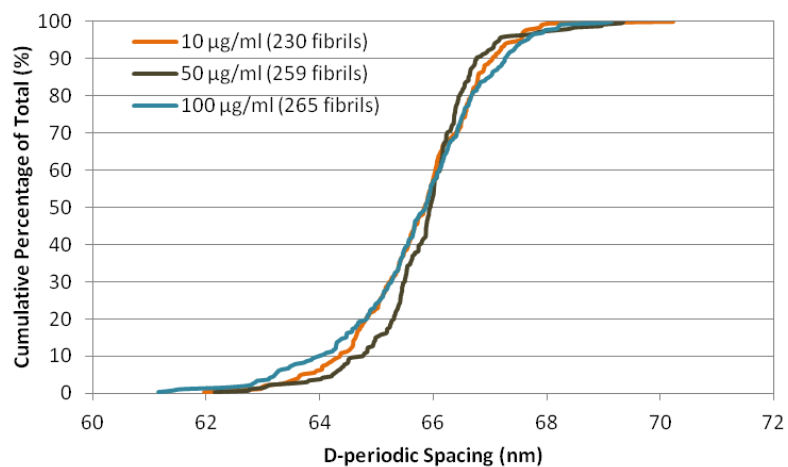
Appendix A.9 CDF representation of D-spacing distributions self-assembled on phlogopite mica at 10, 50 and 100 μg/ml, indicating the lack of concentration dependent changes on phlogopite mica.
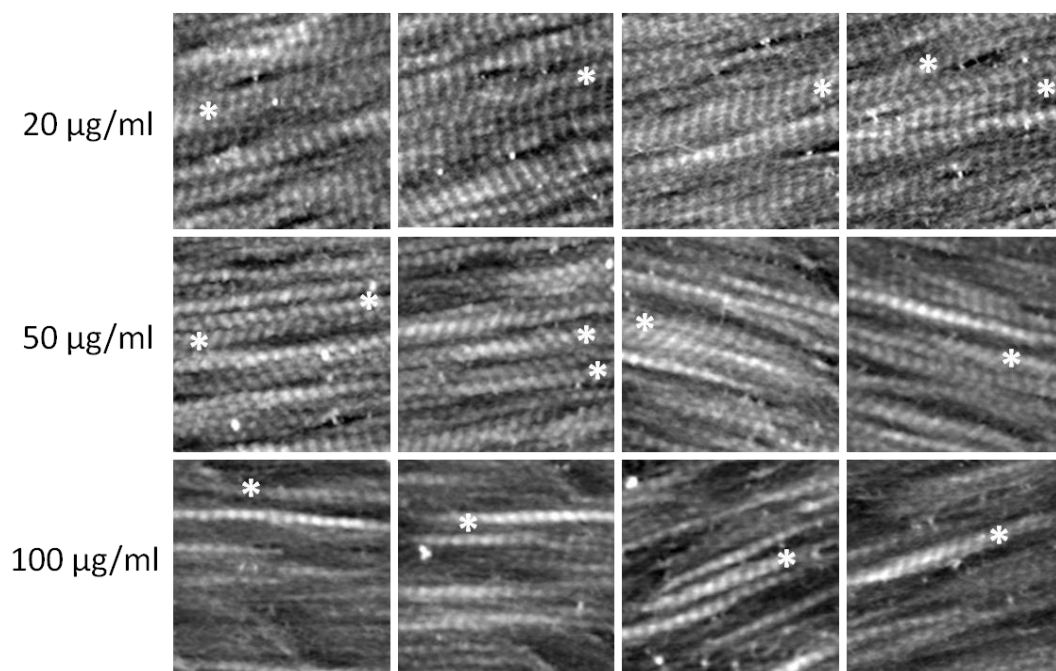
Appendix A.10 Exemplary 1 μm AFM topography images showing tilted D-spacings (marked by asterisks) from 20, 50 and 100 μg/ml samples on muscovite mica.
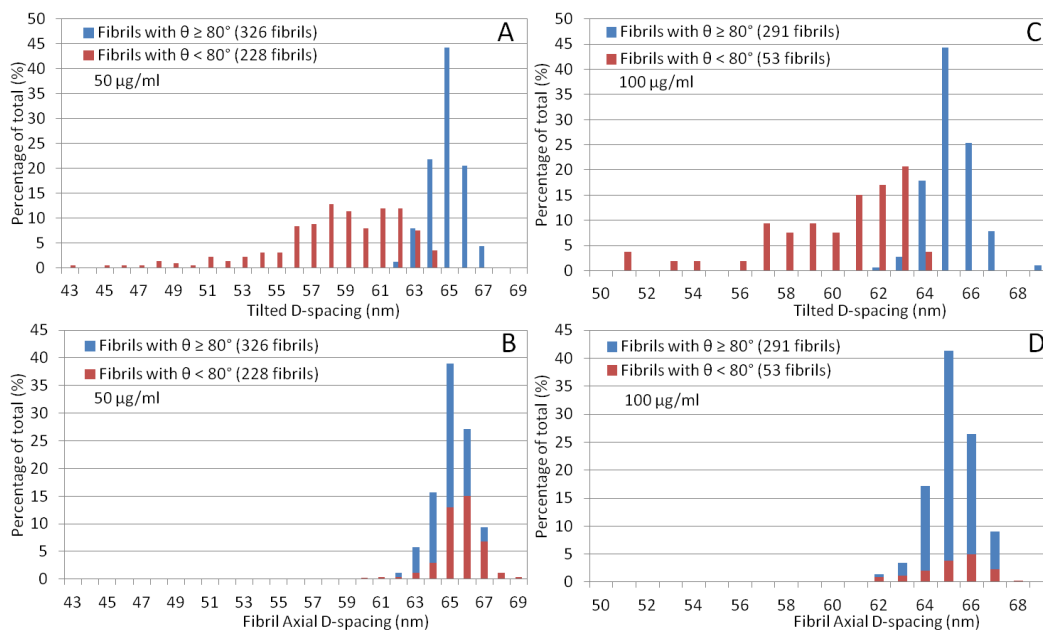
Appendix A.11 The influence of tilt angle on fibril D-spacing at 50 and 100 μg/ml. Panels A-B are D-spacing distribution histograms before and after tilt angle correction in 50 μg/ml. Panels C-D are similar analyses for 100 μg/ml. After tilt angle correction, the tilted D-spacings (θ < 80°) are corrected to the normal distribution range.
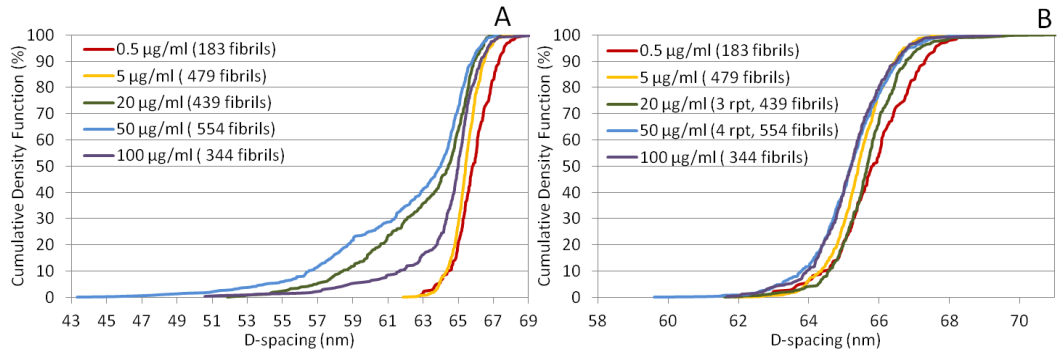
Appendix A.12 The CDF plots of different concentrations (0.5 to 100 μg/ml) on muscovite mica before (panel A) and after (panel B) tilt angle correction.
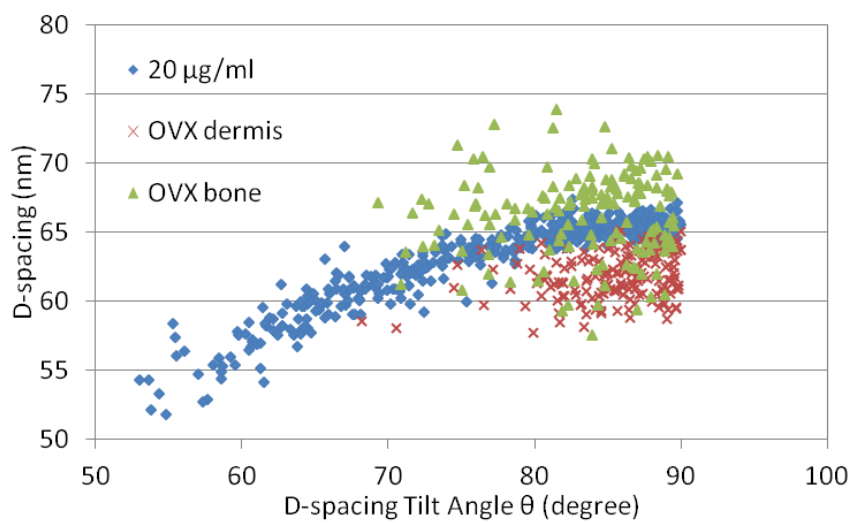
Appendix A.13 Overlaid scatter plots of OVX dermis, bone and 20 μg/ml on muscovite mica.
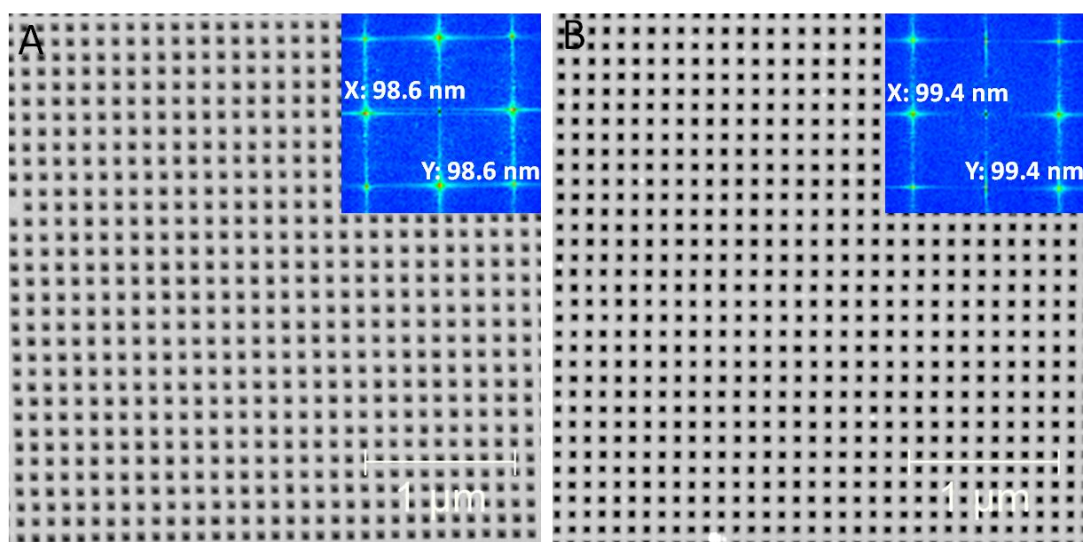
Appendix A.14 Calibration of Agilent 5500 AFM and Nanoscope IIIA AFM using 100 nm x 100 nm calibration grid**.** Panel A is the image of the calibration standard scanned by Agilent 5500 AFM, the insert is the 2D FFT transformation of the image, and the grids on the X and Y directions are measured to be 98.6 nm. Panel B is the image of the calibration standard scanned by Nanoscope IIIA AFM, the insert shows the X and Y measurements are both 99.4 nm.